Felix Egbert Schober, BSc

Parameter Identification for a Drivetrain-Simulation

Master's Thesis

to achieve the university degree of
Master of Science
Master's degree program: Electrical Engineering

submitted to
Graz University of Technology
Faculty of Electrical and Information Engineering

Institute of Automotive Engineering
Member of [**FSI**]

Supervisors:
Dipl.-Ing. Dr.techn. Jürgen Fabian
Dipl.-Ing. Harald Kraus

Graz, June 2016

Acknowledgement

I would like to thank my supervisors Jürgen Fabian and Harald Kraus for the professional support, feedback and assistance during this Master's thesis.

I also want to thank my university colleagues and friends who always encouraged, motivated and entertained me. Special thanks goes to Michael Kiechl and Thomas Anvidalfarei. They supported me with good company, new ideas and approaches.

Furthermore, I would like to thank my parents and my sister. They helped and supported me during all times and situations.

My special thanks goes to my girlfriend Martina, who had to deal with me in stressful situations and always supported me when needed.

Statutory Declaration

Ich erkläre an Eides statt, dass ich die vorliegende Arbeit selbstständig verfasst, andere als die angegebenen Quellen/Hilfsmittel nicht benutzt, und die den benutzten Quellen wörtlich und inhaltlich entnommenen Stellen als solche kenntlich gemacht habe.

Graz, am ....
(Unterschrift)

I declare that I have authored this thesis independently, that I have not used other than the declared sources / resources, and that I have explicitly marked all material which has been quoted either literally or by content from the used sources.

....
(date) (signature)

Abstract

Simulations are getting more important in the automotive industry. With the help of appropriate simulations automotive original equipment manufacturers (OEMs) can significantly reduce development times and costs. For these simulations input parameters such as engine speed, torque or inertia are required. In case of complex hybrid electric vehicles (HEVs) more parameters are needed to build up a simulation model. In addition to a normal combustion engine an electric motor and battery are included as well as a more complex transmission control unit (TCU) and engine control unit (ECU). Those control units require parameters to calculate control signals for the vehicle to perform near its optimum operation area while driving. Control units such as electronic stability control (ESC) and anti-lock brake system (ABS) are performing better if more specific and accurate input parameters are available.

OEMs and automotive suppliers are working together to improve and optimize passenger vehicles. However, data about parameters are hardly contributed for non-disclosure issues. Global automotive suppliers are using for example test benches, where specific parameters can be easily identified such as the suspension characteristics, drag coefficient or inertias. Companies or research institutes which do not have any testing rigs have to develop other methods to identify parameters with their available measurement equipment.

This thesis deals with the development of a holistic method to identify parameters in real driving situations. The objective is to reduce expenses and time for evaluating required vehicle parameters. Furthermore, the developed identification method on the road has the advantage that OEMs do not have to contribute the parameters.
For this purpose a plug-in hybrid electric vehicle (PHEV) was provided. Within this thesis a roadmap was generated, which specifies the driving manoeuvres. If a manoeuvre on the test street did not yield sufficient data quality, the manoeuvre and/or test road was adapted. Not all driving manoeuvres yielded the expected output.

As a result other manoeuvres were used although at first they seemed unsuitable for the desired parameter. Nevertheless, the roadmap to identify vehicle parameters in real world driving manoeuvres showed promising results. In conclusion, it was possible to identify many parameters in real driving situations.

Kurzfassung

In der Automobilindustrie werden Simulationen immer wichtiger. Mit der Hilfe von diesen können Automobilhersteller die Entwicklungszeit und Kosten senken. Für Simulationsmodelle werden geeignete Eingabe-Parameter, wie z.B. Motordrehzahl und Drehmoment, benötigt. Im Falle von komplexen Hybrid-Fahrzeugen müssen zusätzliche Parameter in der Simulation berücksichtigt werden, da in diesen Fahrzeugen neben einen konventionellen Verbrennungsmotor auch ein oder mehrere Elektromotoren und ein Akkumulator eingebaut sind. Dadurch werden Steuergeräte wie etwa das elektronische Stabilitätsprogramm (ESP) oder das Anti-Blockier-System (ABS) komplexer und benötigen zusätzliche Parameter. Um die Regelqualität dieser Steuergeräte zu verbessern müssen genauere und fahrzeugspezifischere Parameter verwendet werden.

Automobilhersteller und Zulieferer arbeiten eng miteinander zusammen um Fahrzeuge ständig zu verbessern und zu optimieren. Jedoch werden die benötigten Fahrzeug-Parameter aus Geheimhaltungsgründen selten weitergegeben. Global tätige Zulieferfirmen verwenden Prüfstände um bestimmte Parameter, wie Feder-Dämpfer-Charakteristiken, Luft- und Rollenwiderstände oder Trägheiten herauszufinden. Unternehmen sowie Forschungsinstitute besitzen meist solche Prüfstände nicht, deshalb müssen andere innovative Methoden zur Parameteridentifizierung entwickelt werden.

Diese Masterarbeit beschäftigt sich mit der Entwicklung einer Methodik, wie Fahrzeug-Parameter im realen Straßenverkehr identifiziert werden können. Das Ziel ist es die Kosten und Arbeitszeit anderer Methoden, wie die Identifizierung mittels Prüfstände, erheblich zu senken. Ein weiterer Vorteil ist, dass Automobilhersteller nicht die Parameter weiter geben müssen.

Für diesen Zweck wurde ein Plug-in Hybrid zur Verfügung gestellt. Erst wurde ein geeigneter Messplan mit Fahrmanövern und Messstrecken entwickelt und beschrieben. Sobald das Fahrmanöver nicht die entsprechende Qualität erfüllte, musste die Durchführung des Manövers oder die Teststrecke angepasst werden. Manche Fahrmanöver lieferten nicht das gewünschte Ergebnis. Deshalb wurden dann andere Manöver herangezogen obwohl diese als erst nicht zweckmäßig erschienen. Zusammengefasst kann festgestgehalten werden, dass die durchgeführten Testmanöver zur Parameter-Identifizierung zielgerechte Resultate lieferten.

Contents

Acknowledgement i

Statutory Declaration iii

Abstract v

Kurzfassung vii

Contents xi

Abbreviations xiii

Symbols xv

1. Introduction 1
- 1.1. Motivation and Objective 1
- 1.2. Introduction to Hybrid Electric Vehicles 2
  - 1.2.1. Series Hybrid Electric Vehicle 2
  - 1.2.2. Parallel Hybrid Electric Vehicle 2
  - 1.2.3. Power-split Hybrid Electric Vehicle 4
- 1.3. Test Vehicle 4

2. Fundamentals and Methods 7
- 2.1. Coordinate System 7
- 2.2. Longitudinal Vehicle Dynamics 8
- 2.3. Driving Resistance Forces 12
- 2.4. Least square method 13

3. Driving Manoeuvres 15
- 3.1. Assumptions 15
- 3.2. Full Load Manoeuvre 0-100 km/h 15
- 3.3. Full Load Variations 16
- 3.4. Heavy Braking 17
- 3.5. Constant Accelerator Pedal Position 17
- 3.6. Constant Velocity 18
- 3.7. Drive Away 18
- 3.8. Brake Release 18

3.9. Coast Down Manoeuvre . . . 20
3.10. Load Variation . . . 20
3.11. Emergency Braking . . . 21
3.12. Speed Bump Crossing . . . 22
3.13. Real Driving Cycle . . . 22
3.14. Charging Measurement . . . 22
3.15. Misuse Manoeuvres . . . 24
3.16. Tip-in . . . 24
3.17. Tip-out . . . 24
3.18. Constant Braking . . . 25

4. Parameter Identification **27**
4.1. Measurement Equipment and Measurement . . . 27
4.2. Data Acquisition . . . 27
4.3. Dynamic Tyre Radius . . . 30
4.4. Centre of Gravity . . . 33
  4.4.1. Centre of Gravity – x-Position . . . 33
  4.4.2. Centre of Gravity – y-Position . . . 34
  4.4.3. Centre of Gravity – z-Position . . . 35
4.5. Spring - Damper Characteristics . . . 37
  4.5.1. Spring Characteristic Estimation . . . 37
  4.5.2. Damper Characteristic Estimation . . . 40
  4.5.3. Spring Damper Model . . . 41
4.6. Battery Characteristics . . . 46
  4.6.1. Discharge Current and Power . . . 47
  4.6.2. Charging Current and Power . . . 47
4.7. Evaluation of the Traction Motor . . . 49
4.8. Evaluation of the Generator . . . 53
4.9. Driving Resistance . . . 57
4.10. Operation Strategy . . . 60
  4.10.1. Evaluation of the Operation Strategy on the Test Bench . . . 64
  4.10.2. Evaluation of the Operation Strategy in Real Driving Condition Manoeuvres . . . 64
4.11. Braking / Recuperation Strategy . . . 66
4.12. Drivetrain Inertia . . . 69
4.13. Brake Release Torque, End Velocity and Time . . . 70
4.14. Drag Torque . . . 73

5. Summary and Conclusion **79**

List of Figures **I**

List of Tables **V**

Bibliography **VII**

A. Appendix **IX**

Abbreviations

ABS	Anti-lock brake system
AC	Air condition
APP	Accelerator pedal position
ASM	Asynchronous motor
BAT	Battery
CoG	Centre of gravity
EM	Electric motor
ESC	Electronic stability control
EPA	Environment Protection Agency
GPS	Global positioning system
HEV	Hybrid electric vehicle
ICE	Internal combustion engine
OEM	Original equipment manufacturers
OPM	Operation mode
PCU	Power control unit
PHEV	Plug-in electric hybrid vehicle
SoC	State of charge
SM	Synchronous motor
WS	Window size

Symbols

Coordinate systems

O_0	Origin of global coordinate system
x_0	x-Coordinate of the global coordinate system
y_0	y-Coordinate of the global coordinate system
z_0	z-Coordinate of the global coordinate system
GoG	Centre of gravity and origin of the vehicle fixed levelled coordinate system
x_H	x-Coordinate of the vehicle fixed coordinate system
y_H	y-Coordinate of the vehicle fixed coordinate system
z_H	z-Coordinate of the vehicle fixed coordinate system

Parameters and constants

g	Gravitational acceleration

Variables Latin Symbols

a	Acceleration of the vehicle ($\dot{v}$)
a_{BR}	Acceleration of brake release manoeuvres
$\dot{a}$	Acceleration gradient of the vehicle ($\ddot{v}$)
$\dot{a}_{BR}$	Acceleration gradient of brake release manoeuvres
a_r	Rolling resistance coefficient
A_{Front}	Frontal area of the vehicle
APP	Accelerator pedal position
CoG	Centre of gravity of the vehicle
CoG_{Ch}	Centre of gravity of the Chassis
C_F	Centre of front tyre
C_R	Centre of rear tyre
c_d	Drag coefficient
c_F	Front spring coefficient
c_R	Rear spring coefficient
c_{Tyre}	Spring coefficient tyre

C_0	Coefficient which describes primarily the rolling resistance
C_1	Coefficient which describes primarily the linear part of the driving resistance
C_2	Coefficient which describes primarily the drag resistance
D	Damping factor
d_F	Damper coefficient of front suspension
d_R	Damper coefficient of rear suspension
dt_{Tmax}	Time interval of the generator to reach its maximum torque
dt_{end}	Time interval maximum torque of generator to ICE start
dt_{ICE}	Time interval from the start of the generator to ICE start
F_{Acc}	Acceleration resistance
F_{Drag}	Drag resistance
F_{Slope}	Slope resistance
F_{Roll}	Rolling resistance
F_{Res}	Overall driving resistance
$F_{L,F}$	Driving force at front tyre
$F_{L,R}$	Driving force at rear tyre
$F_{N,F}$	Normal force at front axle
$F_{N,R}$	Normal force at rear axle
F_0	Curb weight force
$F_{z,def}$	Deflection force in z direction
F_W	Weight force of additional weight
$\Delta F_{z,F}$	Contact force difference at front axle
$\Delta F_{z,R}$	Contact force difference at rear axle
$F_{x,F}$	Reaction force between the front axle and the chassis
$F_{x,R}$	Reaction force between the rear axle and the chassis
$F_{z,F}$	Contact force of front axle
$F_{z,R}$	Contact force of rear axle
G_{Ch}	Vehicle chassis weight $m_{Ch} \cdot \mathrm{g}$
h_{CoG}	CoG height
h_{Ch}	CoG height from chassis
i_G	Gear ratio
i_{FD}	Ration of the final drive
J	Cost functional
l_F	Length from front axle to the CoG
l_R	Length from rear axle to the CoG
$l_{Wheelbase}$	Length from front axle to rear axle
$l_{Track,F}$	Front track width
$l_{Track,R}$	Rear track width
$l_{y,Right}$	Distance from right side to centre of gravity
$l_{y,Left}$	Distance from left side to centre of gravity
Δl	Length difference
m_{Ch}	Chassis mass

$m_{Ch,F}$	Chassis mass front
$m_{Ch,R}$	Chassis mass rear
m_F	Front tyre mass
m_R	Rear tyre mass
m	Total vehicle mass
$m_{Right,R}$	Vehicle mass measured at the right side rear tyre of the vehicle
$m_{Left,R}$	Vehicle mass measured at the left side rear tyre of the vehicle
$m_{Right,F}$	Vehicle mass measured at the right side front tyre of the vehicle
$m_{Left,F}$	Vehicle mass measured at the left side front tyre of the vehicle
M_P	Instantaneous centre of rotation
r_{dyn}	Dynamic tyre radius
r	Tyre radius
s^*_F	Front tyre slip
s^*_R	Rear tyre slip
$s_{D,F}$	Drive slip of front tyre
$s_{D,R}$	Drive slip of rear tyre
$s_{B,F}$	Brake slip of front tyre
$s_{B,R}$	Brake slip of rear tyre
T_F	Traction/brake torque at front axle
T_R	Traction/brake torque at rear axle
$T_{Roll,F}$	Rolling resistance torque at front axle
$T_{Roll,R}$	Rolling resistance torque at rear axle
$T_{Traction}$	Traction torque
T_{Brake}	Braking torque
T_{Total}	Total braking torque
$T_{BR,max}$	Maximum torque from brake release manoeuvres
t	Time
t_{trc}	Reaction time from traction motor
$T_{Gen,min}$	Maximum torque of generator in generation operation
$T_{Gen,max}$	Maximum torque of generator in motor operation
U_{Stat}	Circumference of static tyre radius
v	Levelled velocity of the vehicle
$v_{BR,max}$	Maximum creeping velocity
$v_{BR,end}$	End velocity of brake release manoeuvres
W_F	Wheel contact area at front tyre
W_R	Wheel contact area at rear tyre
WS	Window Size
x	Measured point
x_{CoG}	Ratio between CoG height and wheelbase length
y	Filtered point
Δz_S	Static spring compression
Δz_F	Length difference front
Δz_R	Length difference rear

Variables Greek Symbols

ϕ	Roll angle
φ	Pitch angle
$\dot{\varphi}$	Angular velocity / pitch-rate
$\dot{\varphi}_{simulated}$	Simulated Pitch-rate
$\dot{\varphi}_{measured}$	Measured Pitch-rate
$\ddot{\varphi}$	Angular acceleration
$\Theta_{T,F}$	Tyre inertia of front tyre
$\Theta_{T,R}$	Tyre inertia of rear tyre
$\omega_{T,F}$	Angular velocity of the front tyre
$\omega_{T,R}$	Angular velocity of the rear tyre
α_{Slope}	Slope angle
Θ_G	Gear inertia
Θ_E	Engine inertia
Θ	Drivetrain inertia
Θ_{Ch}	Chassis inertia
γ	Angle of inclination
$\tau_{0\rightarrow 100}$	Acceleration time from 0 to 100 km/h
τ_{BR}	Time interval to reach the end velocity in brake release manoeuvres

Vectors

$\mathbf{z}$	Result value (least square method)
$\mathbf{e}$	Error vector (least square method)
$\mathbf{x}$	Unknown value (least square method)
$\hat{\mathbf{x}}$	Estimated value (least square method)

Matrices

$\mathbf{A}$	Transition matrix (least square method)

Indices

$(\cdot)_{Ch}$	Chassis
$(\cdot)_F$	Front
$(\cdot)_R$	Rear
$(\cdot)_0$	Initial
$(\cdot)_{mean}$	Mean value
$(\cdot)_{max}$	Maximum value
$(\cdot)_{min}$	Minimum value
$(\cdot)_{Left}$	Left side
$(\cdot)_{Right}$	Right side
$(\cdot)_{measured}$	Measured value
$(\cdot)_{simulated}$	Simulated value

1. Introduction

1.1. Motivation and Objective

Mobility is one of the basic needs of human kind, whereas the passenger car is the most popular transportation method [5]. During the years passenger cars developed from vehicles with only combustion engines to hybrid electric vehicle (HEV) with one or more different energy sources. In the year 2001 only two HEVs were on the European market. The number of HEVs has increased the last 10 years to over 30 different cars. The reasons for the drastic development of HEVs is on the one hand the increasing environmental awareness and on the other hand the scarcity of fossil fuel. [2]

Greenhouse gas emissions are the main reason for the climate change, especially CO_2 emissions. About 22 % of the CO_2 emissions in Europe is contributed by traffic. Therefore, the European Union limits CO_2 emissions from vehicles. Since 2015 only vehicles with a limit of 130 g/km CO_2 emissions are allowed. From the year 2020 a limit from 95 g/km is set. However, at the moment there is a tendency to more powerful and bigger vehicles. [2]

New technologies are needed to achieve the CO_2 emission limits with almost the same driving power. Hybrid electric vehicle technologies provide a good solution to those problems.

With a second energy source the degree of freedom increases, which enables an increase of energy efficiency. If the second drivetrain has a rechargeable energy storage (e.g., a battery) the braking energy can be stored and re-utilized. [2]

The advantages of HEVs are the energy efficiency and therefore the fuel consumption reduction. However, an increase of the degree of freedom increases the complexity of a vehicle. With a more complex car the requirements for the drivetrain as well as control units increase. In addition, the safety, driveability and durability should not suffer from those changes.

Automotive original equipment manufacturers (OEMs) are trying to reduce development time and costs from vehicles. This can be achieved through appropriate numeric simulations. One challenge with more complex vehicles is the increase of the required parameters.

Original equipment manufacturers and automotive suppliers are working together to improve and optimise the efficiency of passenger vehicles. However, automotive suppliers as well as OEMs cannot freely distribute parameters due to non-disclosure agreements. Global suppliers are using test benches to obtain those parameters. Some companies do not have the opportunity or resources to use a test bench. Therefore, a holistic method to identify vehicle parameters in real driving situations is developed in this thesis. One main advantage of the identification in real driving situations is the cost efficiency.

1.2. Introduction to Hybrid Electric Vehicles

The advantage of HEVs is that they have an electric storage (battery) and can easily reuse the braking energy through the electric motor. If the electric motor is used as the main propulsion system, the advantages are high efficiency and noise reduction.
The most common HEVs and their drivetrain layout are shown in Figure 1.1. On the top, the schematics of series HEVs are shown. In the middle section, topologies of parallel HEVs and on the bottom power-split HEVs are displayed.

HEVs can be categorized into:

- Series HEV
- Parallel HEV
- Power-split HEV

1.2.1. Series Hybrid Electric Vehicle

Series HEVs consist of an internal combustion engine (ICE), two electric motors (EMs), and a battery (BAT). The ICE is directly coupled to the first EM, this electric machine operates as a generator and charges solely the battery. The combination of the ICE and generator can be grouped as “charging unit” and in certain drivetrain layouts it is also called range extender. The vehicles propulsion is done by an additional electric motor which is powered by the battery. The ICE does not have a direct connection to the drive axle.
The advantage of this decoupling is that the ICE can operate in its optimal operation point and can thus reduce the fuel consumption. Since the traction motor exclusive drives the vehicle the dimensions have to be adapted to the desired performance. Due to the multiple energy conversions the overall efficiency can be disadvantageous.
In the top of Figure 1.1, different topologies of series HEVs are shown. The difference between these is the propulsion of the tyres. The single engine drives the tyres over a drive-shaft. The tandem or wheel hub-motor variants propel the tyres are separately.

1.2.2. Parallel Hybrid Electric Vehicle

In general, parallel HEVs have an ICE that is directly coupled to the propulsion shaft. In some topologies the ICE is also coupled to an electric motor. Ideally the EM can be disconnected from the ICE. Then the vehicle can be driven solely by the ICE, the electric motor or in combination. The overall driving power can be achieved through

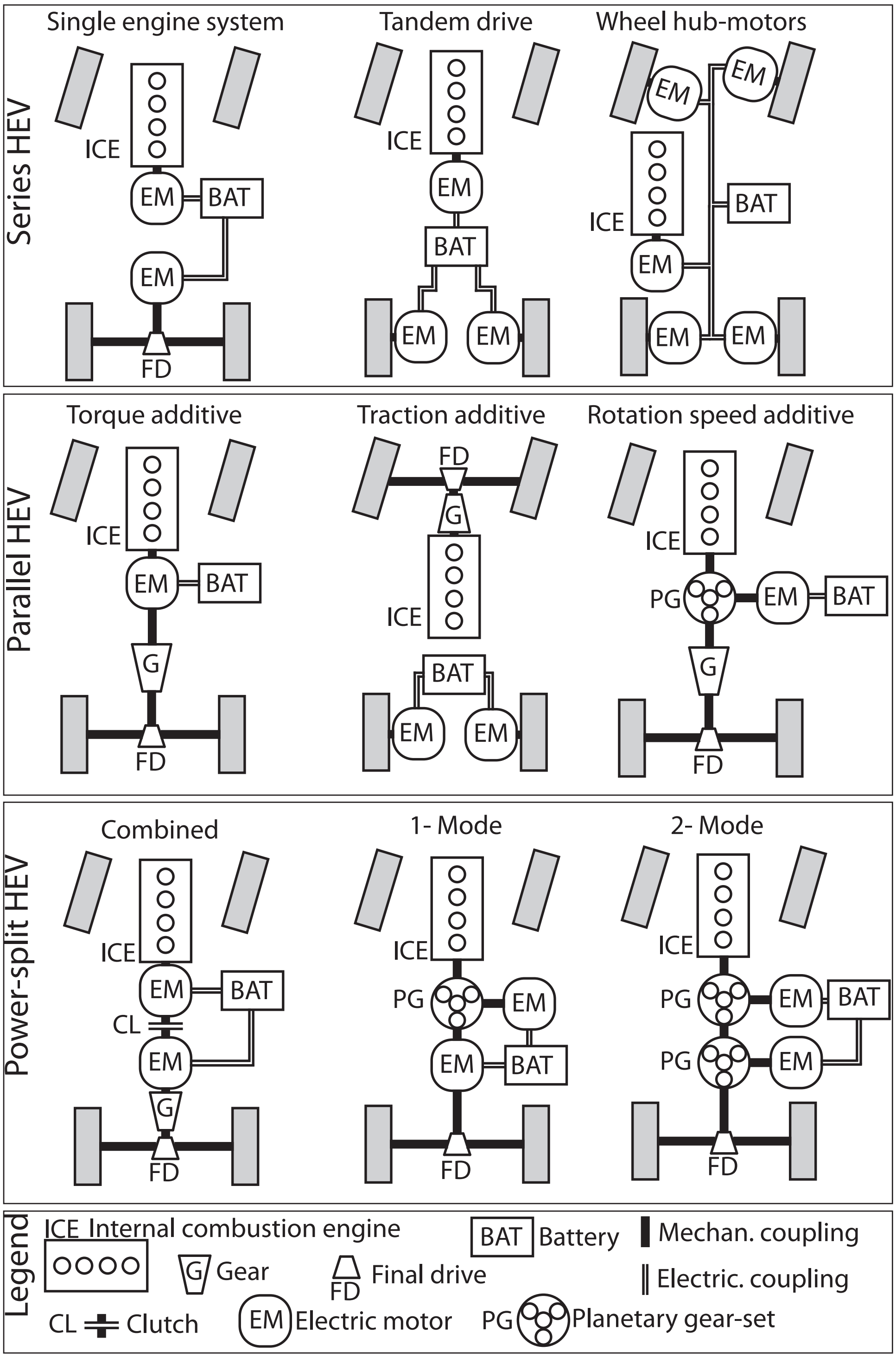
Series HEV
Single engine system
Tandem drive
Wheel hub-motors
Parallel HEV
Torque additive
Traction additive
Rotation speed additive
Power-split HEV
Combined
1- Mode
2- Mode
ICE
EM
BAT
FD
G
PG
CL
Legend
ICE Internal combustion engine
BAT Battery
Mechan. coupling
G Gear
FD Final drive
Electric. coupling
CL Clutch
EM Electric motor
PG Planetary gear-set

Figure 1.1.: Categorization of HEVs, adopted from [5].

addition of rotational speed, traction or torque. [5]

The advantage of parallel HEVs is that the electric motor supports the combustion engine. In all cases the EM can recuperate the braking energy, but the potential is reduced due to the drag of the ICE in certain parallel HEVs topologies. Disadvantageous is that the ICE does not operate in its optimal load point anymore. Furthermore, gears and clutches are needed.

In the middle of Figure 1.1 three topologies of parallel HEVs are shown. If the ICE powers another drive-shaft than the electric motor, the layout is called traction additive. Torque additive is achieved through direct coupling of the ICE and EM. The addition of rotational speed can be achieved with a planetary gear-set.

1.2.3. Power-split Hybrid Electric Vehicle

In power-split HEVs the mechanical power of the ICE is split into an electrical and a mechanical path. The electrical path is gained by a coupled generator. One way to establish the mechanical path is to connect the ICE directly to the drive shaft through a planetary gear-set. On the bottom of Figure 1.1, these topologies (1-2 Mode power-split HEV) are shown in more detail. The Toyota Prius has for example a power-split 1-Mode drivetrain layout.

Another way to establish the mechanical path is with a clutch (combined power-split HEV).

In both cases two electric motors are needed. The advantage of the power-split HEV is that it achieves all features of a HEV. Like, pure electric driving, boosting and optimal operation of the ICE as well as a tow start feature. However, the disadvantages are the increase of the weight, the costs and the complexity of the system due to two electric motors. [22]

1.3. Test Vehicle

The provided test vehicle was a combined power-split HEV. This HEV features an ICE, one generator, one electric motor, clutch as well as a battery.

With these components series and parallel operation can be achieved. Figure 1.2 shows the four of five different operation modes (OPMs). Pure electric drive (OPM 1) and series mode (OPM 5) constitute the series hybrid modi (clutch is disengaged). During pure electric drive the power for the traction motor is delivered by the battery. In series mode the ICE powers the generator which transfers its electric power over an intermediate circuit to the battery and traction motor.

The vehicle can recuperate the braking energy through the traction motor, this described in Figure 1.2 as recuperation mode (OPM 2).

The parallel hybrid mode (clutch is engaged) is described as engine mode (OPM 4). Engine mode is only operated when the vehicle's driving speed is over 100 km/h. Operation

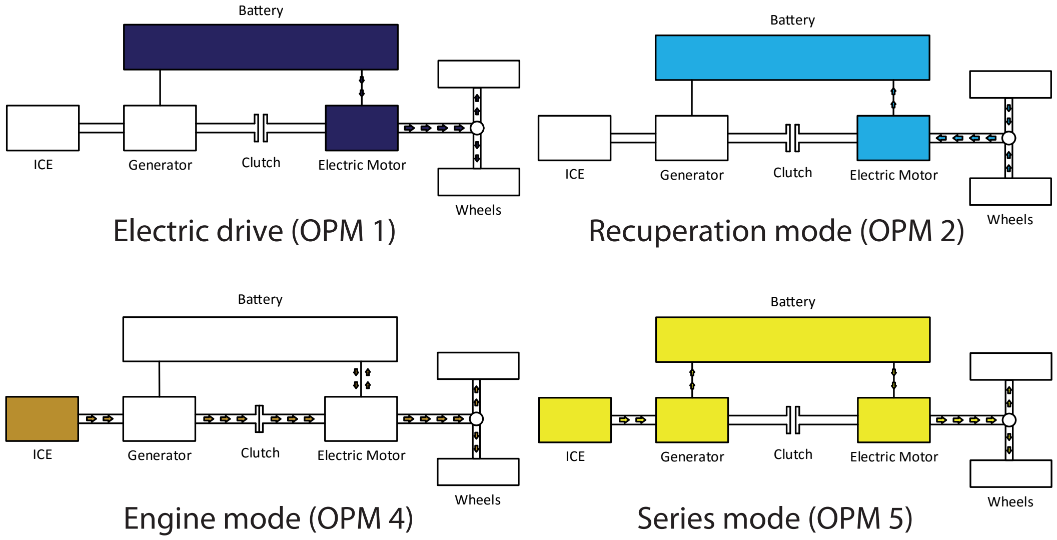
Battery
ICE
Generator
Clutch
Electric Motor
Wheels
Electric drive (OPM 1)
Battery
ICE
Generator
Clutch
Electric Motor
Wheels
Recuperation mode (OPM 2)
Battery
ICE
Generator
Clutch
Electric Motor
Wheels
Engine mode (OPM 4)
Battery
ICE
Generator
Clutch
Electric Motor
Wheels
Series mode (OPM 5)

Figure 1.2.: The four different operation modes of the testing vehicle.

mode 4 is also called load point shifting. This enables the ICE to operate in its optimal load point. The excess power of the ICE is transferred with the help of the generator to the battery. Likewise the vehicle can need more energy than the ICE produces and the remaining energy is achieved through the traction motor. However, during the driving manoeuvres with a vehicle speed of above 100 km/h it was evaluated that the battery SoC is often below 30 %. The acceleration process discharges the battery to a low SoC and therefore the ICE cannot operate in its optimal load point.

Nonetheless, it could be assumed that if the state of charge (SoC) of the battery is high, the electric motor could provide the drivetrain with more power. It is also possible to charge the battery during idling (OPM 3). This thesis did not investigate the charging process in more detail, because it was not in the extant of this thesis. Thus no information of this operation mode is provided. In this thesis, the electric motor that is directly coupled to the ICE is often called as “generator”. The electric motor that is coupled to the drive shaft is often mentioned as “traction” motor.

2. Fundamentals and Methods

This chapter should give an overview of the fundamentals and used methods regarding automotive engineering. It introduces coordinate systems, vehicle dynamics and the resistance forces.

2.1. Coordinate System

In order to describe all movements and forces of a vehicle, a normed coordinate system should be used [4]. There are several orthogonal coordinate systems:

- Inertial system
- Vehicle reference system
- Nominal design position - coordinate system

Inertial system:
Is a “global” coordinate system with its origin fixed on the earth.

Vehicle reference system:
Is a “local” coordinate system with its origin the centre of gravity or in the centre of the vehicle.

Nominal design position - coordinate system:
The nominal design position coordinate system helps to describe the motion of a single object (e.g., tyre or motor). Origin of the coordinate system is then located in the specific object.

In this thesis a vehicle fixed levelled orthogonal coordinate system is used, based on the ISO 70000 standard. The origin of this coordinate system is in the centre of gravity (CoG) and is shown in Figure 2.1.

The six degrees of freedom:

In the three motion dircections:

- in x-direction: Driving
- in y-direction: Lateral movement
- in z-direction: Lifting

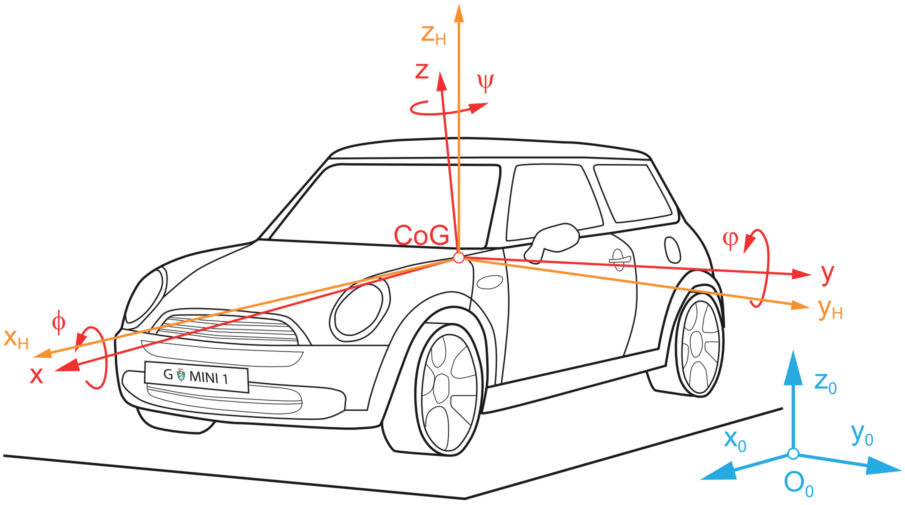

Figure 2.1.: Used coordinate system based on ISO 70000, adopted from [4].

In three rotations:

- Rotation about x-axis: Roll angle ϕ
- Rotation about y-axis: Pitch angle φ
- Rotation about z-axis: Yaw angle ψ

2.2. Longitudinal Vehicle Dynamics

The following text, figures and equations are based on [4].

The equations of motion will be described through Figure 2.2. The indices F is for front and R for rear. The tyre radius for the front and rear tyres are the same and correspond to the dynamic tyre radius ($r_F = r_R = r_{dyn}$)

CoG	Centre of gravity of the vehicle
CoG_{Ch}	Centre of gravity of the chassis
h_{CoG}	CoG height
h_{Ch}	CoG height from chassis
G_{Ch}	Vehicle chassis weight $m_{Ch} \cdot \mathrm{g}$
$F_{x,F,R}$	Reaction force between the front/rear axle and the chassis
$F_{z,F,R}$	Contact force of front/rear axle
$C_{F,R}$	Centre of tyre of front/rear tyre
$l_{F,R}$	Length from front/rear axle to the CoG
a_r	Rolling resistance coefficient
$T_{F,R}$	Traction/brake torque at front/rear axle
$T_{Roll,F,R}$	Rolling resistance torque at front/rear axle
$W_{F,R}$	Wheel contact area at front/rear tyre

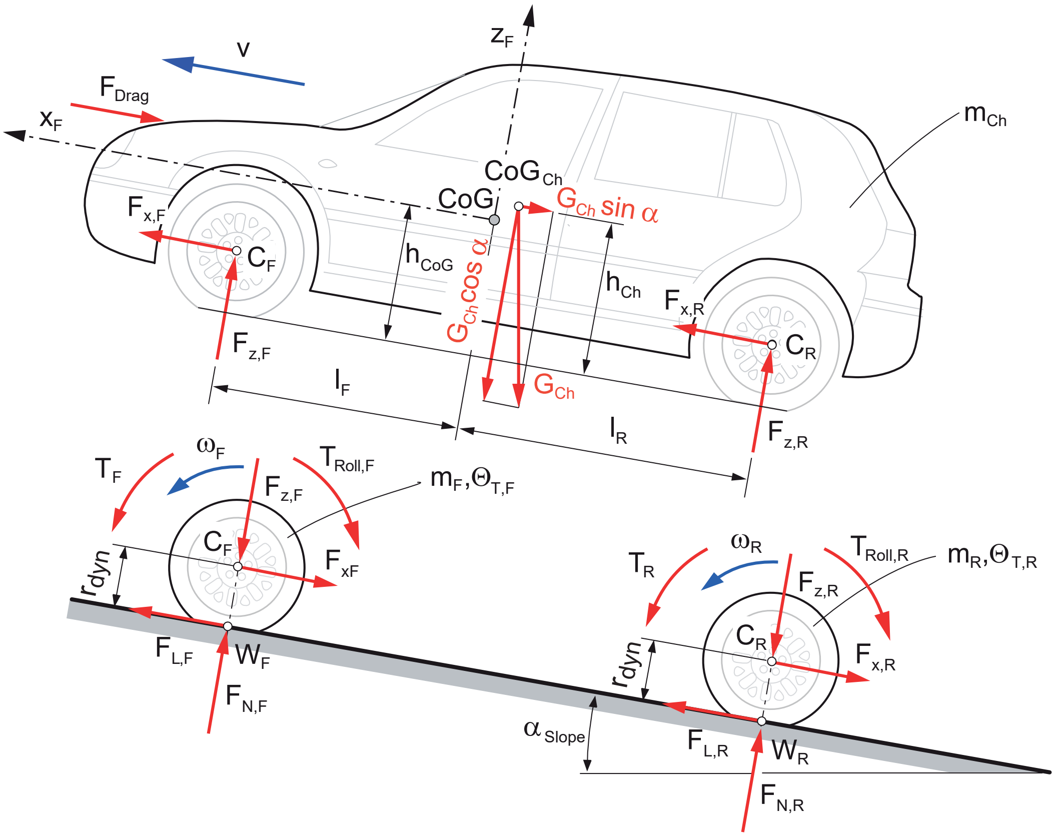
v
F_{Drag}
x_F
z_F
m_{Ch}
CoG_{Ch}
CoG
$G_{Ch} \sin \alpha$
$F_{x,F}$
C_F
h_{CoG}
$G_{Ch} \cos \alpha$
h_{Ch}
$F_{x,R}$
C_R
$F_{z,F}$
G_{Ch}
l_F
l_R
$F_{z,R}$
ω_F
T_F
$T_{Roll,F}$
$m_F,\Theta_{T,F}$
$F_{z,F}$
C_F
F_{xF}
r_{dyn}
$F_{L,F}$
W_F
$F_{N,F}$
ω_R
T_R
$T_{Roll,R}$
$m_R,\Theta_{T,R}$
$F_{z,R}$
C_R
$F_{x,R}$
r_{dyn}
α_{Slope}
$F_{L,R}$
W_R
$F_{N,R}$

Figure 2.2.: Vehicle body, axis, road and it all active forces, adopted from [4]

$F_{L,F,R}$	Driving force at front/rear tyres
$F_{N,F,R}$	Normal force at front/rear axle
m_{Ch}	Chassis mass
$m_{F,R}$	Front/rear tyre mass
m	Total vehicle mass
$\Theta_{T,F,R}$	Tyre inertia at front/rear tyres
$\omega_{T,F,R}$	Angular velocity of the front/rear tyres
v	Levelled velocity of the vehicle
a	Acceleration of the vehicle ($\dot{v}$)
r_{dyn}	Dynamic tyre radius
F_{Drag}	Drag force
α_{Slope}	Slope angle

$T_{F,R} > 0$: Traction torque
$T_{F,R} = 0$: Free ride
$T_{F,R} < 0$: Brake torque

Vehicle body:

$$F_x : \quad m_{Ch} \cdot a = F_{x,F} + F_{x,R} - F_{Drag} - F_{Slope} \tag{2.1}$$

$$F_z : \quad 0 = -m_{Ch} \cdot \mathrm{g} \cdot \cos\left(\alpha_{Slope}\right) + F_{z,F} + F_{z,R} \tag{2.2}$$

$$T_y : \quad 0 = -T_F - T_R - (h_{Ch} - r_{dyn}) \cdot (F_{x,F} + F_{x,R}) - l_{Ch,F} \cdot F_{z,F} + l_{Ch,R} \cdot F_{z,R} \tag{2.3}$$

Axis:
Following equations apply to front and rear axis

$$F_x : \quad m_{F,R} \cdot a = F_{L,F,R} - F_{x,F,R} \tag{2.4}$$

$$F_z : \quad 0 = -m_{F,R} \cdot \mathrm{g} \cdot \cos\left(\alpha_{Slope}\right) - F_{z,F,R} + F_{N,F,R} \tag{2.5}$$

$$T_y : \quad \Theta_{T,F,R} \cdot \dot{\omega}_{F,R} = -T_{F,R} - r_{dyn} \cdot F_{L,F,R} - T_{Roll,F,R} \tag{2.6}$$

By summation of Equations (2.1), (2.4) and (2.6), three differential equations are achieved which describe the complete longitudinal motion of a vehicle.

$$(m_{Ch} + m_F + m_R) \cdot a = F_{L,F} + F_{L,R} - F_{Drag} - F_{Slope} \tag{2.7}$$

$$\Theta_{T,F} \cdot \dot{\omega}_F = r_{dyn} \cdot F_{L,F} - T_{Roll,F} \tag{2.8}$$

$$\Theta_{T,R} \cdot \dot{\omega}_R = r_{dyn} \cdot F_{L,R} - T_{Roll,R} \tag{2.9}$$

The tyre slip is introduced as:

$$s^*_{F,R} = \begin{cases} \frac{1}{1-s_D} & \text{for traction slip} \\ 1 & \text{for free rolling wheel} \\ 1 + s_B & \text{for brake slip} \end{cases} \tag{2.10}$$

With the particular drive slip s_D, given for the front tyre:

$$s_{D,F} = \frac{\omega_{T,F} \cdot r_{dyn} - v}{r_{dyn} \cdot |\omega_{T,F}|} \tag{2.11}$$

and braking slip s_B:

$$s_{B,F} = \frac{\omega_{T,F} \cdot r_{dyn} - v}{|v|} \tag{2.12}$$

The slip is applied to Eq. (2.4) and (2.6).

$$\left(m_{F,R} + s^*_{F,R} \cdot \frac{\Theta_{F,R}}{r^2_{dyn}} \right) \cdot a = -F_{x,F,R} + \frac{T_{F,R}}{r_{dyn}} - \frac{T_{Roll,F,R}}{r_{dyn}} \tag{2.13}$$

if the Eq. (2.1) is also added:

$$\begin{aligned} &\left(m_{Ch} + m_F + m_R + s^*_F \cdot \frac{\Theta_F}{r^2_{dyn}} + s^*_R \cdot \frac{\Theta_R}{r^2_{dyn}} \right) \cdot a = \\ &\qquad \frac{T_F + T_R}{r_{dyn}} - \frac{T_{Roll,F} + T_{Roll,R}}{r_{dyn}} - F_{Drag} - F_{Slope} \end{aligned} \tag{2.14}$$

The inertias from the axis $\Theta_{F,R}$ include also parts of the drivetrain (inertia from the shafts, traction motor and gearbox). If the slip from the wheels are neglected Eq. (2.14) is reduced to:

$$\begin{aligned} &\left(m_{Ch} + m_F + m_R + \frac{\Theta_F}{r^2_{dyn}} + \frac{\Theta_R}{r^2_{dyn}} \right) \cdot a = \\ &\qquad \frac{T_F + T_R}{r_{dyn}} - \frac{T_{Roll,F} + T_{Roll,R}}{r_{dyn}} - F_{Drag} - F_{Slope} \end{aligned} \tag{2.15}$$

In case of a front driven vehicle the inertia from the front Θ_F includes the ratios from the gear i_G, from the final drive i_{FD}, the engine inertia Θ_E and the inertia of the front tyre $\Theta_{T,F}$, see Figure 2.3. $\Theta_{T,R}$ is the inertia of the rear tyre.

$$\Theta_F = \Theta_{T,F} + i^2_{FD} \left(\Theta_G + i^2_G \cdot \Theta_E \right) \tag{2.16}$$

$$\Theta_R = \Theta_{T,R}$$

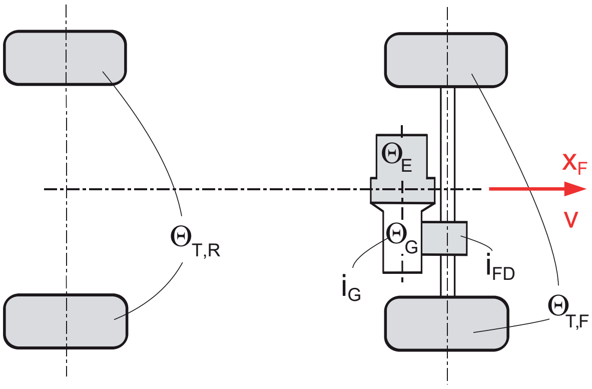

Figure 2.3.: Vehicle with front powered drivetrain and gearbox.

Eq. 2.15 can be again simplified by:

- The vehicle mass can be summarized: $m = (m_{Ch} + m_F + m_R)$
- The rolling torque can be rewritten to: $F_{Roll} = (T_{Roll,F} + T_{Roll,R}) / r_{dyn}$
- Inertias from front and rear can be summarized: $\Theta = \Theta_F + \Theta_R$

$$\left(1 + \frac{\Theta}{m \cdot r_{dyn}^2}\right) m \cdot a = -\left(F_{Drag} + F_{Slope} + F_{Slope}\right) + \frac{T_F + T_R}{r_{dyn}} \tag{2.17}$$

If the inertia is also neglected Eq. (2.17) is reduced to:

$$m \cdot a = -\left(F_{Drag} + F_{Slope} + F_{Slope}\right) + \frac{T_F + T_R}{r_{dyn}} \tag{2.18}$$

When T_F and T_R are combined and substituted with the traction and brake torque of the vehicle Eq. (2.18) is reformulated by:

$$m \cdot a = -\left(F_{Drag} + F_{Slope} + F_{Slope}\right) + \frac{T_{Traction}}{r_{dyn}} + \frac{T_{Brake}}{r_{dyn}} \tag{2.19}$$

2.3. Driving Resistance Forces

Acceleration resistance:

$$F_{Acc} = m \cdot a \tag{2.20}$$

m	Vehicle mass in kg
a	Acceleration in $\mathrm{m/s^2}$

Drag resistance:

$$F_{Drag} = \frac{1}{2} \cdot \rho \cdot c_d \cdot v^2 \cdot A_{Front} \tag{2.21}$$

F_{Drag}	Drag resistance in N
ρ	Air density in kg/m^3
c_d	Drag coefficient
v	Velocity in m/s
A_{Front}	Vehicle front area in m^3

Slope resistance:

$$F_{Slope} = m \cdot \mathrm{g} \cdot \sin(\alpha_{Slope}) \tag{2.22}$$

F_{Slope}	Slope resistance in N
g	Gravitational acceleration in m/s^2
α_{Slope}	Slope angle in rad

Rolling resistance:

$$F_{Roll} = m \cdot \mathrm{g} \cdot a_r \cdot \cos(\alpha_{Slope}) \tag{2.23}$$

F_{Roll}	Rolling resistance in N
a_r	Rolling resistance coefficient

2.4. Least square method

The least square method is a good approach to determine an overdetermined system[1]. With this approach a precise solution cannot be achieved, but an estimated value. The error of this estimated value is as small as possible in terms of least squares.

The following equations are based on [21].

General solution:
Overdetermined system:
System has k equations and n unknowns, whereas $k > r$:

$$\mathbf{z} = \mathbf{A}\mathbf{x} \tag{2.24}$$

$\mathbf{x}$...Unknown value

---

[1] A overdetermined system is a system that has more equations k than unknowns n

Since, no exact solution can be determined, an estimated value ($\hat{\mathbf{x}}$) can be given that the error vector ($\mathbf{e}$) is as small as possible:

$$\mathbf{e} = (\mathbf{z} - \mathbf{A}\hat{\mathbf{x}}) = \begin{bmatrix} e_1 \\ e_2 \\ \vdots \\ e_m \end{bmatrix} \tag{2.25}$$

The cost functional for the least square method is:

$$J = e_1^2 + e_2^2 + \cdots + e_m^2 \tag{2.26}$$

$$J(\hat{\mathbf{x}}) = \mathbf{e}^T\mathbf{e} = (\mathbf{z} - \mathbf{A}\hat{\mathbf{x}})^T (\mathbf{z} - \mathbf{A}\hat{\mathbf{x}}) \tag{2.27}$$

The cost functional has to be a minimum, therefore:

$$\frac{\partial J(\hat{\mathbf{x}})}{\partial \hat{\mathbf{x}}} := \begin{bmatrix} \frac{\partial J}{\partial \hat{x}_1} & \frac{\partial J}{\partial \hat{x}_2} & \cdots & \frac{\partial J}{\partial \hat{x}_n} \end{bmatrix} = \mathbf{0}^T \tag{2.28}$$

By reshaping the cost functional comply to:

$$J(\hat{\mathbf{x}}) = \mathbf{e}^T\mathbf{e} = \mathbf{z}^T\mathbf{z} - 2\mathbf{z}^T\mathbf{A}\hat{\mathbf{x}} + \hat{\mathbf{x}}^T\mathbf{A}^T\mathbf{A}\hat{\mathbf{x}} \tag{2.29}$$

Following the gradient of the cost functional to:

$$\frac{\partial J(\hat{\mathbf{x}})}{\partial \hat{\mathbf{x}}} = -2\mathbf{z}^T\mathbf{A} + \hat{\mathbf{x}}^T \left(\mathbf{A}^T\mathbf{A} + \left(\mathbf{A}^T\mathbf{A}\right)^T\right) = \mathbf{0}^T \tag{2.30}$$

For the optimal estimate value:

$$-2\mathbf{z}^T\mathbf{A} + 2\hat{\mathbf{x}}^T\mathbf{A}^T\mathbf{A} = \mathbf{0}^T \tag{2.31}$$

$$\hat{\mathbf{x}} = \left(\mathbf{A}^T\mathbf{A}\right)^{-1}\mathbf{A}^T\mathbf{z} \tag{2.32}$$

It has to be noted that A has to invertible. The expression $\left(\mathbf{A}^T\mathbf{A}\right)^{-1}\mathbf{A}^T$ can be achieved in MATLAB with the function `pinv(A)` and is known as pseudoinverse. Whereas, MATLAB has an implemented least square method function: `x=lsqlin(A,z,[],[])`.

3. Driving Manoeuvres

3.1. Assumptions

- The vehicle is symmetric over the x-axis
- Left and right wheel have the same characteristic
- Left and right suspension have the same characteristic
- Manoeuvres are performed with closed windows
- Manoeuvres are performed with almost the same weight
- Manoeuvres are performed at dry streets
- Tank should be at least half-full
- SoC $> 27\,\%$[1]

3.2. Full Load Manoeuvre 0-100 km/h

Manoeuvre description

Initially, the vehicle has to stand entirely still. After an immediate brake release the accelerator pedal is fully pressed (APP = 100 %). This manoeuvre ends, when a vehicle speed of 100 km/h is reached. An example is given in figure 3.1.

Identifiable parameters

- Acceleration gradient
- Duration from standstill to 100 km/h
- Response time of the traction motor
- Min/max battery currents of the battery
- Drivetrain inertia
- ICE start up behaviour

---

[1] This value was evaluated through the test manoeuvres. Above 27 % the operation strategy does not change significantly

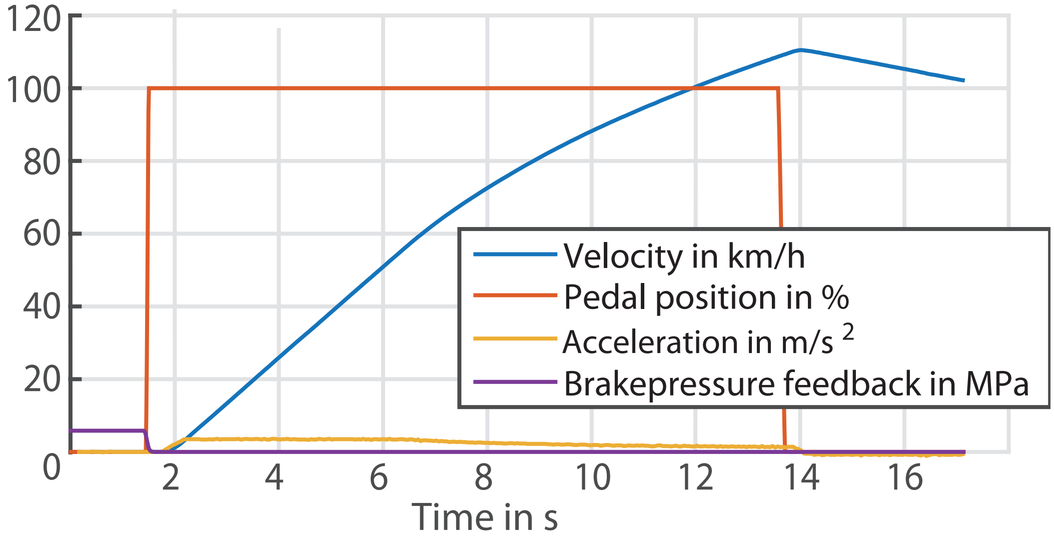

Figure 3.1.: Example of a full load manoeuvre.

Table 3.1.: Full load variation examples.

Start speed in km/h	End speed in km/h
60	100
80	120
40	140
40	70

3.3. Full Load Variations

Manoeuvre description

The vehicle accelerates to a predefined starting speed. After the starting velocity is maintained for a few seconds, the vehicle accelerates again with full throttle until the defined end speed is reached. In Table 3.1 examples for these variation are given.
The identifiable parameters are similar to those stated in 3.2. However, the starting velocities are different and hence the vehicle responses to different speed levels can be evaluated.

Identifiable parameters

- Acceleration gradient

- Duration from starting speed to end speed
- Response time of the traction motor
- Min/max battery currents
- Drivetrain inertia
- ICE start up behaviour

3.4. Heavy Braking

Manoeuvre description

The vehicle drives downhill and the brake pedal is pressed in such a way that the expected recuperation is a maximum. The provided test vehicle has an indicator installed into the control penal. The heavy braking manoeuvre should be done with different starting velocities.

Identifiable parameters

- Maximum recuperation current or min. battery current, respectively
- Maximum recuperation torque or min. traction motor torque, respectively
- Braking strategy

3.5. Constant Accelerator Pedal Position

Manoeuvre description

The vehicle drives with almost constant accelerator pedal position and varying loads. The loads can be changed by driving uphill and adding additional weight.

Identifiable parameters

- Operation mode
- Pedal map
- Operation strategy (quasi-static)

3.6. Constant Velocity

Manoeuvre description

In these manoeuvres the vehicle drives with almost constant velocity and varying loads. The loads can be changed with additional weight and/or driving up- or downhill.

Identifiable parameters

- Operation mode
- Pedal map
- Operation strategy (quasi-static)

3.7. Drive Away

Manoeuvre description

The vehicle has to stand still. While holding the brake pedal the desired accelerator pedal position is adjusted. After releasing the brake pedal the accelerator pedal position should not change. The vehicle accelerates to a constant vehicle velocity. This procedure is done with different accelerator pedal positions of 15 %, 30 %, 40 % and 50 %.

Identifiable parameters

- Acceleration gradient
- Duration till constant velocity is achieved
- Response time of traction motor

3.8. Brake Release

Manoeuvre description

The vehicle has to stand still on a even street. Release the brake and let the vehicle accelerate without using the accelerator pedal till the vehicle reaches a constant speed.

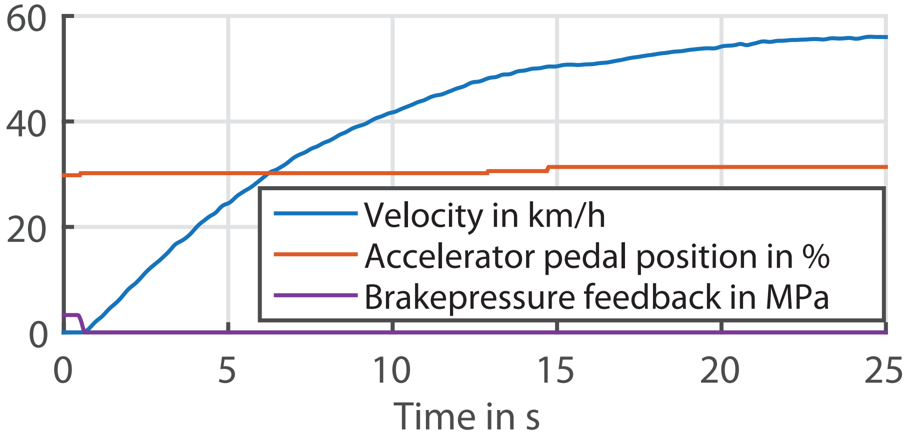

Figure 3.2.: Example of a drive away manoeuvre.

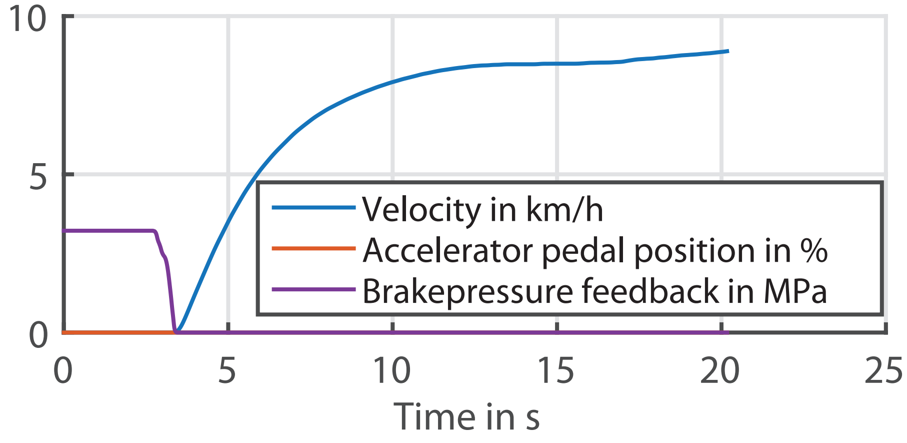

Figure 3.3.: Example of a brake release manoeuvre.

Identifiable parameters

- Acceleration gradient
- Duration to reach end velocity
- Vehicle end velocity

3.9. Coast Down Manoeuvre

Manoeuvre description

The vehicle accelerates to 135 km/h subsequently the drivetrain is disengaged by shifting the gear lever in the neutral position. To calculate the driving resistances, the velocity is measured from 125 km/h to 15 km/h with a sample rate of 1 Hz. The ideal test road should be even and no wind gusts should occur.

In real driving situations such a test road is nearly impossible to find, therefore the manoeuvres are performed in pairs. One manoeuvre in one direction and the other one in the exact opposite direction.

At least four pairs of these coast down manoeuvres should be performed. Before these manoeuvres the vehicle and tyres have to warm up. This manoeuvre is based on [10].

Additional coast down manoeuvres are performed with D(rive)- and B(rake)- lever position. Coast down manoeuvres are also performed with different starting velocities.

Identifiable parameters

- Inertias from drive train
- Rolling resistance
- Drag coefficient
- Recuperation torque in D/B lever position
- Recuperation current in D/B lever position
- Vehicle behaviour

3.10. Load Variation

Manoeuvre description

The vehicle accelerates to a predefined velocity and maintains there for a few seconds to ensure constant vehicle performance. Afterwards the vehicle accelerates with 100 % accelerator pedal position to a given inter-speed. When this inter-speed is reached, the accelerator pedal is released (without additional braking) and the vehicle decelerates to the terminal speed.

Another variant is that the vehicle accelerates to the starting velocity and hold for few seconds and then the accelerator pedal is released till the inter-speed is achieved. After reaching the inter-velocity the vehicle should accelerate with 100 % pedal position till the end speed is reached. In Table 3.2 examples are given table for the load variation manoeuvres. Figure 3.4 shows a load variation with an starting velocity of 70 km/h and an inter-speed of 50 km/h and an end velocity with 70 km/h.

Table 3.2.: Load variation examples.

Start speed in km/h	Inter-speed in km/h	End speed in km/h
30	50	30
70	50	70

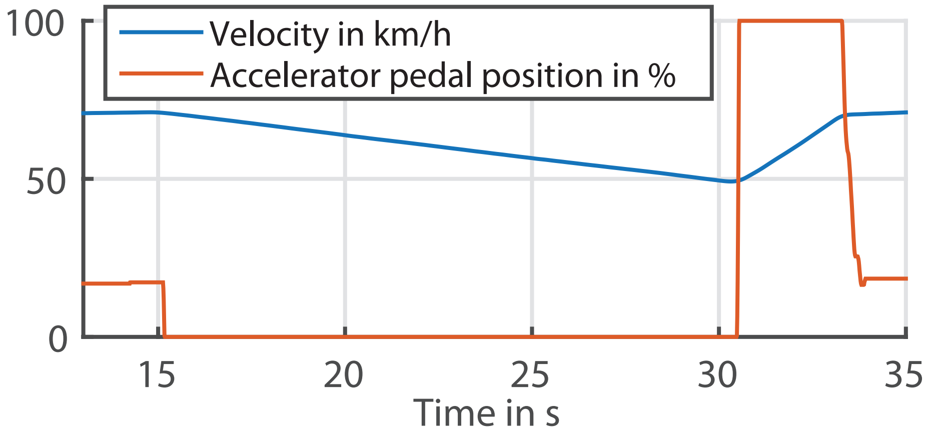

Figure 3.4.: Load variation manoeuvre example.

Identifiable parameters

- Vehicle response behaviour
- Acceleration gradient
- Drag coefficient
- Recuperation torque
- Braking strategy

3.11. Emergency Braking

Manoeuvre description

This manoeuvre is performed in a blocked zone. The vehicle accelerates to a constant velocity of 50 km/h and an emergency brake is initiated.

Identifiable parameters

- Inertia from vehicle chassis around the pitch axis
- Braking strategy

3.12. Speed Bump Crossing

Manoeuvre description

This manoeuvre is used for the spring / damper characteristic determination. For this reason the vehicle passes over a known speed bump with 10 km/h, 20 km/h and 30 km/h.

Identifiable parameters

- Spring characteristic
- Damper characteristic

3.13. Real Driving Cycle

Manoeuvre description

On a predefined test circuit several rounds are performed with different battery states of charge. The velocity profile as well as the route characteristic are recorded. The cycle profile is shown in Figures 3.5 and 3.6.

Identifiable parameters

- Fuel consumption
- Real vehicle behaviour
- Braking strategy
- Generator performance

3.14. Charging Measurement

Manoeuvre description

Start the energy measurement equipment and plug in the charging cable to charge the vehicle.

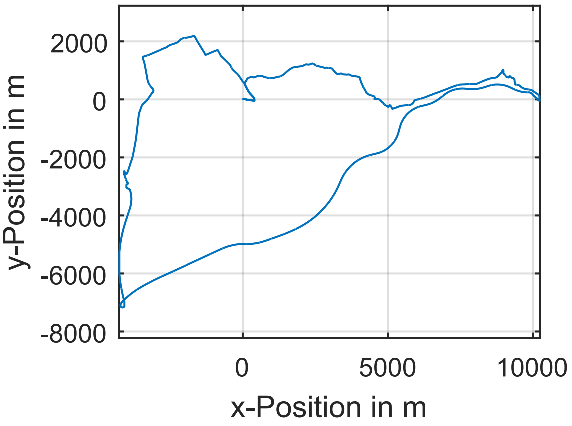

Figure 3.5.: Relative x- and y- Position of the real driving cycle.

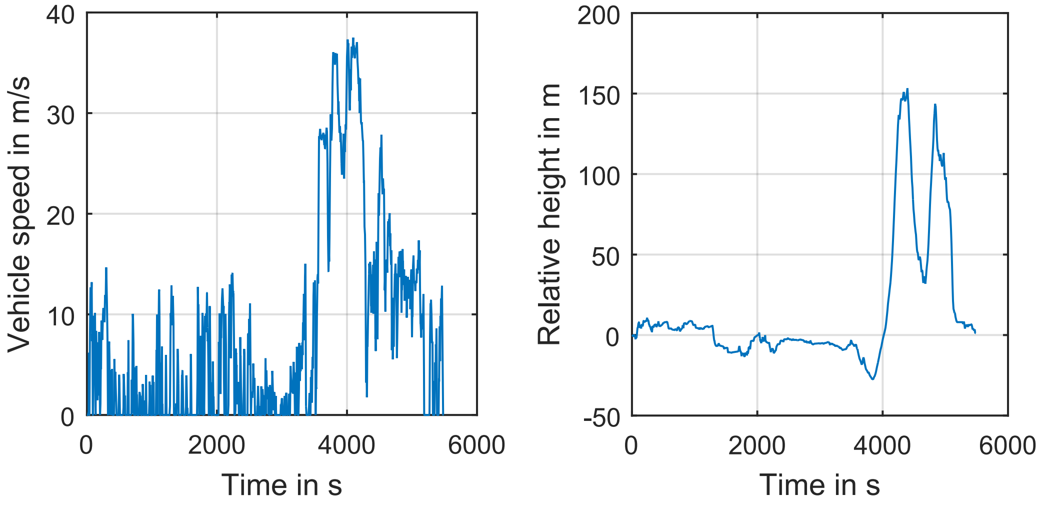

Figure 3.6.: Velocity and height profile over the time of the real driving cycle.

Identifiable parameters

- Charging behaviour
- Maximum charging current
- Maximum charging power

3.15. Misuse Manoeuvres

Manoeuvre description

The driving pedal is almost periodically tipped. Another variation tip the pedal irregulary.

Identifiable parameters

- Vehicle behaviour

3.16. Tip-in

Manoeuvre description

The vehicle accelerates to a predefined starting velocity and maintains for a few seconds to achieve a constant vehicle behaviour. An immediate full throttle phase is initiated.

Identifiable parameters

- Vehicle response
- Jerk

3.17. Tip-out

Manoeuvre description

The vehicle drives with a certain accelerator pedal position and immediately the throttle is realeased.

Identifiable parameters

- Vehicle response
- Jerk

3.18. Constant Braking

Manoeuvre description

The vehicle drives at a certain velocity and a braking manoeuvre is initiated with constant brake pedal position.

Identifiable parameters

- Braking strategy
- Recuperation torque
- Recuperation current
- Recuperation power

Table 3.3.: Manoeuvre and parameter overview.

Driving Manoeuvre	**Parameter**	**Scope of work**	**Verified**
Full Load 0→100 km/h	Acceleration gradient	✓	✓
	Duration	✓	✓
	Response time of traction motor	✓	✓
	Min/Max battery currents	✓	✓
	Drivetrain inertia	✓	✓
	ICE start up	✓	✓
Full Load Variations	Acceleration gradient	x	x
	Duration	x	x
	Response time of traction motor	✓	✓
	Min/Max battery currents	✓	✓
	Drivetrain inertia	✓	✓
	ICE start up	✓	✓
Heavy Breaking	Max. recuperation current	✓	✓
	Max. recuperation torque	✓	✓
	Braking strategy	✓	✓
Constant accelerator pedal position	Operation mode	✓	✓
	Pedal map	✓	✓
	Operation strategy	✓	✓

Constant velocity	Operation mode	✓	✓
	Pedal map	✓	✓
	Operation strategy	✓	✓
Drive away	Behaviour	x	x
	Acceleration gradient	x	x
	Duration	x	x
Brake-Release Delay	Duration	✓	✓
	End velocity	✓	✓
	Acceleration gradient	✓	✓
Coast-Down Manoeuvre	Inertias from drive-train	✓	x
	Rolling resistance	✓	✓
	Drag coefficient	✓	✓
	Recuperation torque	✓	✓
	Recuperation current	✓	✓
	Behaviour	x	x
Load Variation	Vehicle response behaviour	x	x
	Acceleration gradient	x	x
	Drag torque	✓	✓
	Braking strategy	✓	✓
Emergency Breaking	Inertia from chassis	x	x
	Braking strategy	✓	✓
Speed Bump Crossing	Spring-Characteristic	✓	✓
	Damper-Characteristic	✓	✓
Real Driving Cycles	Fuel consumptions	x	x
	Real vehicle behaviour	x	x
	Braking strategy	✓	✓
Charging	Charging behaviour	x	x
Misuse	Vehicle behaviour	x	x
Tip-in	Vehicle response	x	x
	Jerk	x	x
Tip-out	Vehicle response	x	x
	Jerk	x	x
Constant braking	Braking strategy	✓	✓
	Recuperation torque	✓	✓
	Recuperation current	✓	✓
	Recuperation power	✓	✓

4. Parameter Identification

4.1. Measurement Equipment and Measurement

The installed measurement equipment is shown in Figure 4.1. The 12 V batteries were powering the measurement computer, the measurement instruments, the external hard drive disc, the W-LAN antenna as well as the measurement instruments. The W-LAN antenna allowed to connect a control device. With this device the measurement was started and stopped. Furthermore, it allowed to evaluate the past measurements. The measurement computer was the core of the measurement equipment. All signal cables and CAN-Bus data were directed to it. With an external hard drive disc it was possible to extract the measured data from the measurement computer.

Figure 4.2 shows the positions of the current probes. With these probes, the battery, the on board power supply, the power control unit (PCU), the heater and air condition (AC) current was measured. The battery current is the summation of the left and right battery current that were measured by the probes.

Table 4.1 displays the measured parameters and its sources that were needed for the evaluation. Some were measured multiple times to verify the correspondence. Some parameters were added or removed during the driving manoeuvres. For example, the battery currents and voltages from the energy measurement equipment was firstly installed, but secondly removed. However, it was acceptable since the CAN-Bus data yielded the same measurement values. Another example, is the brake pedal position, which was installed at a later time. This was used to verify an accurate position for some evaluations.

During the evaluation it was detected that the generator voltage is the same as the battery voltage. This is reasonable since both are connected to the same intermediate circuit. The generator torque and the actual regeneration torque are the same as well.

For calculation reasons some parameters had to be converted into different unit, e.g., the levelled acceleration from the ADMA, it is measured in g and had to be converted into m/s^2.

4.2. Data Acquisition

The measured data and the data from the CAN-Bus have an asynchronous sampling rate. At the beginning of every new data set, the data was reset to an unified sampling

---

[1] The measurement signal was measured with an unit. The relevant unit should be in kPa.

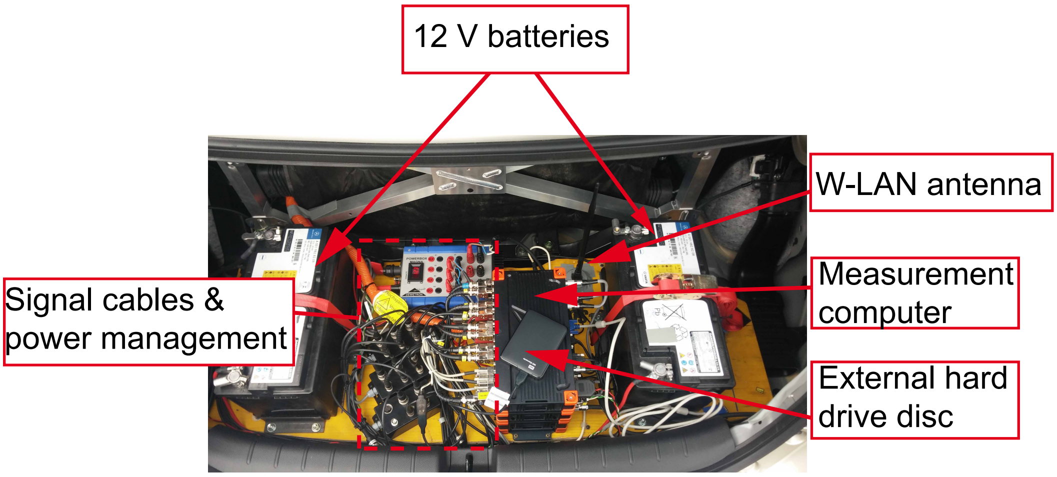
12 V batteries
W-LAN antenna
Signal cables & power management
Measurement computer
External hard drive disc

Figure 4.1.: Measurement equipment.

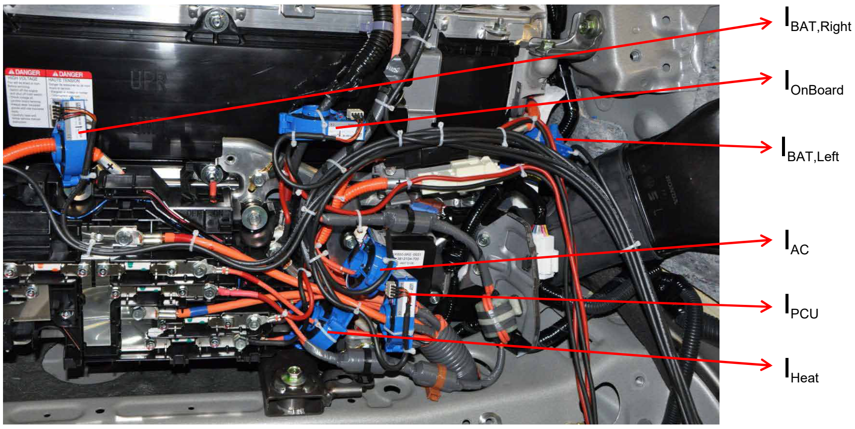
$I_{BAT,Right}$
$I_{OnBoard}$
$I_{BAT,Left}$
I_{AC}
I_{PCU}
I_{Heat}

Figure 4.2.: Current probes positions.

Table 4.1.: Measured parameters.

Name	Unit	Source
Battery SoC	%	CAN-Bus
Battery current	A	CAN-Bus
Battery current	A	Energy measurement equipment
PCU current	A	Energy measurement equipment
Heater current	A	Energy measurement equipment
On board power supply current	A	Energy measurement equipment
Air condition current	A	Energy measurement equipment
Battery power	W	CAN-Bus
Battery voltage	V	Energy measurement equipment
Requested auxiliary power	W	CAN-Bus
Brake pressure feedback to driver	kPa	CAN-Bus
Brake pressure	(kPa)[1]	CAN-Bus
Braking pedal position	V	Potentiometer
Axle torque	Nm	CAN-Bus
Engine rotational speed	rpm	CAN-Bus
Actual regeneration torque	Nm	CAN-Bus
Levelled velocity	m/s	GPS-Antenna
Longitudinal coordinate	Decimal-Deg	GPS-Antenna
Latitude coordinate	Decimal-Deg	GPS-Antenna
Height coordinate	m	GPS-Antenna
Generator torque	Nm	CAN-Bus
Generator rotational speed	rpm	CAN-Bus
Generator voltage	V	CAN-Bus
Operation mode	-	CAN-Bus
Accelerator pedal position	%	CAN-Bus
Pitch	Deg	ADMA
Roll	Deg	ADMA
Yaw	Deg	ADMA
Pitch-rate	Deg/s	ADMA
Roll-rate	Deg/s	ADMA
Yaw-rate	Deg/s	ADMA
Levelled acceleration in x direction	g	ADMA
Levelled acceleration in y direction	g	ADMA
Levelled acceleration in z direction	g	ADMA
Traction motor torque	Nm	CAN-Bus
Traction motor rotational speed	rpm	CAN-Bus

rate of 100 Hz, because 100 Hz is the highest sample rate that can be ascertain from the CAN-Bus. The calculations with an asynchronous data is an elaborate process. With the initialized, data the calculations are much easier. Since some measured signals have an higher sampling rate, some of the data were lost. However, the 100 Hz is a trade-off between data loss and conveniently calculations.
The velocity which is used in every evaluation needs a special focus. The velocity is measured through the GPS-Antenna and hence it is levelled. In addition to the levelled velocity it is filtered with an average mean filter. The feasibility is given by the fact, that the vehicle mass is high, as a consequence, the inertia is also high. The derivatives of original measurement signals have to be filtered, because of numerical issues (e.g., the derivative is the ratio of the difference of two consecutive signal points and the time difference for the corresponding signal points). The average mean filter, also known as moving average filter, is a filter that spans a window over the current data points and averages all values in this window. For example: The window size (WS) is 20 points, the current point is located on the position 25. Now the filter takes the last and the next ten points (from position 15 to 35) and calculates the mean value over these 20 points. Next the filter proceeds to the next point (position 26) and spans there a window of 20 points and averages this window. However, through this filter method a phase shift occurs. As a corrective action the same procedure is used backwards with inbuilt MATALB function `filtfilt`. Eq. (4.1) represents the calculation from one point through the average mean filter. As an example a part from the acceleration of a speed bump crossing is shown in Figure 4.3. Once the unfiltered acceleration is displayed and once the filtered data set.

$$y(n) = \frac{1}{WS}\left(x(n) + x(n-1) + \ldots + x(n-(WS-1))\right) \tag{4.1}$$
$$n = 1, 2, ..., WS$$

y	Filtered point of average mean filter
x	Measured point

In MATLAB it can be implemented as following with the `filtfilt` function:

```
b=ones(WS,1);
a=zeros(WS);
a(1)=WS;
output = filtfilt(b,a,signal);
```

4.3. Dynamic Tyre Radius

The tyre of a vehicle is one of the most important components of a vehicle, the tyres transfer the traction force onto the street and therefore the vehicle is driven forward. On the tyres the weight, centrifugal and other forces are effecting the radius. For a more

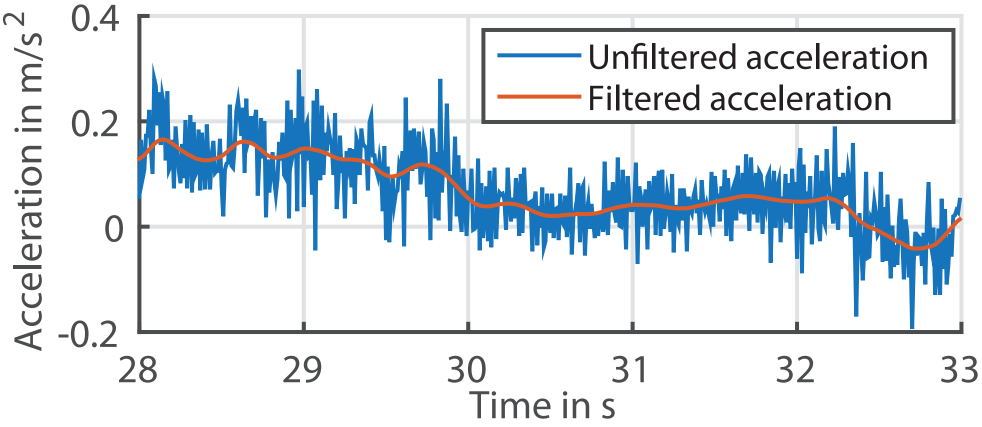

Figure 4.3.: Example of an average mean filter, with a window size of 20 points.

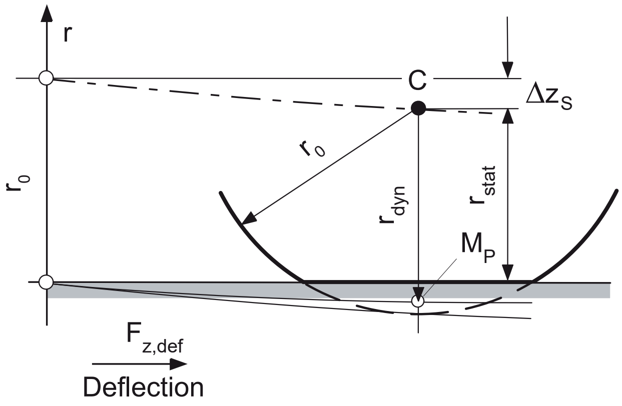

Figure 4.4.: Difference of the tyre radii. The parameter C is the centre of the tyre, M_P the instantaneous centre of rotation and Δz_S is the static spring compression, adapted from [4].

accurate calculation of the vehicle and its parameters not the static tyre radius is needed, but the effective (dynamic) radius. In Figure 4.4 the differences between the dynamic r_{dyn}, the static r_{stat} and the nominal tyre radius r_0 are shown ($r_{stat} < r_{dyn} < r_0$). The nominal radius is the radius that is specified by the manufacturer. As displayed r_{dyn} dependence on the instantaneous centre of rotation M_P. The distance from C to M_P increases with increasing velocity.

Today's vehicles have belt tyres and are constructed with steel-threads. As a result the dynamic rolling circumference U_{dyn} can be assumed as constant [24]. To estimate the difference between the effective and the nominal radius a test was conducted. The DIN 70020 standard states that the dynamic tyre radius is measured at 60 km/h without any

Table 4.2.: Measured tyre parameters.

Tyre dimension		225/50 R17
	r_0	328.5 mm
Measured values	$U_{stat,F}$	4060 mm
	$U_{stat,R}$	4070 mm
Calculated values	$U_{stat_{mean}}$	4065 mm
	r_{stat}	323.5 mm
	r_{dyn}	326.5 mm

driving or braking forces. The rolling circumference defines the dynamic tyre radius. [24]

$$r_{dyn} = \frac{U_{dyn}}{2\pi} \tag{4.2}$$

With the provided measurement equipment such a measurement was not executable. Therefore a similar method was applied with the help of an approximation of the dynamic tyre radius.

$$r_{dyn} \approx \frac{2}{3} r_0 + \frac{1}{3} r_{stat} \tag{4.3}$$

U_{dyn}	Rolling circumference in mm
r_{dyn}	Dynamic tyre radius in mm
r_0	Nominal tyre radius in mm
r_{stat}	Static tyre radius in mm

The vehicle is standing on an even road. The left front and the right rear tyre are marked. The initial positions on the streets are marked too. Afterwards the vehicle is pushed forwards. Two entire rotations of the tyres are conducted. The distance between the markings are measured. The measured distance from the left front tyre is $U_{stat,F}$ and from the right rear tyre $U_{stat,R}$. The dynamic tyre radius is conducted with the measurement equipment and a passenger. This is done to achieve r_{dyn} during testing conditions. The results are shown in Table 4.2. The radius r_0 is the nominal radius that is given through the tyre dimensions, r_{stat} is the calculated radius from the measured averaged distance $U_{stat_{mean}}$. Finally, the dynamic radius r_{dyn} is calculated with Eq. (4.3).

Summary

The dynamic tyre radius $r_{dyn} = 326.5\,\text{mm}$ and is calculated with Eq. (4.3). For this the vehicle was pushed and the rolling circumference was marked on the test road. The results are summarised in Table 4.2.

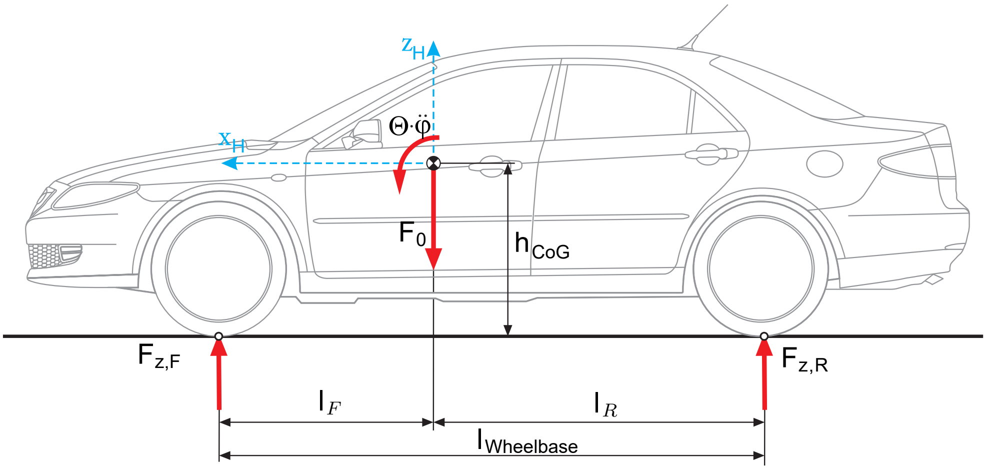

Figure 4.5.: Centre of gravity, adapted from [9].

4.4. Centre of Gravity

4.4.1. Centre of Gravity – x-Position

The centre of gravity (CoG) is also an important parameter of the vehicle. The CoG correlates with the load of the vehicle. Here the centre of gravity is calculated with the curb weight of the vehicle. The CoG is calculated with the principle of angular momentum.

$$0 = F_{z,R} \cdot l_{Wheelbase} - F_0 \cdot l_F \tag{4.4}$$

With the force acting on the rear axle $F_{z,R}$:

$$F_{z,R} = \mathrm{g} \cdot (m_{Right,R} + m_{Left,R}) \tag{4.5}$$

$$F_0 = \mathrm{g} \cdot (m_{Right,R} + m_{Left,R} + m_{Right,F} + m_{Left,F}) \tag{4.6}$$

Now Eq. (4.9) can be transformed to:

$$l_F = \frac{F_{z,R} \cdot l_{Wheelbase}}{F_0} \tag{4.7}$$

The distance from the rear axle to the CoG reads:

$$l_R = l_{Wheelbase} - l_F \tag{4.8}$$

Table 4.3.: Centre of gravity – x-Position results.

$l_{Wheelbase}$ in m	l_F in m	l_R in m
2.77	1.23	1.54

$F_{z,F}$	Force on the front axle in N
$F_{z,R}$	Force on the rear axle in N
F_0	Curb weight mass of the vehicle in N
l_F	Length from the front axle to the CoG in m
l_R	Length from the rear axle to the CoG in m
$l_{Wheelbase}$	Length of the wheelbase in m
g	Gravitational acceleration in m/s^2
$m_{Right,R}$	Vehicle mass measured at the right rear of the vehicle in kg
$m_{Right,F}$	Vehicle mass measured at the right front of the vehicle in kg
$m_{Left,R}$	Vehicle mass measured at the left rear of the vehicle in kg
$m_{Left,F}$	Vehicle mass measured at the left front of the vehicle in kg
m	Total mass of the vehicle in kg
Θ_{Ch}	Inertia of the chassis in kgm^2

Table 4.3 shows the results for the position of the CoG based on the longitudinal axis.

4.4.2. Centre of Gravity – y-Position

The track width of front $l_{Track,F}$ and rear $l_{Track,R}$ axle has a difference of 0.007 m. Therefore, a similar track on the front and rear axle is assumed. The track width is used to calculate the CoG in lateral position. The results are shown in Table 4.4. The distance difference from middle of the car to $l_{y,Left}$ is 0.02 m. As a result the CoG in y-position is almost centred. Thus, it can be assumed that the vehicle is symmetric along the x-axis.

$$0 = F_{z,Left} \cdot l_{Track,F} - F_0 \cdot l_{y,Left} \tag{4.9}$$

The force acting on the left side of the vehicle $F_{z,Left}$ yields:

$$F_{z,R} = \mathrm{g} \cdot (m_{Left,F} + m_{Left,R}) \tag{4.10}$$

The distance from the left side of the vehicle to the CoG position is:

$$l_{y,Left} = \frac{F_{z,Left} \cdot l_{Tack,F}}{F_0} \tag{4.11}$$

$F_{z,Left}$	Contact force on the Left side of the vehicle in N
F_0	Curb weight mass of the vehicle in N
$l_{Track,F}$	Front track width in m
$l_{Track,R}$	Rear track width in m
$l_{y,Left}$	Length from the left side of the vehicle to CoG in m
g	Gravitational acceleration in m/s^2

Table 4.4.: Centre of gravity – y-position results.

$l_{Track,F}$ in m	$l_{y,Right}$ in m	$l_{y,Left}$ in m
1.58	0.81	0.77

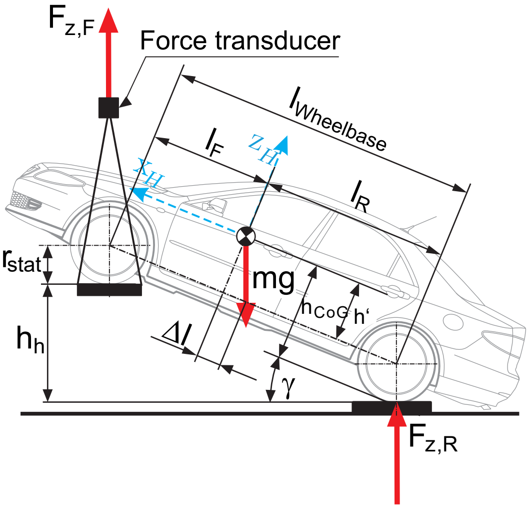

Figure 4.6.: Tilt measurement, adapted from [9].

4.4.3. Centre of Gravity – z-Position

One method to measure the CoG height is through a tilt measurement. Figure 4.6 shows such a measurement. The vehicle is lifted on one axle as high as possible. The force $F_{z,F}$ is measured by a force transducer.

$$T_y = 0: \quad -m \cdot \mathrm{g}\,(l_R - \Delta l) \cdot \cos\gamma + F_{z,R} \cdot l_{Wheelbase} \cdot \cos\gamma = 0 \tag{4.12}$$

m	Total vehicle mass in kg
g	Gravitational acceleration in m/s^2
γ	Angle of inclination in Deg
l_R	Length from rear axle to the CoG in m
Δl	Length difference in m
$F_{z,R}$	Contact force on rear axle in N
$l_{Wheelbase}$	Wheelbase length in m
l_F	Length from front axle to the CoG in m
l_R	Length from rear axle to the CoG in m
r_{stat}	Static wheel radius in m

Eliminating the cosine function in Eq. (4.12):

$$F_R \cdot l_{Wheelbase} = m \cdot \mathrm{g}\,(l_R - \Delta l) \cdot \cos\gamma \tag{4.13}$$

The length difference Δl is calculated by h' and ϕ

$$\Delta l = h' \tan\gamma \tag{4.14}$$

With h' defined as:

$$h' = h_{CoG} - r_{stat} \tag{4.15}$$

Equation (4.13) can be reshaped with Eq. (4.7) and Eq. (4.14) to:

$$F_R \cdot l_{Wheelbase} = F_{z,F} \cdot l_{Wheelbase} - m \cdot \mathrm{g} \cdot h' \tan\gamma \tag{4.16}$$

$$h' = \frac{F_{z,F} \cdot l_{Wheelbase} - F_R \cdot l_{Wheelbase}}{m \cdot \mathrm{g} \cdot \tan\gamma} \tag{4.17}$$

Using the static tyre radius r_{stat}, h_{CoG} reads:

$$h_{CoG} = r_{stat} + h' = r_{stat} + \frac{F_{z,F} \cdot l_{Wheelbase} - F_R \cdot l_{Wheelbase}}{m \cdot \mathrm{g} \cdot \tan\gamma} \tag{4.18}$$

A tilt measurement was not possible without damaging the vehicle, therefore an estimation of the CoG height was used, compare Eq. (4.19). This approximation was introduced by [1]. This approximation can lead to incorrect results. The height of the CoG decreases with additional weight. A heavy SUV has a higher CoG in reality, however using this estimation the height of the CoG decreases. As an example an SUV with the same wheelbase and a curb weight of 2500 kg has a CoG height of 0.44 m. In contrast, a lighter vehicle with the same wheelbase but a different curb weight of 1300 kg has a height of 0.57 m. Consequently, this example shows that the height of a SUV is lower than of the lighter vehicle, which is not the case in reality.

$$x \equiv \frac{h_{CoG}}{l_{Wheelbase}} = 0.26 - 0.04 \cdot \frac{m}{1000\,\mathrm{kg}} \tag{4.19}$$

x_{CoG}	Ratio between CoG height and wheelbase length
h_{CoG}	Height of the CoG in m
m	Total mass of the vehicle in kg

Reformulating Eq. (4.19) leads to the height of the CoG h_{CoG}:

$$h_{CoG} = \left(0.26 - 0.04 \cdot \frac{m}{1000\,\mathrm{kg}}\right) \cdot l_{Wheelbase} \tag{4.20}$$

However, this estimation is necessary, since it was not possible to tilt the vehicle. Table 4.5 shows the results for different weight loads. It is obvious that the vehicle height h_{CoG} decreases with increasing total vehicle mass.

Table 4.5.: Centre of gravity calculation results.

Load	Total mass in kg	CoG height in m
Curb weight	1729	0.5298
Curb weight + Driver	1801	0.5218
Curb weight + Driver + Passenger	1885	0.5124

Summary

In this chapter methods to determine the centre of gravity are introduced. The x-position of the CoG is 1.23 m from the front axle and has a height of about 0.52 m. The y-position is 0.77 m from the left side of the wheels to the CoG. The y-position of the CoG is located almost in centre of the vehicle. Thus, it is assumed that the vehicle is symmetrical along the x-axis. These parameters were calculated with the curb weight of the vehicle. The height is estimated with Eq. (4.20). This was done since it was not possible to tilt vehicle without damaging the front skirt.

4.5. Spring - Damper Characteristics

The spring damper characteristics are evaluated with the help of a spring damper model and an optimisation process. To get reasonable results for the spring and damper coefficients a driving manoeuvre with a pitch-rate deflection is needed, which is achieved with a speed bump crossing. The velocity, pitch and pitch-rate are measured and implemented into a single track model, compare Figure 4.10. The speed bump dimensions implemented are shown in Figure 4.11. Subsequently, the spring damper characteristics are evaluated through an optimisation process. Nevertheless, a first estimation of the spring and damper characteristic is done, to get an idea of the possible parameter range.

4.5.1. Spring Characteristic Estimation

The vehicle is first loaded above the front springs with additional weight to estimate the spring characteristic. The weight is gradual increasing and the forces $F_{z,F}$, $F_{z,R}$ and the lengths Δz_F, Δz_R are measured, see Figure 4.7. The lengths are measured before the weights are loaded to calculate the length differences. The forces are measured with the help of wheel load scales.

Afterwards the rear springs are loaded with the additional weights. Ideally the additional weights are loaded directly above the springs. In this measurement series it was not possible to load the weights directly above the rear suspension. The weights were placed in the trunk. Due to the used load scales placed directly below the tyres, the weight can be placed anywhere near the spring as long as a deflection is measured. The weights

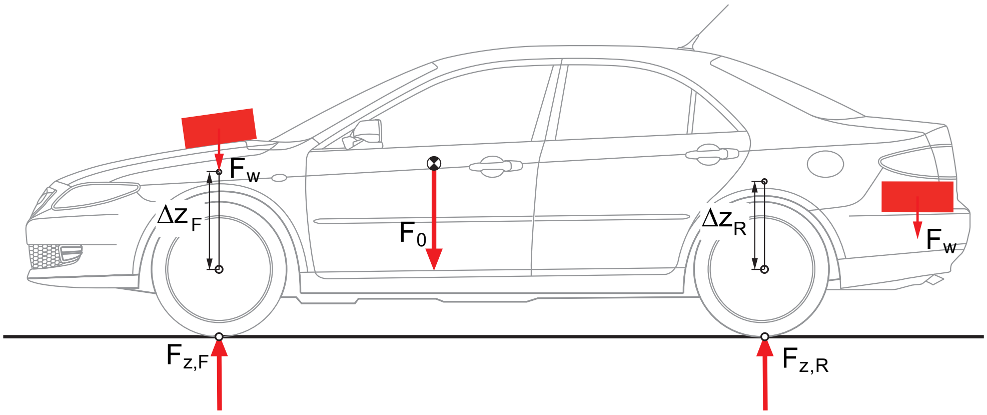

Figure 4.7.: Measurement to estimate the spring compression characteristic, adopted from [9].

should increase symmetrically on the left and right side of the vehicle. A pure negative lifting motion is needed. Otherwise, the vehicle performs not only a pitch but also a roll motion. This can influence the measurement results. This method only enables determination of the linear spring characteristics. In the measurement procedure the weights were increased by 20 kg per increment to a total of 100 kg per spring. Tables A.1 and A.2 in the appendix highlight the measurements results.

The front spring coefficients are calculated with the following equations. The rear spring is determined vice versa. The initial front force $F_{z,F,0}$ without any additional weight is calculated:

$$F_{z,0,F} = \mathrm{g} \cdot (m_{Right,F,0} + m_{Left,F,0}) \tag{4.21}$$

where the front force $F_{z,F}$ with additional weight reads:

$$F_{z,F} = \mathrm{g} \cdot (m_{Right,F} + m_{Left,F}) \tag{4.22}$$

The force difference of the front axle yields:

$$\Delta F_{z,F} = |F_{z,F,0} - F_{z,F}| \tag{4.23}$$

The compression of the spring Δz_F is determined by:

$$\Delta z_F = |l_{F,0} - l_{F,Measured}| \tag{4.24}$$

Finally, the spring constant at the front suspension c_F yields:

$$c_F = \frac{\Delta F_{z,F}}{2 \cdot \Delta z_F} \tag{4.25}$$

Table 4.6.: Results of the spring characteristic of the front spring.

Front

Additional mass in kg	Compression in mm	Force in N	Spring constant c_F in N/m
+20	2	362	90742
+40	7	765	54655
+60	12.5	1167	46695
+80	20	1559	38994
+100	22	1913	43476
Mean value			54913

Table 4.7.: Results of the spring characteristic of the rear spring.

Rear

Additional mass in kg	Compression in mm	Force in N	Spring constant c_R in N/m
+20	5	490	49049
+40	10	922	46107
+60	15	1432	47742
+80	19	1932	50857
+100	24	2413	50276
Mean value			48806

$F_{z,F}$	Force on the front axle in N
$F_{z,R}$	Force on the rear axle in N
$F_{z,F,0}$	Initial force (idle state) in N
l_F	Length from the centre of the front wheel to a marking point above in mm
l_R	Length from the centre of the front wheel to a marking point above in mm
g	Gravitational acceleration in m/s^2
$m_{Right,F}$	Vehicle mass measured at the right front of the vehicle in kg
$m_{Left,F}$	Vehicle mass measured at the left front of the vehicle in kg
$m_{Right,F,0}$	Vehicle mass measured at the Right front of the vehicle without any additional weight in kg
c_F	Front spring constant in N/m

The spring constant in Eq. (4.25) has to be divided by 2, because the forces (masses) from left and right tyres are used. Tables 4.6 and 4.7 show the results of the spring characteristics of the front and rear spring, respectively. The first entry in Table 4.6 with a spring constant of 90742 N/m is extremely high. This can be explained by a reading error during the measurement process. If the length difference is 3 mm instead of 2 mm the spring constant is reduced to about 60500 N/m, which is a more reasonable result. Figure 4.8 describes the linear spring characteristic. The calculation results of the spring forces are shown in Figure 4.9 and a linear progression is apparent.

The initial values of the spring damper model are the mean values of the evaluated spring constants in Tables 4.6 and 4.7. The mean value of the front and rear spring are 54913 N/m and 48806 N/m, respectively.

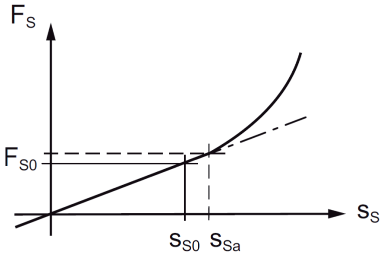

Figure 4.8.: Linear progressive spring characteristic. Distance s_{S0}, describes the end of the linear compression. At the distance s_{Sa} an additional spring is engaged. Adopted from [4].

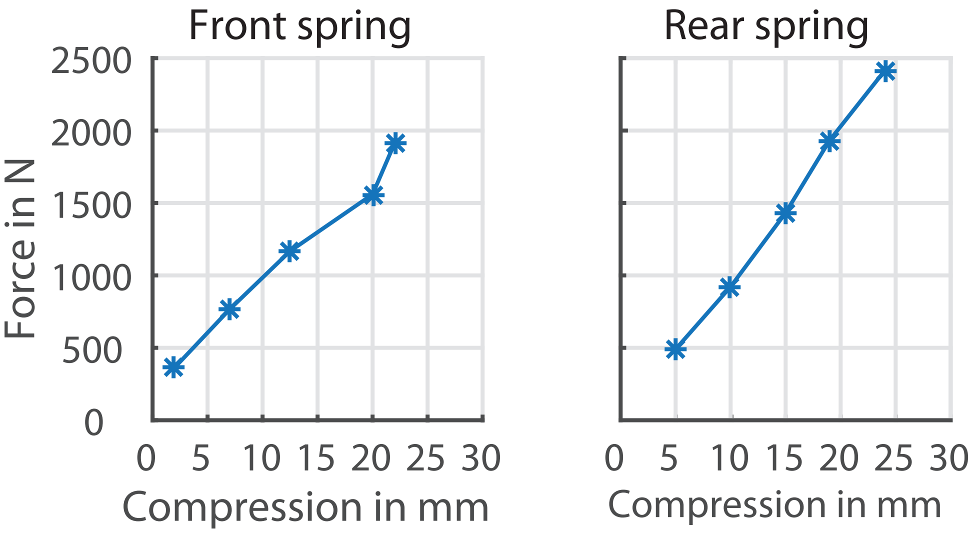

Figure 4.9.: Spring characteristics.

4.5.2. Damper Characteristic Estimation

Some assumptions are made in order to determine the damper coefficient. First of all, it is assumed that the damper has only a linear characteristic. Second, the left and right damper are symmetrical and therefore have the same performance. The damper is calculated with the damping factor D, see Eq. (4.26). Since the test vehicle was a rather comfortable car the damping factor was assumed with $D = 0.3$. According to [4], this indicates a comfortable setting. To calculate the damping coefficient the spring constants must be known in advance. Therefore, the mean spring coefficients from 4.5.1 were used. Moreover, the mass of an axle and two tyres are estimated with 100 kg. Last, the spring constant of the tyres is much greater than the spring constant of the actual spring $c_{Tyre} \gg c_{Spring}$. Consequently, the tyre spring characteristic can be neglected

and an external force is damped only by the suspension of the vehicle.
In Eq. (4.26) m_{Ch} is divided by four, because only one quarter of the chassis mass acts on one damper. Since in a single track model the left and right suspensions are combined to one single device Eq. (4.26) is divided by 2. The damper coefficient in Eq. (4.26) is calculated for the front suspension.

$$D = \frac{d_F}{2\sqrt{c_F \cdot \frac{m_{Ch}}{4}}} \tag{4.26}$$

D	Damping factor
d_F	Damping coefficient of front suspension in Ns/m
c_F	Spring constant of front suspension in N/m
m_{Ch}	Mass of the chassis in kg

Table 4.8 shows the results of the estimated front and rear damper characteristics.

Table 4.8.: Damper coefficients.

d_F	d_R
2929 Ns/m	2761 Ns/m

According to [23], the linear damping coefficient of a vehicle with about the same mass is in the range of 2600 and 3600 Ns/m.

4.5.3. Spring Damper Model

The spring damper model is based on a simple single track model, shown in Figure 4.10. The whole model is implemented in SIMULINK and its parameter are than optimised with the function `fminsearch`.
Since the CoG in Chapter 4.4 was calculated with the curb mass without the measurement equipment and passengers the mass distribution for the speed bump crossing manoeuvres has to be recalculated, which is directly implemented in the MATLAB-script. Because of the new mass distribution, the quarter-vehicle model mass and thus the dampers are calculated again with the equations in Chapter 4.5.2. The mass of the chassis and the tyre masses are modelled as mass points. The suspension mass is assumed with 100 kg. The springs have no inclination angle in contrast to real conventional vehicles. Moreover, no spring and damper conversions are implemented. Furthermore, the instantaneous pitch centre is assumed to be in the CoG. The slip of the wheels are neglected.

The inertia of the chassis was assumed to be a thin rod. The mass distribution affects the inertia and is calculated by Eq. (4.27).

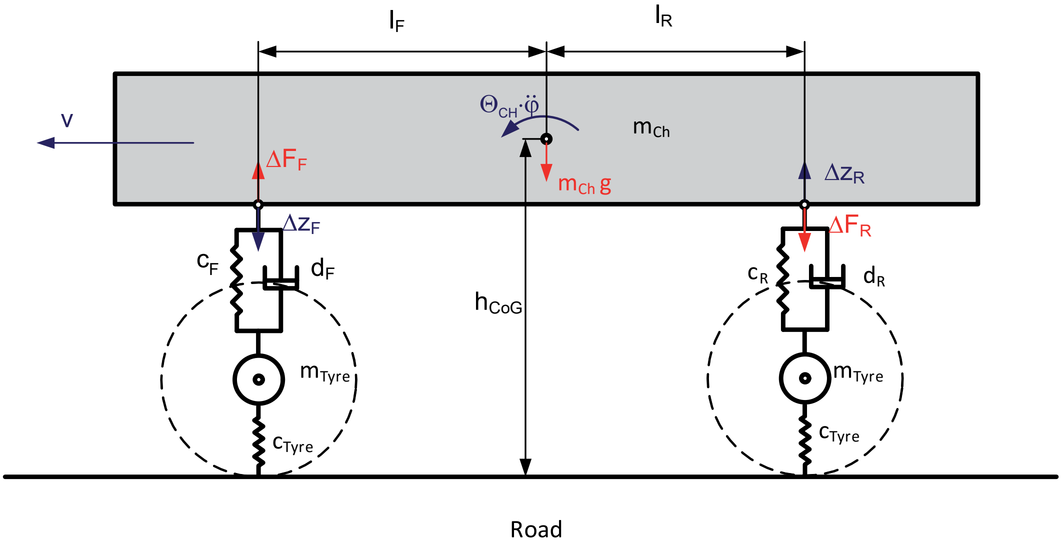

Figure 4.10.: Spring damper simulation model, adapted from [4].

$$\Theta_{Ch} = \frac{m_{Ch,F} \cdot l_F^2}{3} + \frac{m_{Ch,R} \cdot l_R^2}{3} \tag{4.27}$$

The speed bump was measured with a laser operating distance measuring instrument (i.e., Hilti PD 30) every 10 mm over a total distance of 3 m. At first, the suspension simulation was performed with the measured points of the bump. However, the result was not satisfying since the bump shape has a deep impact on the results. Therefore, the measured points were aligned. Interpolation of the measured bump points had no effect on the simulation model and the results since SIMULINK interpolates automatically grid points. Smoothing the bump provided a better solution. The implemented MATLAB function `fit` and the smoothing method `smoothingspline` were used for this purpose. Equation (4.28) shows the method of the spline fitting. The smoothed bump is shown in Figure 4.11, where the crosses are the measured points and the curve consists of the smoothed and interpolated values. The "new" bump matches 98 % of the original measurement points.
A virtual road was constructed for the simulation model so that the model has a 10 m tuning phase before and after the bump. Thus, the simulation model avoids undesired transients at start and end of the simulation manoeuvre. Moreover, the test road in the simulation has to have a certain distance so that the whole vehicle can cross the bump.

The implemented smoothing spline s uses a smoothing parameter p and weights w_i. The smoothing spline method minimizes the parameter s for each data point x_i [11], compare

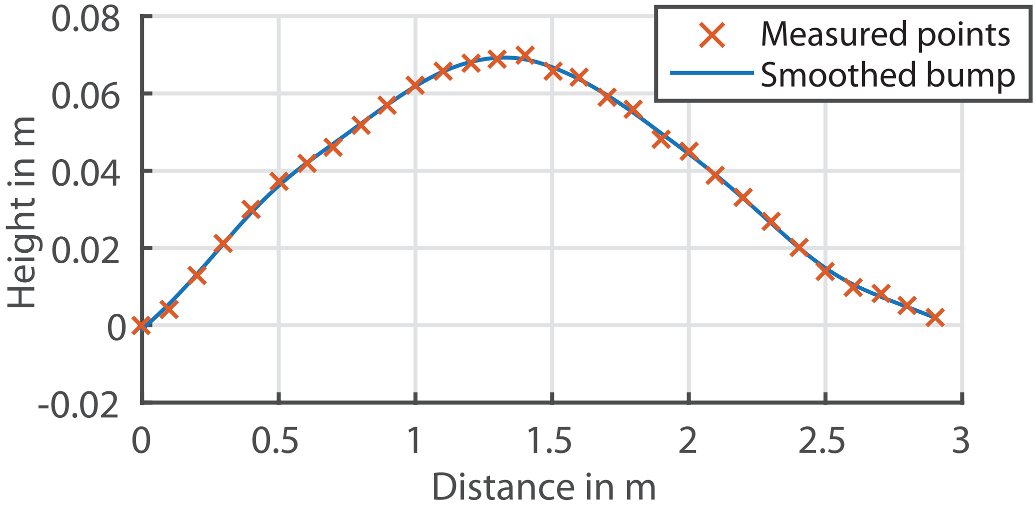

Figure 4.11.: Speed bump. Measured points in red, fitted and interpolated curve in blue.

Eq. (4.28).

$$\min_s \left\{ p \sum w_i \left(y_i - s(x_i)\right)^2 + (1-p) \int \left(\frac{d^2 s}{dx^2}\right)^2 dx \right\} \tag{4.28}$$

where the smoothing parameter p is set to 0.999.

In general, the spring-damper characteristic was solved with the function `fminsearch` which optimises the pitch-rate of the simulation model in order to fit best the given pitch-rate of the measurements. The used cost functional is shown in Eq. (4.29). It calculates the area between the measured and the simulated pitch-rate $\dot{\varphi}_{measured}$ and $\dot{\varphi}_{simulated}$, respectively. The cost functional is squared to achieve a positive error-areas which are then accumulated. Otherwise, in certain situations the cost functional is small, but the actual single errors are high, e.g., if "positive" errors are compensated by "negative" ones.

$$J = \int_0^{t_{end}} \left|\dot{\varphi}_{simulated} - \dot{\varphi}_{measured}\right|^2 \mathrm{d}t \tag{4.29}$$

A more sophisticated approach is to use a weighted cost functional, for instance that the area before the bump starts has little influence of the cost functional (i.e., little weight value) or the biggest deflection is rated higher (i.e, high weight value). This is beneficial, since before the actual simulation starts an area difference is already calculated. The speed bump crossing manoeuvres were performed at least two times over two different bumps with different starting velocities of approximately 10, 20 and 30 km/h. The outcome of the simulations are different to the results from the the spring and damper estimations in Chapters 4.5.1 or 4.5.2. This can be explained by the assumptions made

Table 4.9.: Simulation results in comparison to the estimated values.

	Unit	Measurement with 20 km/h	Measurement with 10 km/h	Estimated values
Front spring	N/m	26856	55618	54913
Rear spring	N/m	11871	47722	48806
Front damper	Ns/m	1031	2830	2929
Rear damper	Ns/m	2413	2900	2761
Cost functional value	-	3670	2586	-

for the simulation. For instance, the tyre spring characteristics were estimated with 200000 N/m [2] and not measured. Moreover, the height of the CoG of the vehicle and the inertia of the chassis Θ_{Ch} were estimated.

In some measurement records the pitch-rate had an offset. The most promising method to eliminate this offset was to subtract the mean value of the overall pitch-rate. The starting condition of the simulation was not always clear. Therefore, every time a new measurement record was initialised the starting point was manually set to achieve a certain similarity of the simulated and measured pitch-rate. The speed bump geometry has a big impact on the simulation. Therefore, a better precise measurement of the bump is recommended, e.g., with increments every 5 mm over a distance of at least 5 m . This has the advantage that the “flat” street is included and the real road characteristics can be better implemented in simulation. In addition, the bump is not evenly built. The left side of the bump has a much steeper incline and decline than the right side. However, with a single track model it is impossible to account for this difference. Thus, the model is once simulated over the left and once simulated over the right side of the speed bump.

In Figure 4.12 two different measurements and simulations are shown. The left hand side shows one speed bump crossing with 20 km/h and on the right hand side one with 10 km/h is given. The red lines are the measured pitch and pitch-rates and the green lines are the final optimisation results. The grey lines are the outcomes of various iterations. The measurement on the right was performed over the “flatter” side of the bump and the results of the optimisation are similar to the estimated spring and damper values in Chapters 4.5.1 and 4.5.2. However, the congruence of the simulated and measured pitch-rate is very small.

The other simulation has good congruence of the simulated and measured pitch and pitch-rates but the actual spring and damper values have a big difference to the estimations. The actual results of both simulations are displayed in Table 4.9. These different measurements were picked because the measurement with 20 km/h has the best congruence of the simulated and measured pitch-rate but poor results regarding the initial estimations. In contrast, the measurement with 10 km/h has almost the worst congruence of all simulations but the best numerical values in reference to the spring-damper-estimation values in Chapter 4.5.1 and 4.5.2.

---

[2] According to [23], the tyre spring stiffness of a vehicle with about the same mass is 220000 N/m.

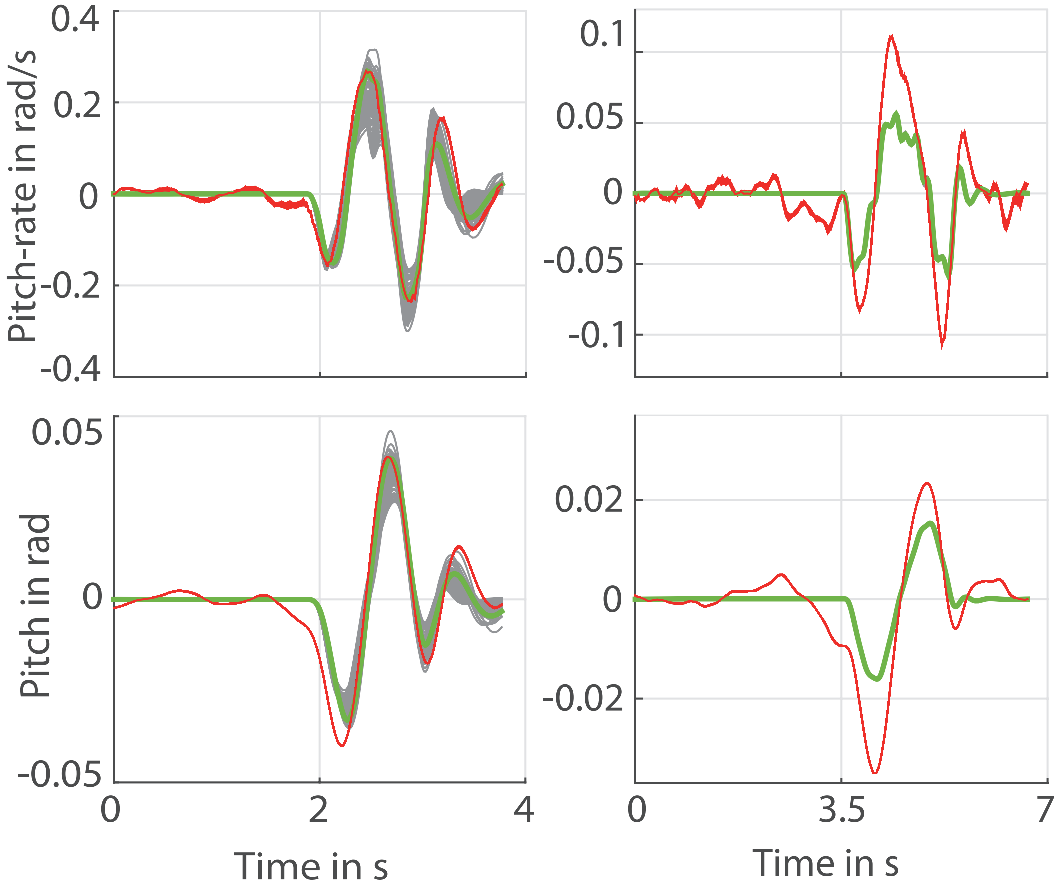

Figure 4.12.: Left: the pitch-rate and pitch with a good congruence of simulated and measured pitch and pitch-rate is shown. The optimisation process was performed with 20 km/h. Right: the pitch-rate and pitch have bad congruence and were performed with 10 km/h. The red lines are measured values and the green lines are the final optimisation results.

Another method to measure the spring damper characteristic is to use the relative acceleration of the suspension determined by a cable potentiometer or a wheel vector sensor. With this measurement equipments the relative length, velocity and acceleration of the suspension can be measured. The wheel vector sensor has the advantage that the wheel movement can also be measured. The relative length as well as the velocity or the acceleration can be used in the simulation model instead of the pitch-rate. Figure 4.13 shows on the left side a cable potentiometer and on the right side a wheel vector sensor. However, it was not possible to install one of these measurement instruments onto the vehicle, because no blocked testing area was available.

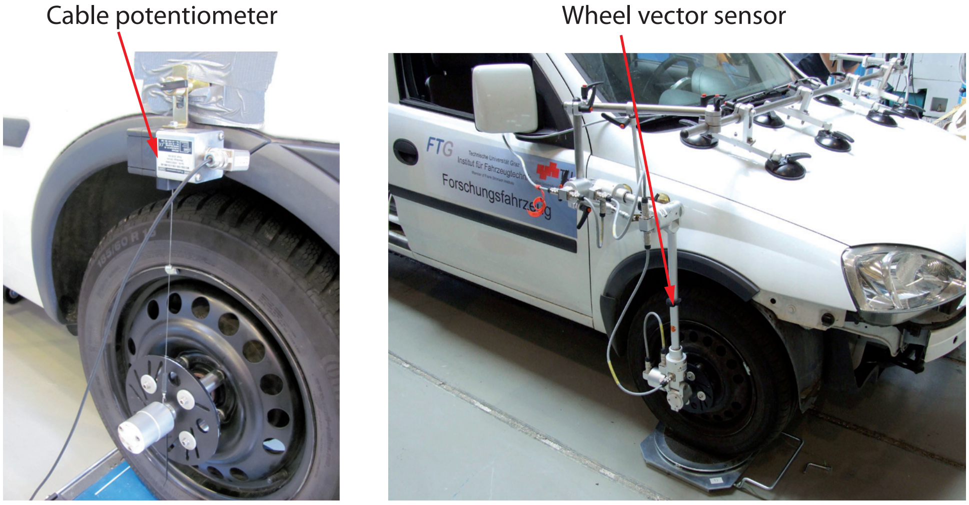

Figure 4.13.: Cable potentiometer and wheel vector sensor to measure the relative velocity of the suspension, adopted from [9].

Summary

The spring damper coefficients that are calculated with the simulation model differ partially from the results of the initial spring and damper estimations. The results from the simulation with a good congruence of the pitch and pitch-rate have spring coefficients below 26 kN/m. In contrast, the spring coefficient from the estimations are about 50 kN/m. The results of the simulation with bad congruence of the simulated and measured pitch and pitch-rate have similar coefficients as the values from the estimations. The many assumptions and simplifications that are made for the simulation model (e.g. simple single track model, estimated CoG height, only linear domain of the spring-damper characteristics, ...) may explain the difference. Using the acceleration of the suspension instead of the pitch-rate may inprove the optimisation results. A simple cable potentiometer or a wheel vector sensor is then needed. However, it was not possible to install such an equipment on the test vehicle due to saftey reasons, thus the pitch-rate was used.

4.6. Battery Characteristics

In this chapter the battery current and power are discussed. It is assumed that, the maximum discharge current can be identified with full load manoeuvres. In contrast, the maximum charging current and power is assumed to be evaluated with heavy braking manoeuvres. At first, the battery current was measured with an additionally installed energy measurement equipment, compare Chapter 4.1. Due to the effect that the mea-

Table 4.10.: Discharging battery characteristics.

	Unit	Mean value	Standard deviation
Peak current	A	247.88	7.82
Continuous current	A	113.99	7.91
Max. peak power	kW	73.60	2.34
Continuous power	kW	35.05	2.32

surement equipment samples the battery current and voltage with a high sample rate of 50 kHz, it has much more outliers than the CAN-Bus data. Those outliers are caused by measurement or parasitic errors. An average mean filter, compare Chapter 4.2, is used to smooth the measurement results. However, the CAN-Bus data and the energy measurement equipment data was compared and both data sets yielded the same results. To avoid the outliers of the measurement equipment the CAN-Bus data was used for further calculations.

4.6.1. Discharge Current and Power

In Figure 4.14 a full load manoeuvre is represented, with the velocity and pedal position. Moreover, the battery current, voltage and power are shown. The peak values of the battery current and power are highlighted as well as the continuous current and power. The voltage has its lowest value at the peak of the battery current, this is evident since the battery has the highest load at this moment. In Table 4.10 the peak power is at about 70 kW and the maximum discharge current at about 250 A. The continuous current has a mean value of about 115 A and the battery has a continuous power output of ≈ 35 kW. At high accelerations the slip of the tyres are controlled by the Anti-lock brake system (ABS) and electronic stability control (ESC) unites. Therefore, it is possible that these control unites avoid maximum vehicle acceleration. Due to safety reasons the control units were not turned off, since the manoeuvres were performed in the real driving situations. Further measurements showed that the battery was not only limited to the discharge current but also to the maximum peak discharge power.

4.6.2. Charging Current and Power

The recuperation current and power are evaluated with the help of heavy braking manoeuvres. These manoeuvres are more difficult to perform, because a test road with a steep decline is needed. It was a problem to achieve a high recuperation performance since it was not possible to switch of the ABS control unit . Thus, it was assumed that during the heavy braking manoeuvres the recuperation display on the control panel of the test vehicle indicates the maximum recuperation. However, analyses showed that the proposed method was not optimal for this propose.

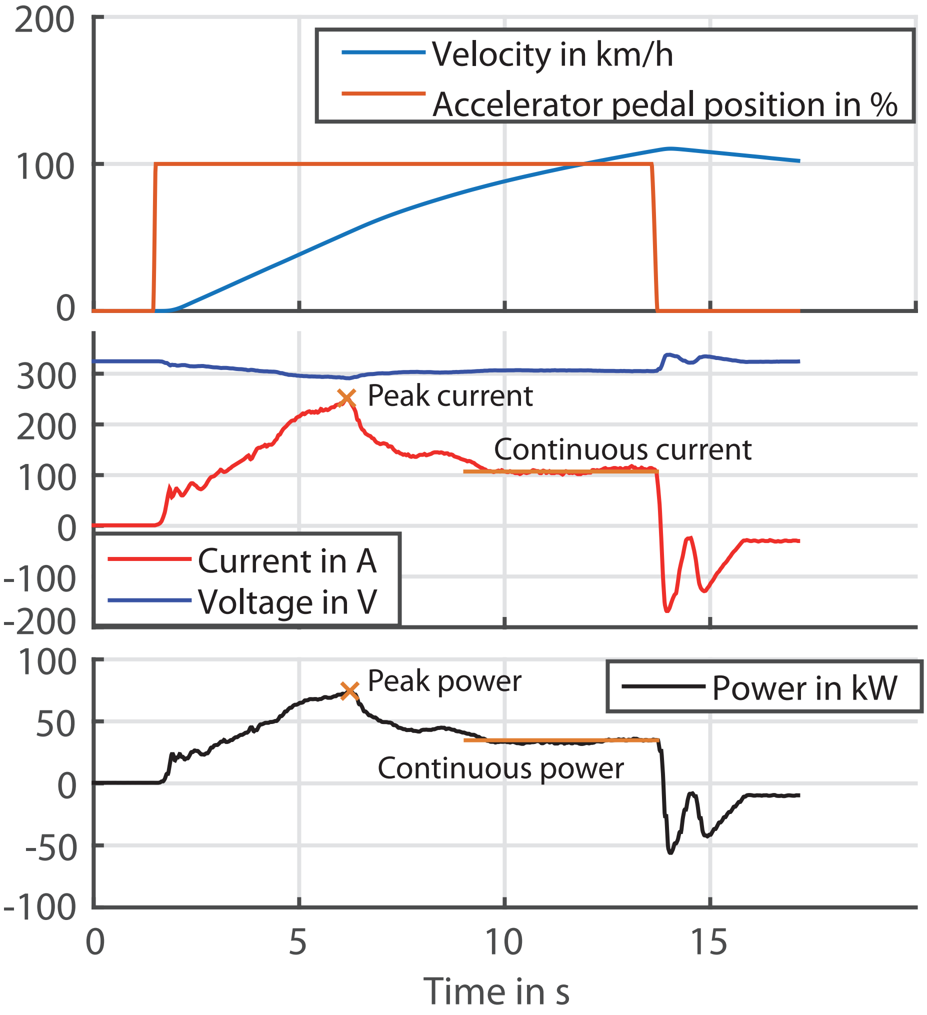

Figure 4.14.: Full load acceleration manoeuvre with battery current, voltage and power.

During a heavy braking or emergency braking the slip of the tyres cannot be neglected. Moreover, the anti-lock brake and electronic stability control system interferes at such manoeuvres. Thus, the maximum recuperation was not achieved. Figure 4.15 shows such a manoeuvre. The starting velocity was about 55 km/h and then the brake pedal is immediately pressed. This results in a recuperation current of about 80 A. Afterwards the vehicle accelerates to over 60 km/h again and the brake pedal is pressed till the vehicle stands still. During this process the control panel was used to estimate the maximum recuperation. It was assumed that with this manoeuvre the maximum peak current could be evaluated.

However, in some full load measurement files very high recuperation currents and power

Table 4.11.: Charging battery characteristics.

	Unit	Mean value	Standard deviation
Peak recuperation current	A	145.75	27.70
Max. recuperation power	kW	48.26	1.00

peaks were detected. These results were also taken into account.
During emergency braking manoeuvres no recuperation current was detected. Consequently, the vehicle does not recuperate during emergency braking. One reason for this behaviour could be a safety issue, since it is better to stop a vehicle immediately than having longer braking distance and a higher SoC in such situations. It is also possible that the high deceleration gradient of the vehicle is to steep to recuperate some energy of the braking manoeuvre. The recuperation current and power limited to about 150 A and 50 kW.

Summary

The battery characteristics were evaluated by heavy braking and full load manoeuvres, respectively. The power limitations are +70 kW and -50 kW. The maximum discharge current is at +250 A and the maximum recuperation current at -150 A. The heavy braking manoeuvres are certainly one of the most difficult manoeuvres to perform and are maybe not suited to achieve a clear measurement results, since the slip of tyres are regulated by the ABS and ESC.

4.7. Evaluation of the Traction Motor

In this chapter the traction motor is evaluated with the help of full load manoeuvres. The reaction time of the traction motor is evaluated as well as the maximum acceleration and maximum acceleration gradients. Furthermore, the time which the test vehicle needs to reach a velocity of 100 km/h from standstill is measured. Figure 4.16 displays a full load manoeuvre. In the upper figure the velocity, the accelerator pedal position, the acceleration and the brake pressure feedback to the driver are shown. The brake pressure feedback is used as an indicator when the brake pedal is released. Since, the brake pedal position was not measured when full load manoeuvres were performed. The value $\tau_{0 \to 100}$ is the acceleration time from 0 to 100 km/h. In the figure below the reaction time of the traction motor t_{trc} is analysed.

Table 4.12 shows the results of traction motor characteristics. The time to reach 100 km/h from standstill is 9.28 s. The reaction time of the traction motor is 0.29 s. According to [7], a combustion engine has a response time between 0.1 and 1 s. An electric motor has a much quicker response time than a conventional ICE. The jerk of the vehicle was evaluated with the acceleration gradient. Jerks are an indicator for driving comfort,

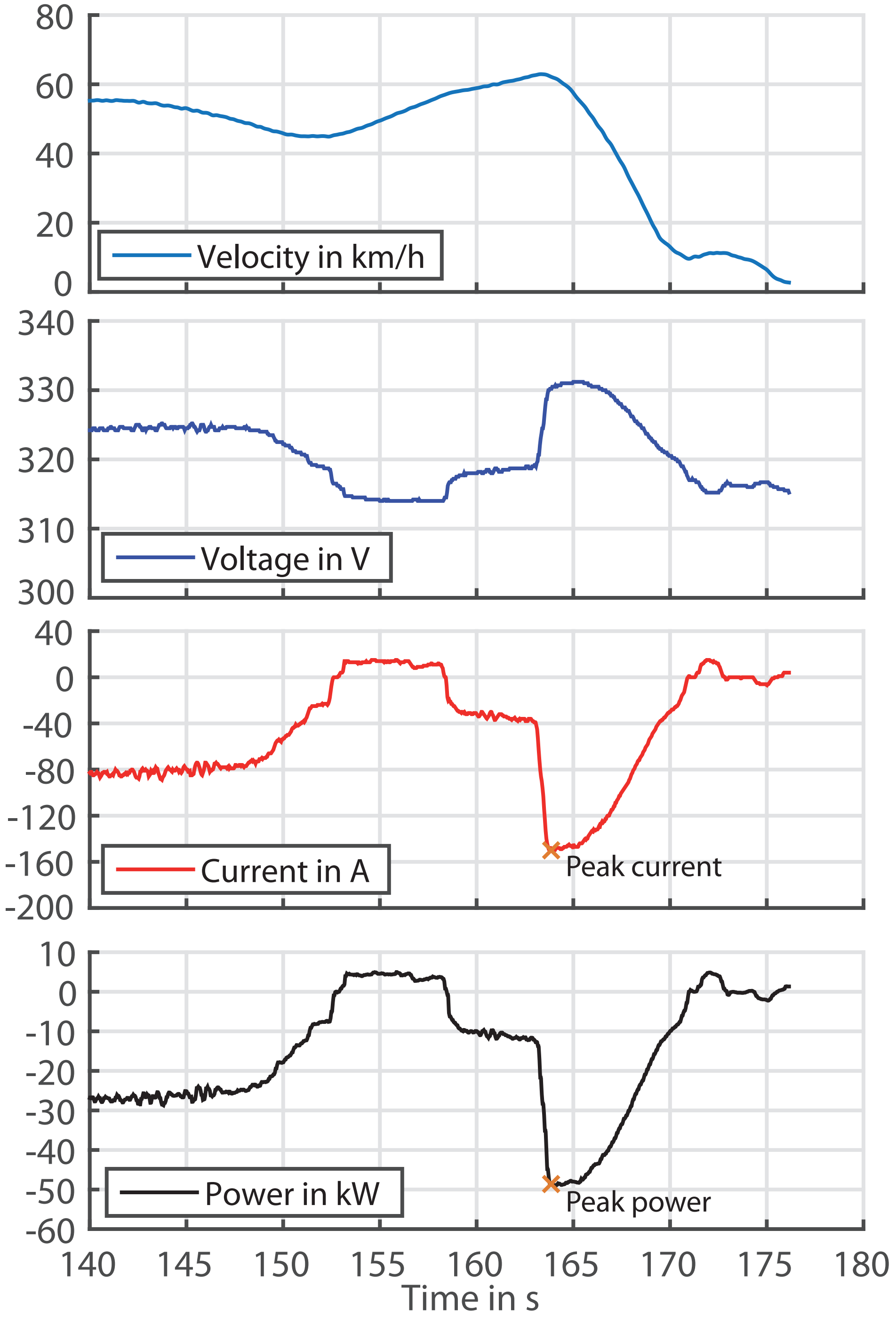

Figure 4.15.: Velocity, battery voltage, battery current and battery power during a heavy braking manoeuvre.

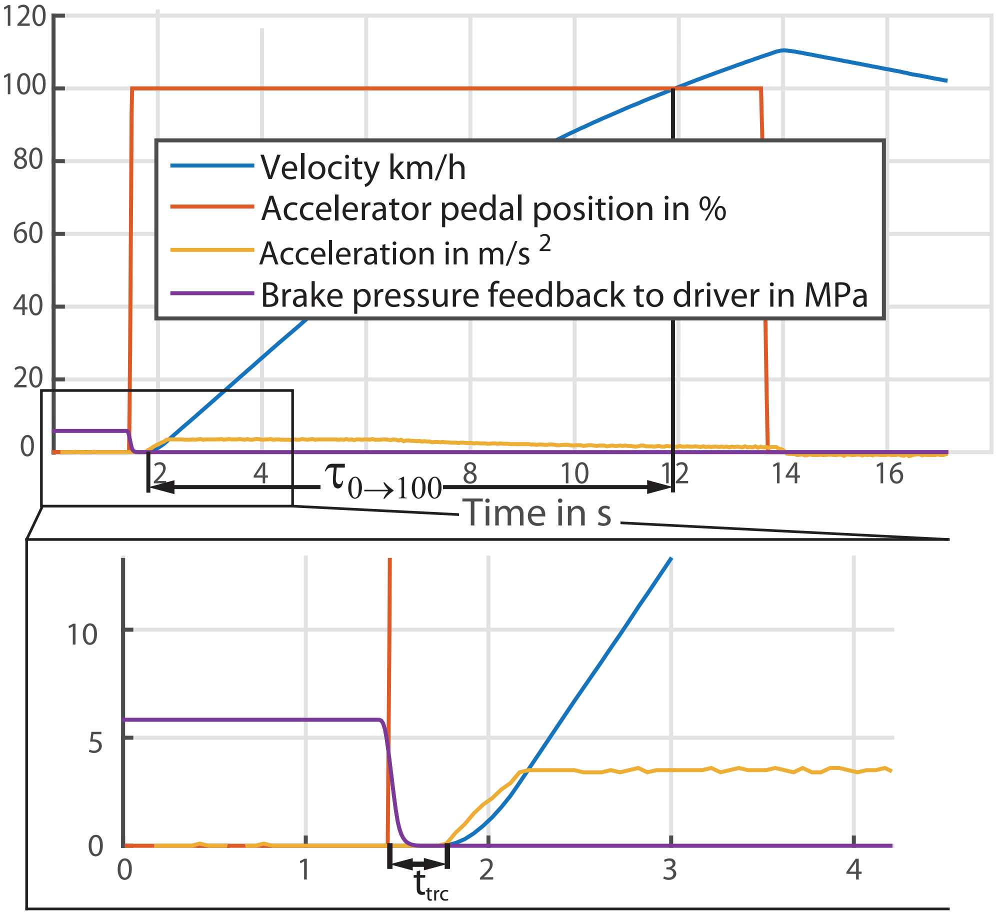

Figure 4.16.: Full load acceleration manoeuvre with the reaction time of the traction motor and the time difference between zero and 100 km/h.

Table 4.12.: Results of the full load manoeuvres.

	Unit	Mean value	Standard deviation
Acceleration time $\tau_{0 \to 100}$	s	9.28	0.74
Reaction time t_{trc}	s	0.29	0.04
Max. acceleration	m/s^2	3.80	0.24
Max. acceleration gradient	m/s^3	7.75	0.79

Table 4.13.: Jerks and comfort levels [25].

Jerks in m/s^3	Comfort level
± 1	Comfortable
± 2	Acceptable
± 10	Only in emergency situations

Table 4.14.: Acceleration time $\tau_{0 \to 100}$.

Vehicle	Acceleration time from 0 to 100 km/h $\tau_{0 \to 100}$ in s
Mercedes CLA 250 [17]	6.6
Mini Cooper S 3 [16]	6.8
BMW i3 [6]	7.2
Nissan Altima 2013 2.5 SL [18]	7.70
Audi A4 Avant 1.4 TFSI [14]	9
Test vehicle	9.28
Lexus CT 200h [16]	10.3

safety and driveability of a vehicle. Hybrid electric and electric vehicles suffer more from jerks than normal gasoline or diesel driven vehicles. Conventional vehicles have sufficient damper elements such as torque converters and flexible joints in the drivetrain [8]. The authors in [25] classify the acceleration gradient into comfort levels, see Table 4.13. The evaluated acceleration gradient is $7.75\,m/s^3$. This is rated as extremely uncomfortable, compare [25]. However, such a manoeuvre describes the performance of the vehicle and not its comfort level. Since, the acceleration gradient was calculated with the deviation of the velocity profile numerical errors occurred. Thus higher values than the real acceleration gradient were determined.

In Table 4.14 acceleration times from 0 to 100 km/h $\tau_{0 \to 100}$ are displayed. In comparison to other vehicles the test car has a relative low acceleration performance. Reasons for that are that the vehicle was loaded with the test equipment and two passengers. Moreover, the drivetrain layout (compare Chapter 1.3) does not enable immediate high traction power (i.e., the ICE has to start up before the traction motor can use the entire propulsion power). The anti-lock brake system and electronic stability control were also activated during all manoeuvres. These safety mechanisms regulate the tyre slip and can therefore decrease the traction power.

Summary

The test vehicle needs about 9.3 s to reach 100 km/h from standstill. Which is in comparison to other vehicle a rather low acceleration performance. Another relevant parameter for the safety and driveability of the vehicle is the acceleration gradient which is

7.75 m/s^3. The analysis shows one advantage of the electric traction motor that is its almost instantaneous dynamic response compared to a conventional ICE driven vehicle.

4.8. Evaluation of the Generator

This chapter analyses the start-up behaviour of the generator. The ICE cannot start on its own and needs a starting motor. The coupled generator can tow-start the ICE. The ICE needs a certain rotational speed at which it can deliver power to the generator or directly to the drivetrain. This starting procedure of the generator and ICE occurs also in other manoeuvres (e.g., driving at too low SoC), but in this chapter the actual results are based only on full load manoeuvres.

The generator is technically an electric motor and has to perform at first as an electric motor to overcome the inertias of shafts and the ICE. The maximum torque $T_{Gen,max}$ is the torque that the generator can produce when it is in motor operation mode. The maximum negative torque $T_{Gen,min}$ is the maximum torque that the generator can produce when it operates in the generation mode. Table 4.15 shows that the minimal and maximum torques are almost the same. Furthermore, the time interval of the generator to reach its maximum torque dt_{Tmax} and to start the ICE dt_{ICE} is determined. Additionally, the rotational speeds at dt_{Tmax} and dt_{ICE} are evaluated. Figure 4.17 gives an example of the start up. At first, the generator starts in motor operation mode to overcome the inertias and to tow-start the ICE. After dt_{ICE} the generator switches from motor to generation operation. Since at this time the idle rotational speed of the ICE is reached and it can produce power itself. This power is then directly delivered to the remainder drivetrain or the generator. The rotational speed of the generator at dt_{end} is about 2370 rpm. Considering the gear ratio between the generator and ICE the rotational speed of the generator corresponds to ICE starting speed given in the data sheet.

Table 4.15.: Results of the generator characteristics of full load manoeuvres.

	Unit	Mean value	Standard deviation
Max. generator torque $T_{Gen,max}$	Nm	84.76	0.12
Time duration dt_{max}	s	0.26	0.03
Rotational speed at t_{Tmax}	rpm	1124.17	148.51
Torque gradient $T_{Gen,max}/dt_{Tmax}$	Nm/s	322.84	40.48
Time duration dt_{end}	s	0.32	0.02
Time duration dt_{ICE}	s	0.58	0.02
Rotational speed at t_{end}	rpm	2376.24	15.56
Min. torque $T_{Gen,min}$	Nm	83.27	1.74
Max. rotational speed	rpm	12082.43	19.54
Min. power	kW	102.85	1.53

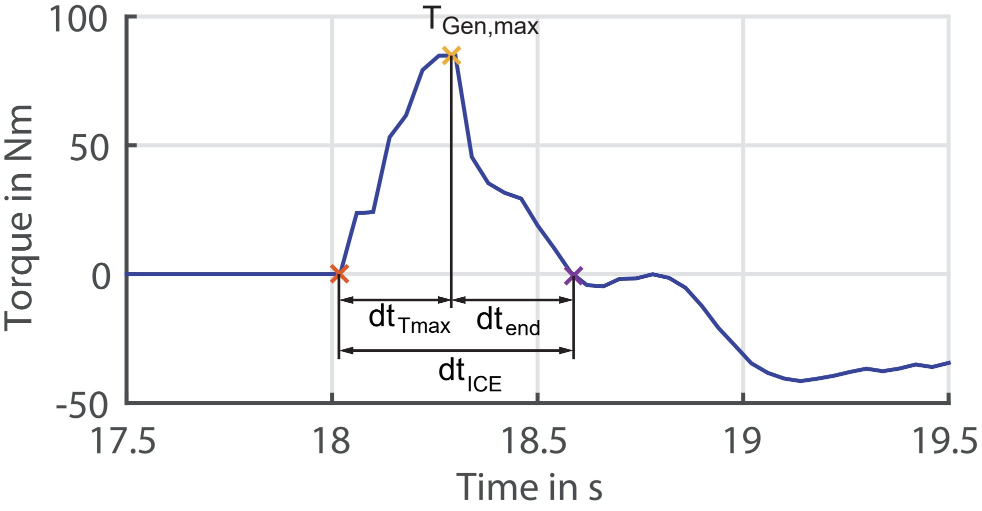

Figure 4.17.: Start up of the generator. Generator torque over time of a full load manoeuvre.

Figure 4.18 displays a full load manoeuvre with the traction motor and generator torques as well as the rotational speeds of the traction motor, ICE and generator. In addition, the battery current and the generator power are given. The torques and rotational speeds are shown component-wise (e.g., no gear ratios are considered). The generator start up was also evaluated with a low SoC of the battery (≈27 %). These situations showed the same start up behaviour. Since the battery cannot solely provide the traction motor the needed traction power, the generator powered additionally the traction motor. During low SoC driving situations, the ICE has to start up more often so that the generator can produce additionally traction power. Figure 4.19 shows such an example with low SoC of the battery. When the traction motor requires high power the generator and the ICE has to start up. The starting procedure of the generator is shown in the sub-plot where the torque is displayed. It has similar behaviour as seen in Figure 4.17.

Furthermore, the generator behaviour is determined in situations where the traction motor changed from propulsion to recuperation mode. At low vehicle speeds the generator did not react to the changes. However, at high speeds (above 100 km/h) the traction motor changed from the propulsion to recuperation mode. The generator converts the energy of the ICE into electrical energy, compare Figure 4.20. At first, the vehicle accelerates to a high velocity and the clutch between the ICE and the drivetrain is closed. In this case all rotational speeds of every single component is similar considering the corresponding gear ratios. However, in Figure 4.20 the operation mode sub-plot displays that the OPM is series mode (OPM 5) but actually the clutch is engaged, thus the vehicle operates in its engine mode (OPM 4). For a more detailed description compare “Observations” in Chapter 4.14.

After the acceleration the vehicle coasts and the traction motor does recuperate the

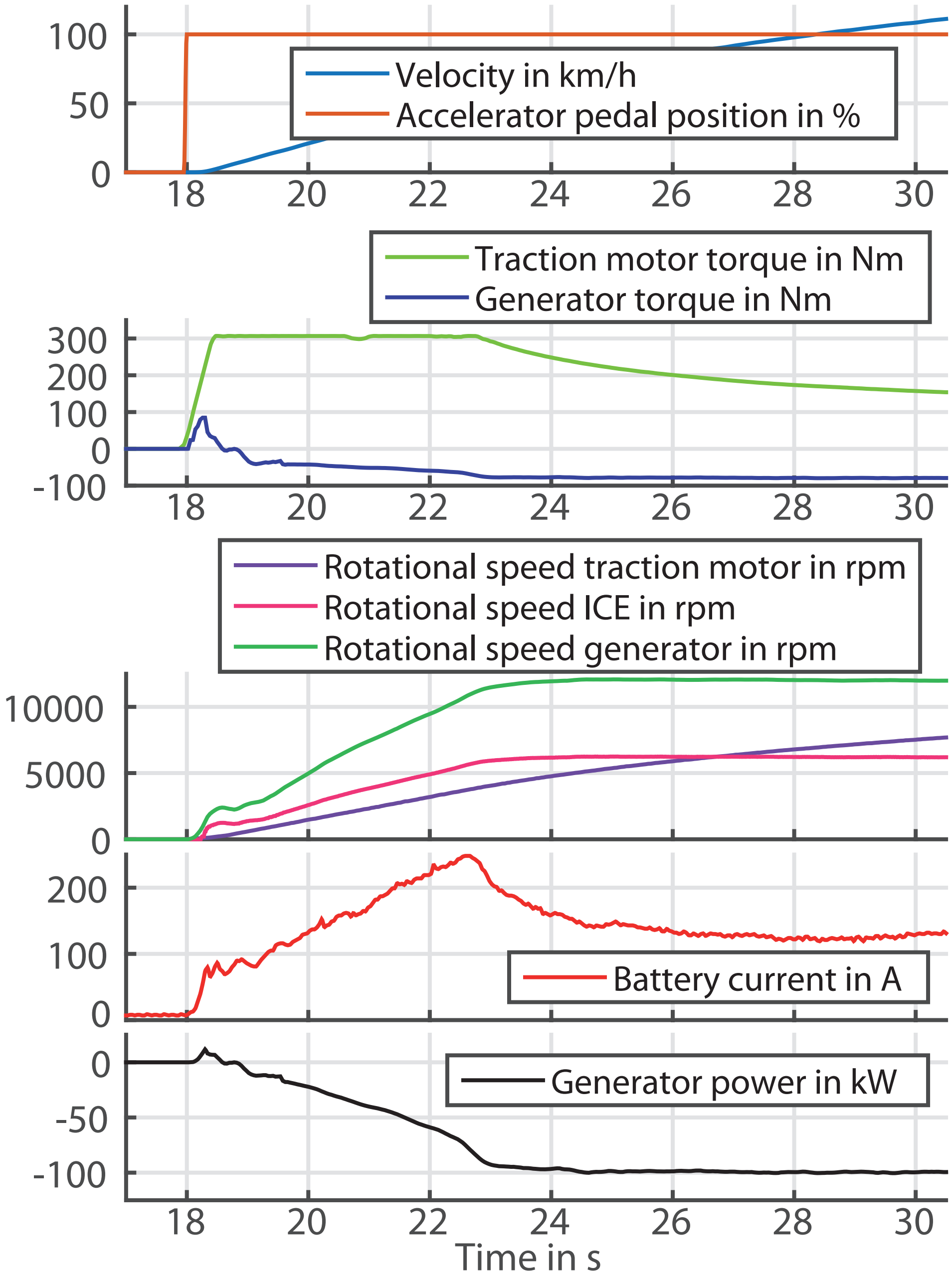

Figure 4.18.: Generator evaluation from a full load manoeuvre

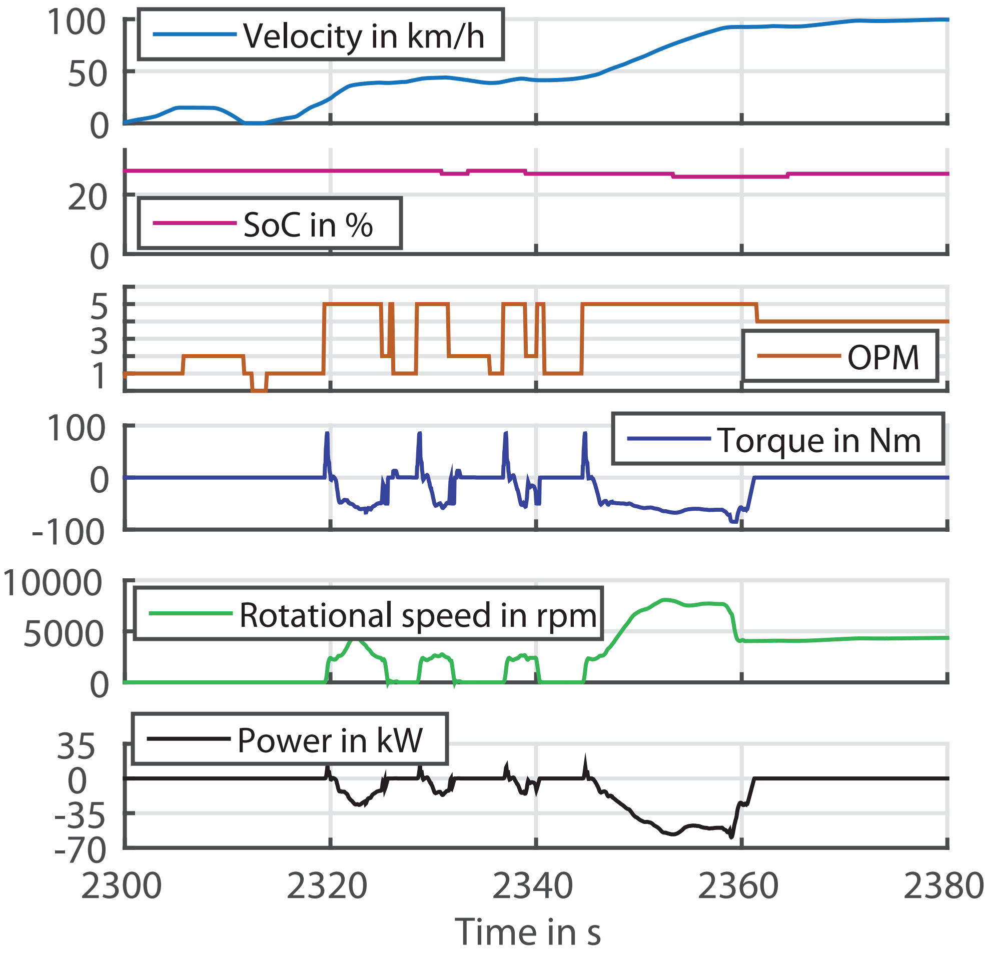

Figure 4.19.: Generator behaviour with low SoC (≈27 %).

driving energy into electrical energy. The vehicle is still in engine mode but the torques from the generator and ICE are zero. After a while the clutch opens and the rotational energy of the ICE is converted by the generator. At 28 s, the generator has a negative torque of about -50 Nm.

Summary

The results of the evaluation of the generator are shown in Table 4.15. The mean time to start the ICE is 0.58 s. At this time the generator has a rotational speed of 2370 rpm, and shifts from motor to generator operation mode. All parameters were evaluated with the help of full load driving manoeuvres. At low battery SoC the generators has to tow start the ICE more often to produce additionally energy by the generator. At higher

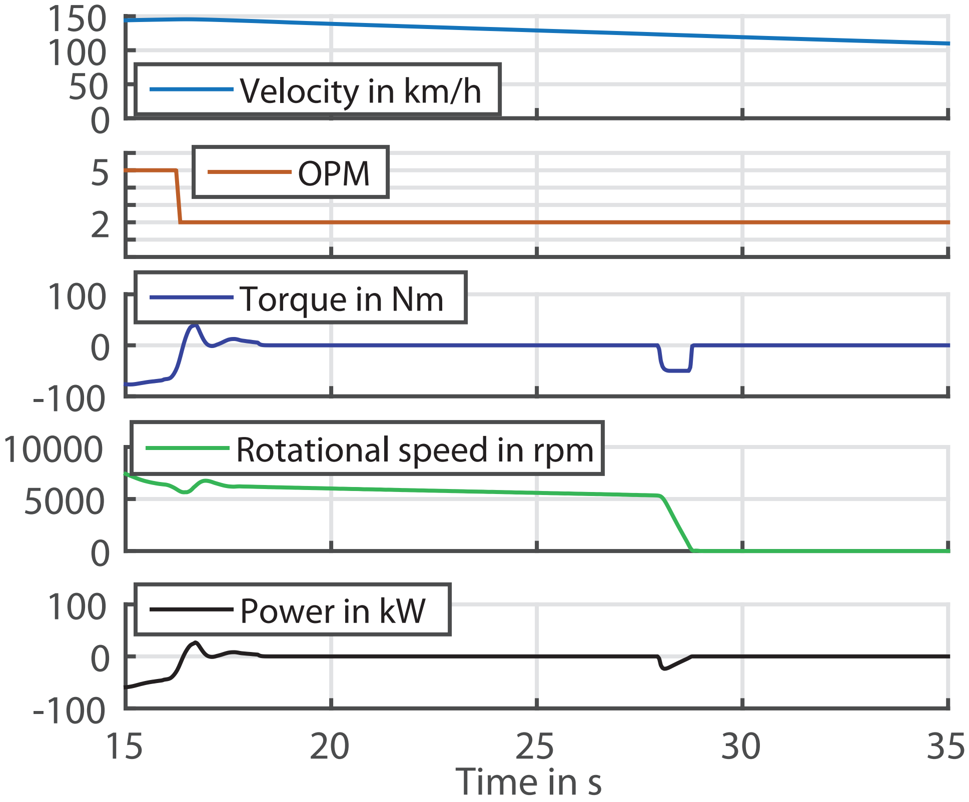

Figure 4.20.: Generator behaviour of switching from engine mode to recuperation mode.

velocities, the clutch is engaged thus the ICE is coupled to the remainder drivetrain, and the traction motor changes from propulsion to recuperation mode. In case of a disengaged clutch the rotational energy of the ICE is then converted to electric energy by the generator. In conclusion, the starting procedure of the generator is always the same independent of the driving state, compare Figure 4.17.

4.9. Driving Resistance

The driving resistance of a vehicle can be presented in two ways. One way is to calculate three coefficients C_0, C_1, and C_2 as shown in Eq. (4.30). These coefficients are described in literature as “street values”, where F_{Res} is the overall driving resistance of the vehicle, C_2 is primarily the drag resistance, C_1 characterizes the linear part of the driving resistance and C_0 forms mainly the rolling resistance [10].

$$F_{Res} = C_2 \cdot v^2 + C_1 \cdot v + C_0 \tag{4.30}$$

Table 4.16.: Results of the coast down manoeuvres.

	C_0 in N	C_1 in N(m/s)	C_2 in N/(m/s)^2
Evaluated coefficients	130.91	4.07	0.33
Reference values (EPA)	102.62	0.796	0.40
Driving resistance coefficients	a_r	$c_d \cdot A_{Front}$	c_d
	-	in $1 \cdot \mathrm{m}^2$	-
	0.008	0.73	0.34

F_{Res}	Overall driving resistance in N
v	Velocity in m/s
C_2	Coefficient which describes primarily the drag resistance
C_1	Coefficient which describes primarily the linear part of the driving resistance
C_0	Coefficient which describes primarily the rolling resistance

Another way to describe the driving resistance is the summation of the drag, slope, and rolling resistances F_{Drag}, F_{Roll}, F_{Slope}, which are defined in Chapter 2.3. In order to evaluate the required coefficients of the driving resistance coast down manoeuvres are performed without engaged gear. No additional driving pedal was activated. Therefore, $T_{Traction}$ and T_{Brake} are zero, compare Eq. (4.31).

$$m \cdot a = -\left(F_{Drag} + F_{Roll} + F_{Slope}\right) + \underbrace{\frac{T_{Traction}}{r_{dyn}}}_{=0} + \underbrace{\frac{T_{Brake}}{r_{dyn}}}_{=0} \tag{4.31}$$

m	Vehicle mass in kg
a	Vehicle acceleration in m/s
F_{Drag}	Drag resistance in N
F_{Roll}	Roll resistance in N
F_{Slope}	Slope resistance in N
$T_{Traction}$	Traction torque in Nm
T_{Brake}	Brake torque in Nm
r_{dyn}	Dynamic tyre radius in m

In Figure 4.21 the velocities of the performed coast down manoeuvres are plotted. Two of eight tests were unsuccessful, because of the irregular progression of the velocity. The difference between the failed and successful attempts is caused by a big slope differences of the test streets, wind gusts or varying road conditions. Other influences of the driving resistances are weather impacts like rain, snow, hail and even the ambient temperature.

Table 4.16 presents the coefficients of the coast down manoeuvres. The parameters are calculated with the least square method, compare Chapter 2.4. With the help of the determined coefficients the overall driving resistance was calculated, see Figure 4.22. In

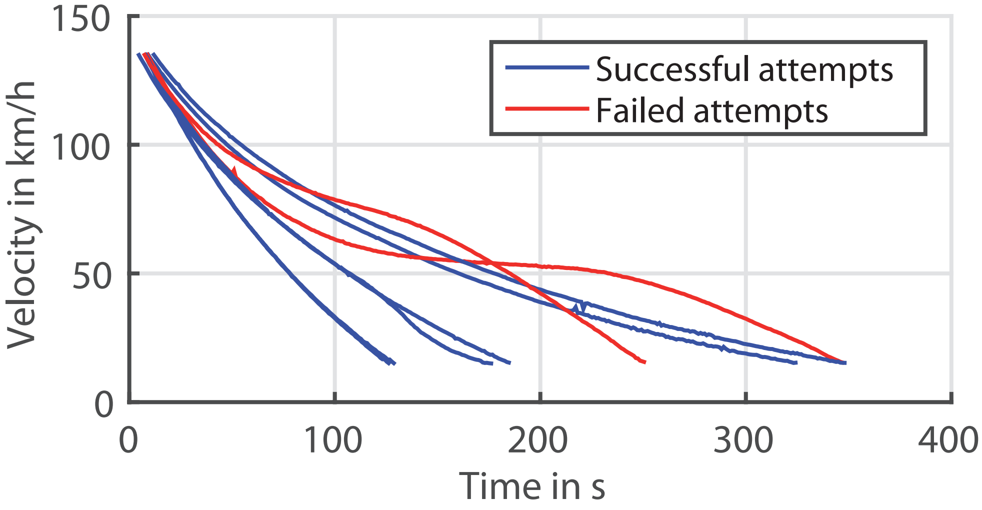

Figure 4.21.: The velocities of eight coast down manoeuvres. Two of the eight are failed coast down attempts.

the table the “street” values and additionally the reference values of the *Environmental Protection Agency* (EPA) are given. Furthermore, the resistance coefficients for F_{Drag}, F_{Roll} and F_{Slope} are shown. The product $c_d \cdot A_{Front}$ includes the frontal area of the test vehicle. It was not possible to determine the frontal area of the manufacturer. Consequently, a value of $2.1\,\mathrm{m}^2$ is estimated. With this assumption the drag coefficient c_d was calculated.
Passenger cars have frontal areas in the range of 1.5 to $2.5\,\mathrm{m}^2$. A low rolling resistance tyre in 2008 had a rolling coefficient a_r of 0.008 at low velocities. In 2030 tyres with a coefficient of 0.004 will be expected. The drag coefficient c_d is in the range of 0.24 to 0.4. [3]

The total driving resistance is calculated once with the “street values” with all coast down attempts. Furthermore, the driving resistance is calculated with only the successful attempts and once with the reference values, given in Table 4.16. The higher rolling resistance occurs due to winter tyres which were mounted on the test vehicle. They cause an offset in the overall driving resistance, compare Figure 4.22. As mentioned before wind gusts, slopes and other weather conditions have an impact on the calculated resistances. The real driving velocity is measured via a GPS-Antenna that is attached onto the vehicle. However, this antenna and the needed cabling influences the drag coefficient significantly. The coefficient calculation with all attempts led to negative result for the primarily linear driving resistance. Thus, the progression of the resistance with all attempts is partial decreasing, compare the red line in Figure 4.22.

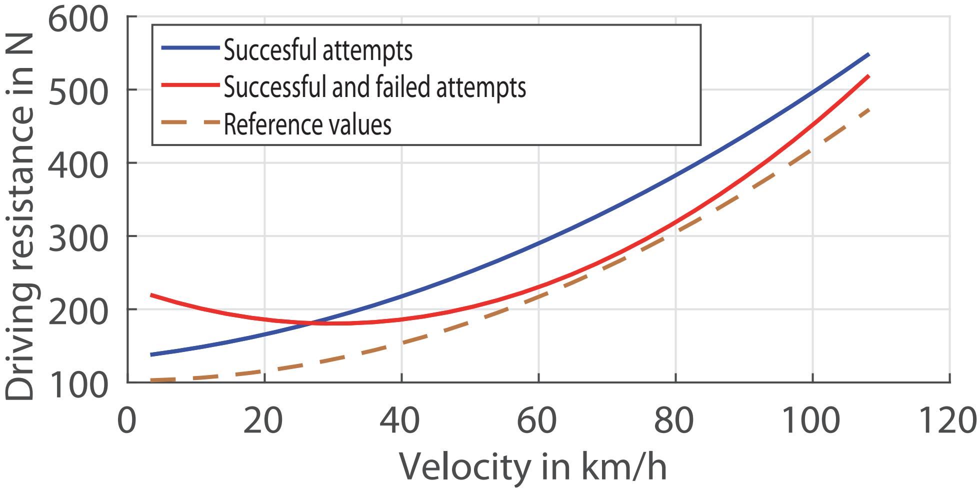

Figure 4.22.: The overall driving resistance was calculated either with only successful or all attempts. Furthermore, it was calculated with the reference values given by the institution EPA.

Summary

The total driving resistance of a vehicle can be calculated through the velocities of coast down manoeuvres without a gear engaged. The method of least squares was used. The results of the coefficients are represented in Table 4.16. Figure 4.22 shows the overall driving resistance, once calculated with all attempts, once only with the successful attempts and once with the given reference values. More successful attempts lead to more accurate results. The coefficients with only successful attempts differ from the reference values, since the reference values were evaluated with the help of a test bench. For this the vehicle has to spend 24 hours in the test bench area under predefined conditions to acclimatise. This was not the case with the performed real driving manoeuvres. There slopes and weather impacts influence the coast down manoeuvres. Furthermore, a GPS-Antenna was attached to the vehicle, which increased the drag coefficient. In addition, the vehicle was equipped with winter and not with summer tyres. This explains also the difference between the in the values given in Table 4.16. All influences mentioned before explain the different curves in Figure 4.22.

4.10. Operation Strategy

A hybrid electric vehicle needs an intelligent operation strategy in order to increase fuel efficiency. The operation strategy was evaluated with a combination of constant velocity, constant accelerator pedal position, quasi-static acceleration and quasi-static velocity manoeuvres. The results of these manoeuvres are gathered and displayed in a so called pedal map. In the following chapter an “increasing” and “decreasing” pedal are introduced. Whereas the "increasing" pedal map indicates constant (but positive) acceleration or constant accelerator pedal positions. In contrast, the "decreasing" pedal map is characterised by constant (but negative) acceleration or negative pedal positions. In real driving situations not all load points can be achieved. Therefore, the results of a test bench are included in the pedal maps.

The operation strategy is influenced by the following parameters:

- Driving with D(rive) or B(rake) mode
- HV button on/off
- ECON button on/off
- Auxiliary units
- Accelerator pedal
- Braking pedal
- Driving velocity
- Acceleration
- State of charge of the battery
- External circumstances like weather and street conditions

The test vehicle, gives the opportunity to select between the D(rive) mode or B(rake) mode. Drive mode is used for normal driving. In brake mode the regenerative braking while driving down hill or coasting is increased. Is the HV button pressed, the vehicle drives at low to moderate speeds solely electrical. If the HV button is pressed for more than 3 s the ICE is starts and charges the battery while idling. By pressing the ECON button the vehicle provides a visualisation of the driving style and the fuel efficiency. Furthermore, the performance of the climate system is adjusted to increase fuel efficiency. The auxiliary units (e.g., heater, air condition, radio) influence the battery SoC or increases the load of the ICE.

Static pedal map

A static pedal map is determined if one load point is measured and maintained for a few seconds. At this point the operation mode should not change. A transition between operation modes are located if two nearby load points have different operation modes. Many static load points must be determined at the border of two operation modes areas. This method is visualized in Figure 4.23. The red points represent different load points. The various colours represent the different operation modes. This method has a big drawback, in particularly it is time intensive, since every load point has to be reached separately.

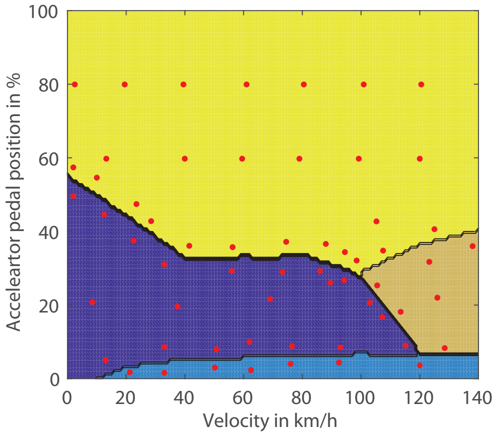

Figure 4.23.: Static pedal map. The various colours represent different operation modes. The red points represent different load points.

Quasi static pedal map

If a slightly increasing or decreasing accelerator pedal position as well as an increasing or a decreasing velocity are allowed a quasi-static pedal map can be identified. Therefore, with one driving manoeuvre more transition points can be obtained. In Table 4.17 a list of all possible configuration are shown. Where red is the transition of the operation mode, green is the velocity v and blue is the accelerator pedal position APP. Configuration 1, 2 and 3 represents the transition for the "increasing" pedal map and 4, 5 and 6 for the "decreasing" pedal map. Number 3 and 6 are difficult to achieve. Figure 4.24 clarifies the approach of a quasi-static pedal map. One arrow represents one driving manoeuvre. The various colours in the map represents the different operation modes. On the left side of the figure manoeuvres with a slightly increasing velocity and pedal position are represented. The driving manoeuvre is selected in such way that a transition from one operation mode to another is performed. With this method a quasi-static pedal map in real driving situations is obtained. On a test bench the velocity or the accelerator pedal position can be maintained constant. This is shown on the right side of Figure 4.24. The same procedure is made with decreasing velocities and accelerator pedal position for the "decreasing" pedal map.

Many different parameters influence the operation strategy. Thus, for the quasi-static pedal map restrictions are made. The HV and ECON button, compare Chapter 4.10, are off during all test manoeuvres as well as auxiliary unites, except lights and other safety units. The vehicle is only driven in driving mode D. The pedal map is limited to 140 km/h. The brake pedal should not be activated during the driving manoeuvres,

Table 4.17.: List of all possible driving manoeuvres. Green: Velocity v of the vehicle; Blue: Accelerator pedal position APP; Red: Transition of the operation mode.

Nr.		Description
1	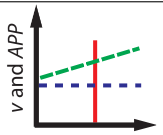	v = increasing $APP \approx$ constant
2	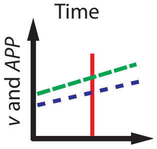	v = increasing APP = increasing
3	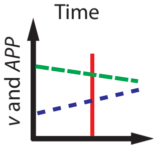	v = decreasing APP = increasing
4	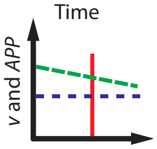	v = decreasing $APP \approx$ constant
5	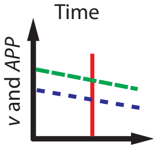	v = decreasing APP = decreasing
6	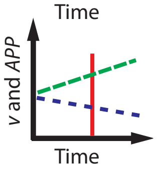	v = increasing APP = decreasing

except in hazardous situations. The acceleration should not be greater than $\pm 0.25\,\mathrm{m/s^2}$[3] and the accelerator pedal position should not change rapidly. During the assessment of the first driving manoeuvres it was evaluated that the operation strategy hardly changes while driving above a SoC of 27 %. Therefore, the pedal maps are evaluated for below and above a SoC of 27 %.

For the following figures the operation mode classification is again highlighted, compare Chapter 1.3:

- Electric Drive → OPM 1
- Recuperation mode → OPM 2

---

[3] With an acceleration of $\pm 0.25\,\mathrm{m/s^2}$ the increase or decrease of the velocity can be neglected.

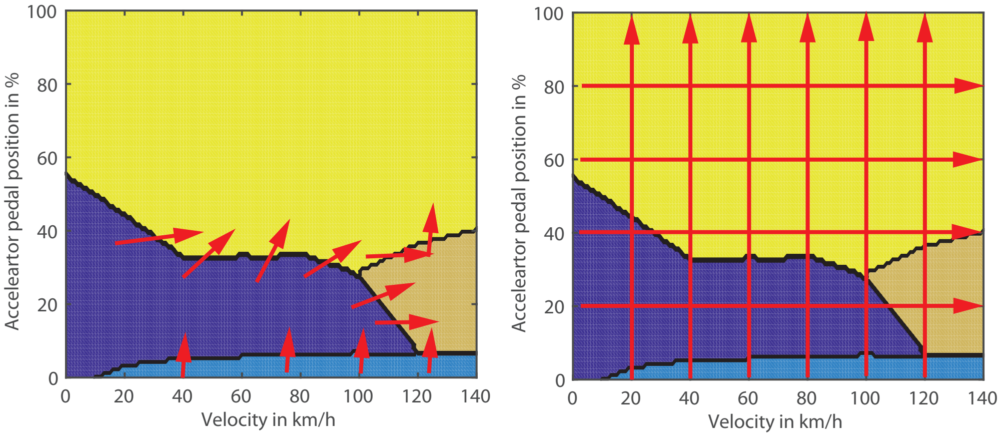

Figure 4.24.: Left: Quasi-static pedal map for real driving manoeuvres with driving manoeuvres just over the transition. Right: Quasi-static pedal map on a test bench with driving manoeuvres with constant APP or v. The different colours represent different operation modes. Red arrows represent quasi-static manoeuvres.

- Idling mode → OPM 3
- Engine mode → OPM 4
- Series mode → OPM 5

4.10.1. Evaluation of the Operation Strategy on the Test Bench

The advantage of a test bench is that a certain velocity can be set and the accelerator pedal position can be changed. Or the pedal position can be hold and the velocity can increase or decrease. The test bench manoeuvres were performed from 20 to 140 km/h in steps of 20 km/h and the accelerator pedal was changed from 0 to 50 % in 10 % steps. Figure 4.25 represents the results of transition points of the test bench manoeuvres. On the left side the points with a battery SoC below 27 % and on the right side above are shown. Since some transition points are evaluated multiple times the average value of these are calculated.

4.10.2. Evaluation of the Operation Strategy in Real Driving Condition Manoeuvres

In real driving manoeuvres it is difficult to repeat the exact same load points, due to changing driving situations. However, if a similar manoeuvre is performed the transition

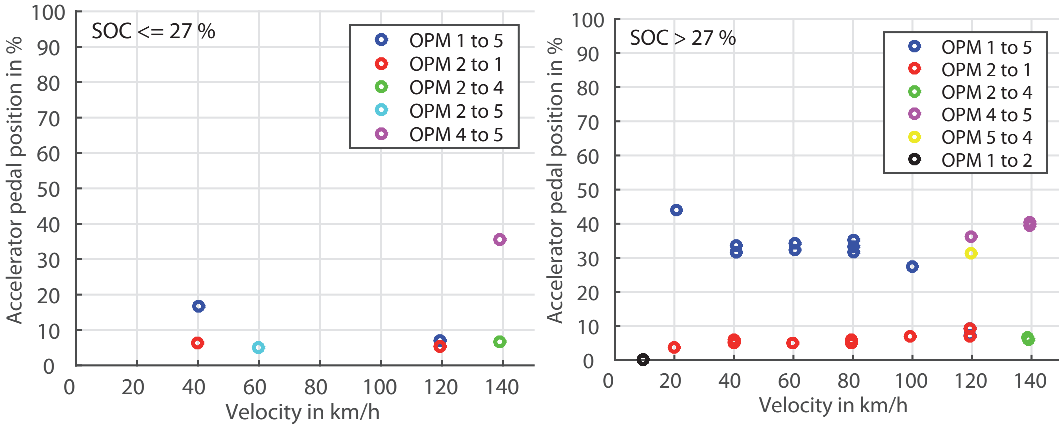

Figure 4.25.: Transition points achieved from the test bench.

point of the operation mode should accumulate in the same area. In the following figures only the transition points and pedal map of SoC values above 27% are represented. The results for a lower SoC and the “decreasing” pedal map are shown in the Appendix (A.1, A.2). With the “increasing” and the “decreasing” pedal maps a combined pedal map with a hysteresis can be determined, compare Appendix A.3. Figure 4.26 is divided into four sub figures. Sub-figure 1 displays all transition points of every quasi-static manoeuvre. As mentioned before it is assumed that similar manoeuvres results in similar transition points. The transition points of sub-plot 1 are averaged in 5 km/h intervals and displayed in sub-figure 2. In addition to the transition points of the driving manoeuvres in real situations the transitions of the test bench are shown and included in sub-figure 3. With further optimisation a pedal map is constructed as represented in sub-figure 4.

Summary

Pedal maps can either be obtained by static or quasi-static driving manoeuvres. Since it is easier and more time efficient quasi-static manoeuvres are used in this thesis. The operation modes depend on all kind of influences, thus restrictions were introduced (e.g. , driving mode D, accelerations up to 0.25 $\mathrm{m/s^2}$, HV button off). During the evaluation of the real driving manoeuvre not all transition can be achieved. Therefore, in the quasi-static pedal map the transition points of the test bench are also included. Furthermore, the operation strategy does not change significantly at a battery’s SoC above 27 %. The quasi-static “increasing” pedal map above 27 % SoC is displayed in sub-figure 4 in 4.26. The “decreasing” pedal map can be found in the Appendix A.1 as well as the pedal maps for below 27 % A.2. When the “increasing” and “decreasing” pedal map is combined a pedal map with a hysteresis can be obtained, compare Figure A.3.

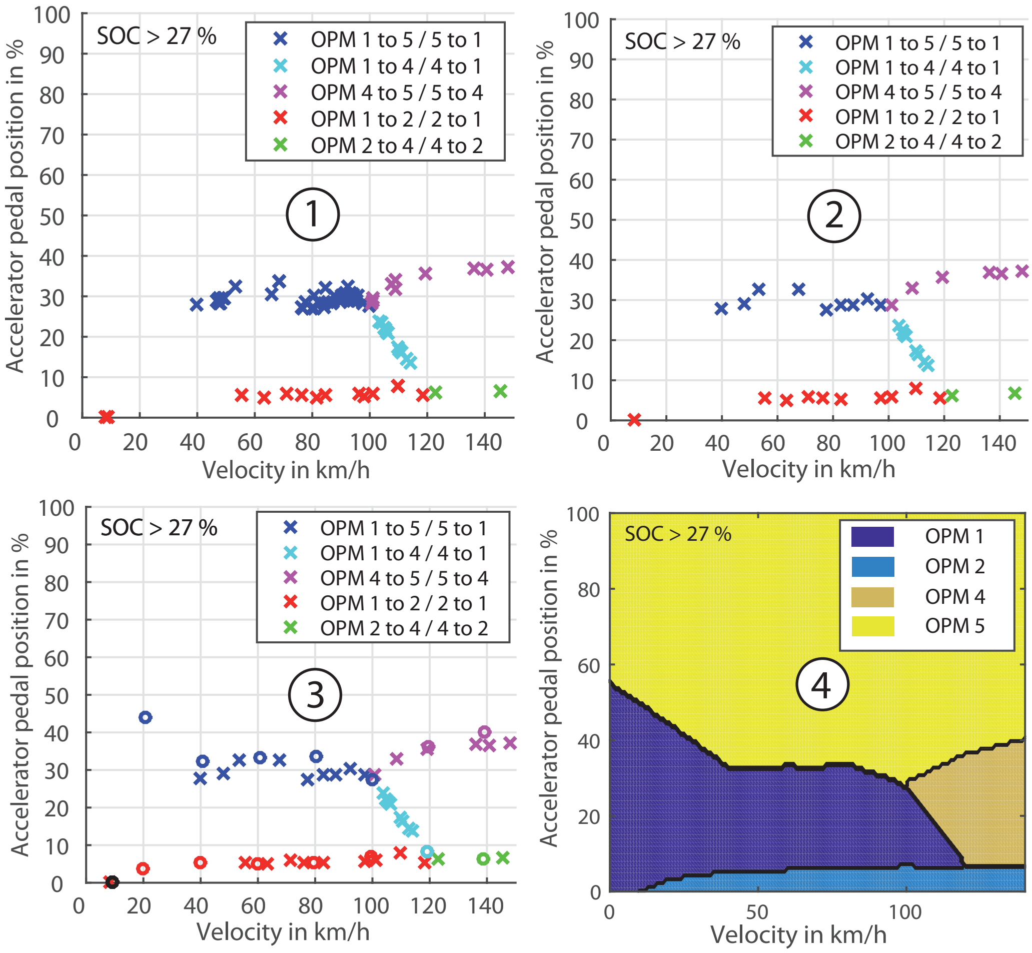

Figure 4.26.: Quasi static "increasing" pedal map for real driving manoeuvres. 1: All transition points from real driving situations. 2: The points are averaged with a 5 km/h increment. 3: Additionally, the transitions points from the test bench are included. 4: With further optimisation the quasi-static pedal map is obtained.

4.11. Braking / Recuperation Strategy

In addition to the operation strategy (positive torque), the braking strategy (negative torque) of the vehicle has a major impact on the performance of a HEV. Therefore, different braking, coast down and recuperation manoeuvres were analysed. The total braking torque T_{Total} consists of the recuperation torque and the braking torque. The recuperation torque $T_{Traction}$ represents the proportion of the total braking torque that the traction motor can recuperate. The rest is converted into heat by the conventional friction brakes T_{Brake}.

The braking torque is defined as negative, therefore in Eq. (4.32) it is added to $T_{Traction}$. A restriction is that the brake torque must be greater than -250 Nm on the axle otherwise it is set to zero. The reason is that 250 Nm on every brake corresponds to 62.5 Nm at each tyre. This is interpreted as torque ripple and is thus neglected. With the equation of motion the brake and total torque are calculated. The traction motor torque $T_{Traction}$ is known due to a measurement signal.

$$(m \cdot a) \cdot r_{dyn} = -\left(F_{Drag} + F_{Roll} + F_{Slope}\right) \cdot r_{dyn} + T_{Traction} + T_{Brake} \tag{4.32}$$

$$T_{Brake} = \left(F_{Drag} + F_{Roll} + F_{Slope}\right) \cdot r_{dyn} - T_{Traction} + (m \cdot a) \cdot r_{dyn} \tag{4.33}$$

$$T_{Total} = T_{Brake} + T_{Traction} \tag{4.34}$$

a	Acceleration in m/s^2
m	Vehicle mass in kg
T_{Total}	Total braking torque in Nm
T_{Brake}	Braking torque in Nm
$T_{Traction}$	Traction motor torque in Nm
r_{dyn}	Dynamic wheel radius in m
F_{Drag}	Drag resistance in N
F_{Roll}	Roll resistance in N
F_{Slope}	Slope resistance in N

Figure 4.27 shows the braking strategy with is evaluated with different braking manoeuvres. Different manoeuvres led to similar braking behaviour. The red line represents the maximum recuperation torque of the traction motor. All measured and calculated values correspond to the axle level (e.g., all necessary gear ratios are considered). The blue points are the recuperation torque of the traction motor and the cyan points are the total braking torque that the driver requires for braking. The remainder is converted into heat by the conventional friction brakes. The traction motor has its maximum recuperation power between 6 and 54 km/h. At higher velocities the recuperation power is falling with its given maximum recuperation torque, due to the given motor characteristics. The two cyan lines that are more than five times higher than the limit of the traction motor are emergency braking manoeuvres. As mentioned in Chapter 4.6.2 the traction motor does not recuperate at such braking manoeuvres. Figure 4.28 displays the evaluated recuperation strategy. In general, the vehicle tries to recuperate any torque that is in area 1. Any torque higher (area 2) is converted by conventional friction brakes. The torque is normalised to the maximum possible recuperation torque. In situations where the total torque is in the recuperation area but the brake pedal is pushed rapidly the vehicle may not recuperate the braking energy.

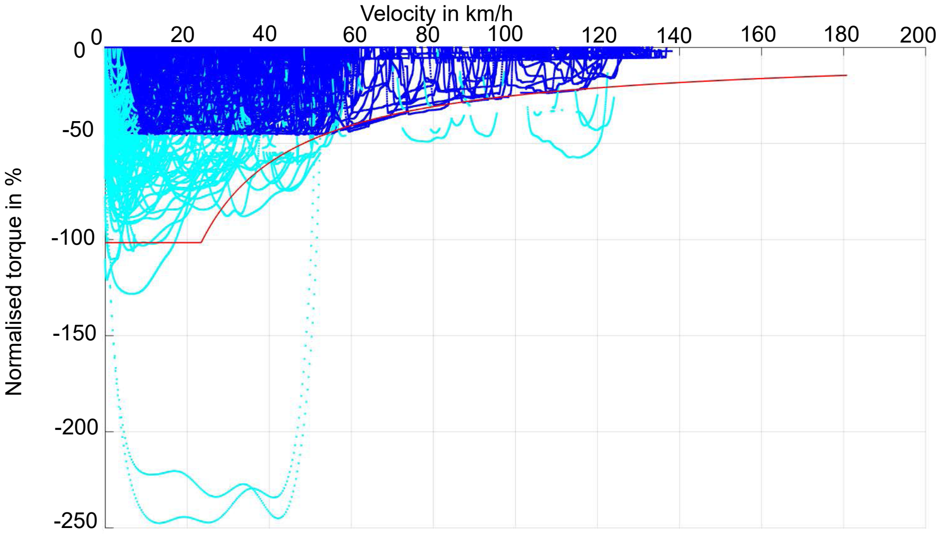

Figure 4.27.: Braking strategy. The cyan points represent the braking torque, the blue points the traction motor torque and the red line the max. recuperation characteristic of the traction motor.

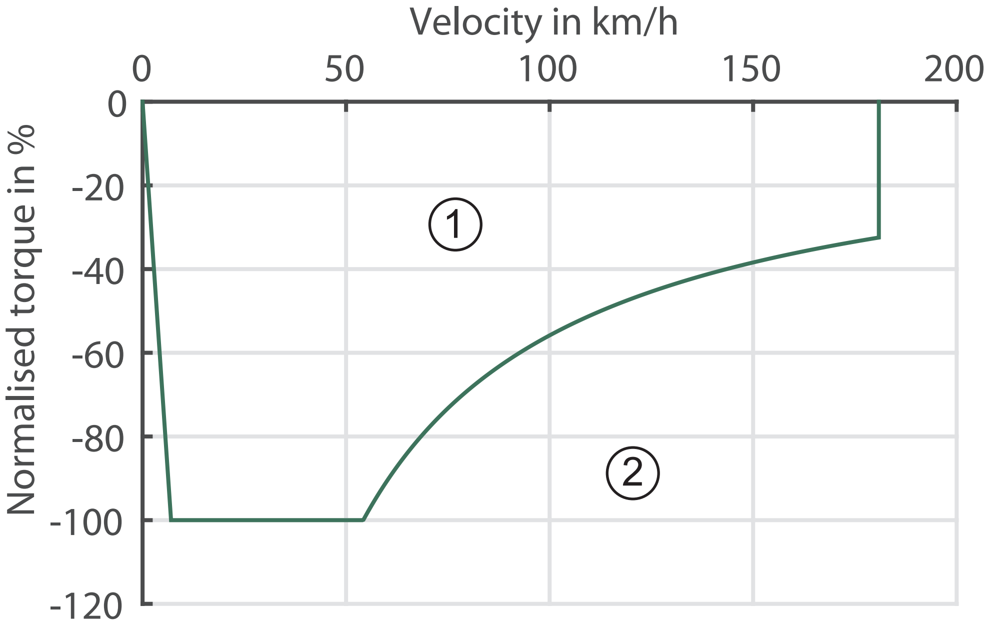

Figure 4.28.: Traction motor recuperation limit.

Summary

Different braking manoeuvres allow the determination of the braking strategy, compare Figure 4.27. The current and power limitations of the battery limit the recuperation overall potential. As a conclusion, the braking strategy attempts to recuperate the braking energy if possible for the traction motor. But there are exceptions e.g., when the brake pedal is pushed rapidly. The possible influence of tyre slip is neglected. Moreover, it is assumed that no interference of ABS or ESC occur.

4.12. Drivetrain Inertia

The drivetrain inertia is determined with full load accelerations with the method of least squares. The rotational and translational equation of motion using the correlation of the drivetrain inertia in Chapter 2.2 reads:

$$\left(1+\frac{\Theta}{m \cdot r_{dyn}^2}\right) m \cdot a = -\left(F_{Drag}+F_{Roll}+F_{Slope}\right)+\frac{T_{Traction}}{r_{dyn}}+\frac{T_{Brake}}{r_{dyn}} \tag{4.35}$$

m	Vehicle mass in kg
r_{dyn}	Dynamic tyre radius in m
Θ	Drivetrain inertia in kgm^2
a	Vehicle acceleration in m/s^2
F_{Drag}	Drag resistance in N
F_{Roll}	Roll resistance in N
F_{Slope}	Slope resistance in N
$T_{Traction}$	Traction motor torque in Nm
T_{Brake}	Braking torque in Nm

When calculating the inertia it is important that only a positive or a negative acceleration occurs. Otherwise, it is inaccurate due to the alternation of the acceleration. The inertia is evaluated with an acceleration manoeuvre, thus the brake torque is zero. The traction motor has a fixed gear ratio to the wheels and is therefore always coupled to the driven wheels, thus Θ is the sum of the inertias of the drivetrain. This includes the inertia of the gears, the transmission, the traction motor and the wheels. The ICE is only connected to the drivetrain in rare cases. Thus, for further simulations the ICE inertia is estimated. The drivetrain inertia is relative small in comparison to the vehicle inertia and therefore influenced easily . At first, the drivetrain inertia was calculated with coast down manoeuvres without an engaged gear. When the inertia is calculated while coasting then $T_{Traction}$ in Eq. (4.35) is zero since the traction motor does not drive the wheels. In this case the drag coefficient, rolling resistance and the inertia are unknown. Those parameters were determined with the method of least squares. However, the inertia was negative and the drag and rolling coefficients too high. A constraint least square method was used instead, where no negative values are allowed and the roll and drag coefficients have to be in a certain predefined range. Again, no reasonable results were obtained.

Therefore, instead of the coast down manoeuvres full load acceleration manoeuvres were chosen where only positive accelerations occur. In addition, the following assumptions were made to simplify the equation and therefore the solution.

Assumptions:

- $A_{Front} = 2.1\,\mathrm{m}^2$
- $a_r = 0.008$
- $c_d = 0.3$
- No transmission losses

The drag coefficient value c_d is assumed to be in the range of 0.3 ± 0.1 [15], [20] for the test vehicle. In the calculation of the coast down manoeuvre a drag coefficient of 0.34 is calculated with an assumed front area of $2.1\,\mathrm{m}^2$. The assumption that the transmission has no losses is feasible because the inertias of the gear and the transmission shafts can be neglected in comparison to the inertias of the traction motor and wheels. The calculated inertia is based on the axle level and not on the traction motor level, compare Eq. 2.16. Reformulating Eq. (4.35) leads to:

$$\underbrace{-\left(F_{Drag} + F_{Roll} + F_{Slope} + m \cdot a\right) + \frac{T_{Traction}}{r_{dyn}^2}}_{\mathbf{z}} = \underbrace{\frac{a}{r_{dyn}^2}}_{\mathbf{A}} \cdot \underbrace{\Theta}_{\hat{\mathbf{x}}} \tag{4.36}$$

With the least square method described in Chapter 2.4 the inertia $\Theta = 0.14\,\mathrm{kgm}^2$.

$$\hat{\mathbf{x}} = \left(\mathbf{A}^T\mathbf{A}\right)^{-1}\mathbf{A}^T\mathbf{z} \tag{4.37}$$

Summary

The inertia is calculated with the least square method and full load acceleration manoeuvres. In addition, some assumptions have been made and an inertia of $\Theta = 0.14\,\mathrm{kgm}^2$ is calculated. According to [7], an ICE with an open clutch is in the range from 0.15 to $0.30\,\mathrm{kgm}^2$. Powerful electric motors are in the same range.

4.13. Brake Release Torque, End Velocity and Time

If the brake pedal is released the vehicle creeps. The brake release manoeuvre is described in Chapter 3.8. Figure 4.29 shows the torque of the traction motor depending on its rotational speed or the vehicle speed. Table 4.18 represents all results. These results are mean values of four measurements. Furthermore, in Figure 4.29, the torque from some measurements are not converting towards zero. This can be explained that all manoeuvres were performed in a parking area with a certain slope.

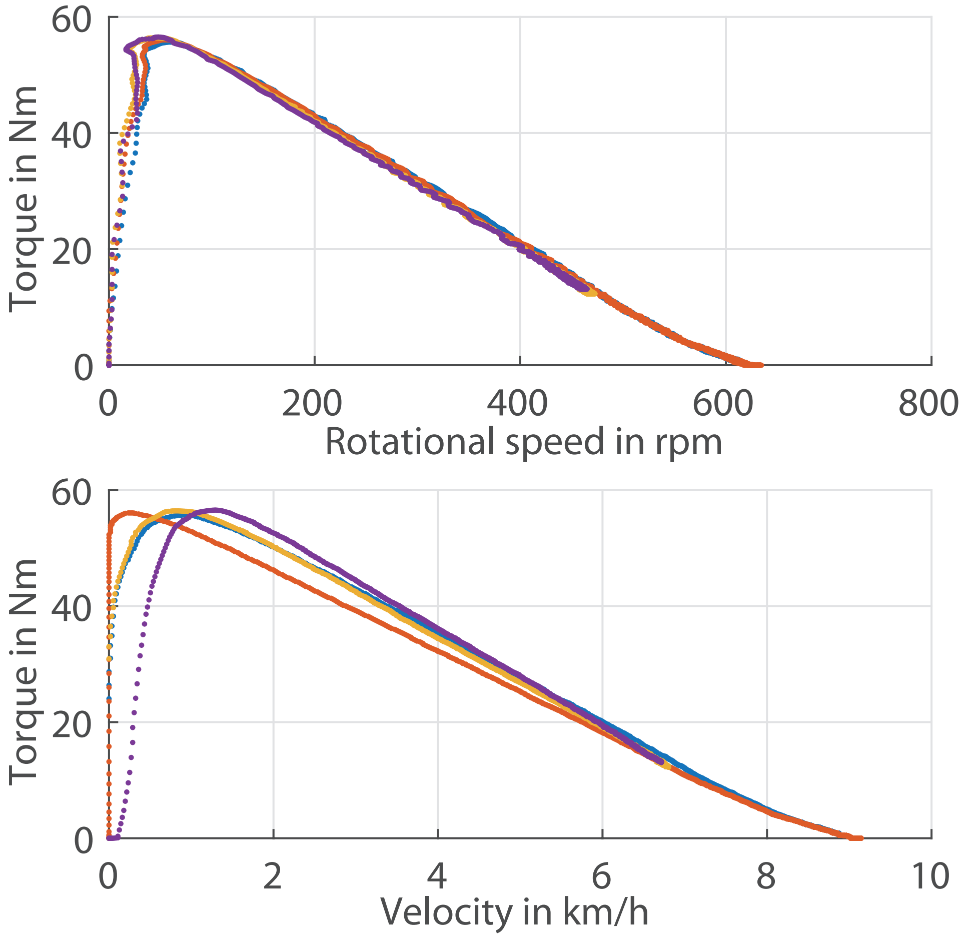

Figure 4.29.: Torques from brake release manoeuvres correlated to the traction motor.

In Figure 4.30 the acceleration and the velocity of a brake release manoeuvre is shown. The maximum creeping velocity $v_{BR,max}$ is reached when the acceleration is zero for the first time. The end velocity $v_{BR,end}$ represents the final creeping velocity. It is defined as 99 % of the maximum creeping velocity $v_{BR,max}$. The parameter τ_{BR} represents the time which is needed to reach the end velocity. In Table 4.18 the parameters are shown. In addition to the velocities and time the maximum torque $T_{BR,max}$, acceleration a_{BR} and acceleration gradient $\dot{a}_{BR}$ are displayed. The maximum torque is influenced by the slope and rolling resistances as well as the inertias of the drivetrain. The drag resistance is negligible, because the velocity is relatively low (<10 km/h).

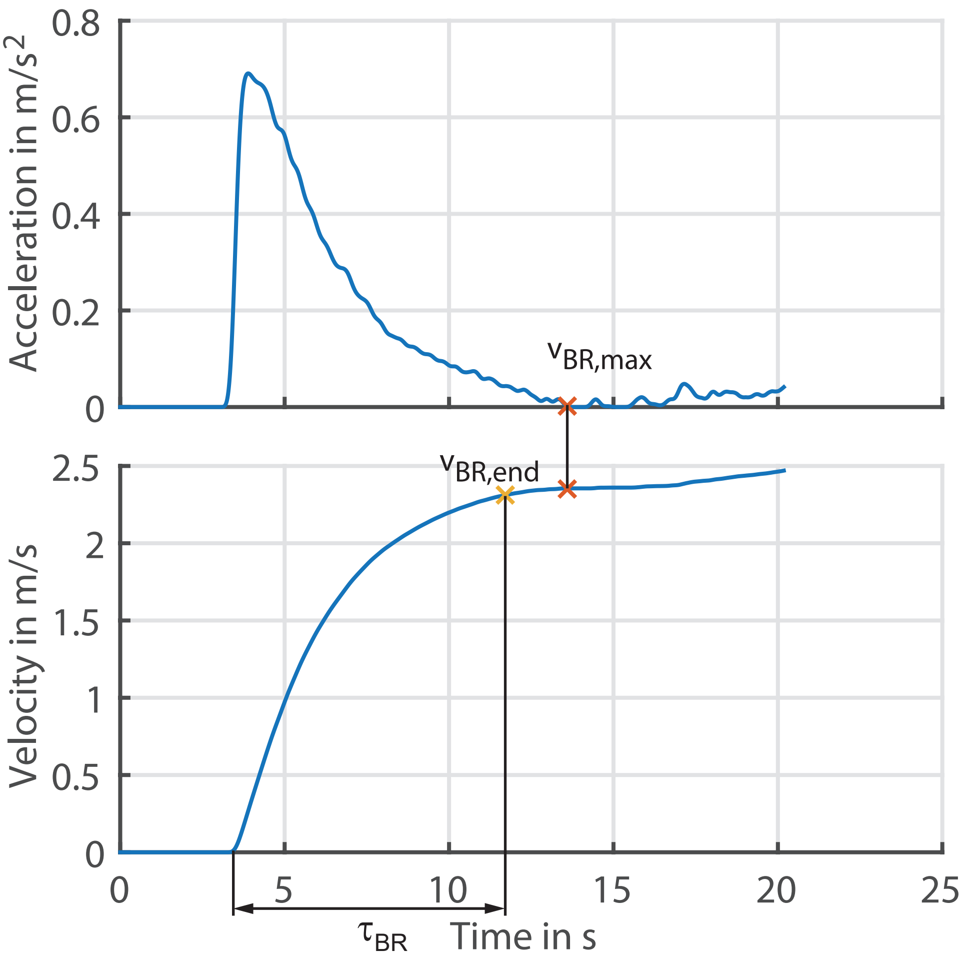

Figure 4.30.: Acceleration and velocity of a brake release manoeuvre.

Table 4.18.: Results of the brake release manoeuvres.

	Unit	Mean value	Standard deviation
Max. torque $T_{BR,max}$	Nm	56.16	0.39
Max. velocity $v_{BR,max}$	km/h	7.25	1.06
End velocity $v_{BR,end}$	km/h	7.11	1.05
Time interval τ_{BR}	s	9.00	0.45
Max. acceleration a_{BR}	m/s^2	0.58	0.09
Max. acceleration gradient $\dot{a}_{BR}$	m/s^3	1.46	0.21

Summary

The driving manoeuvre for the brake release is straightforward. Nevertheless, only three of four manoeuvres were correct measured. Different driving conditions (e.g., slopes) have an impact on the results. The end velocity is about 7 km/h. In comparison a Tesla Model S has a creeping velocity of approximately 5 mph (≈8 km/h) [19]. The time which is needed to reach the end velocity is about 9 s. The max. torque to overcome the driving resistances is about 56 Nm. The maximum acceleration gradient is $1.46\,\mathrm{m/s^3}$. According to Table 4.13 this jerk is comfortable for the passengers.

4.14. Drag Torque

The drag torque of the traction motor is determined with coasting down manoeuvres with engaged gear. Figure 4.31 shows the drag torque of the traction motor depending on the rotational speed or the driving velocity. The maximum torque is about -20 Nm and occurs at around 40 km/h, which corresponds to a traction motor rotational speed of 2800 rpm. The plot combines fourteen measurements, which are all coherent. In comparison, an ICE has small drag torque at low velocities or rotational speeds and increases over the rotational speed [12], [13]. When an ICE coasts down, no fuel is injected but air still inrushes into the piston chamber. The piston moves up and down with the rotational speed and compresses the inrushed air. As a result at higher rotational speeds the friction losses and the energy which is needed to compress the air increases. The same manoeuvre were performed with the gear B engaged. The maximum drag torque is about -50 Nm at around a rotational speed of the electric motor of 4000 rpm or 60 km/h. Appendix A.4 shows the corresponding results . Furthermore, coast down manoeuvres were performed on a test bench. The comparison is shown in the Appendix A.5. Both methods yield the same results.

Brake release torque and drag torque combined

Figure 4.32 represents the drag torque and the torque from the brake release measurements. The torque from the break release approaches to zero at around 9 km/h, which correspond to a rotational speed of the traction motor of 640 rpm. Likewise the drag torque converges towards zero at the same velocity and rotational speed.

Observation

During the analyses of the drag torque, an operation state was found where the clutch between the ICE and the driving axle is engaged. In electric drive (OPM 1), recuperation (OPM 2) or series operation mode (OPM 5) the clutch is disengaged and the torque of the traction motor and the actual torque on the axle should correlate. Figure 4.33 shows

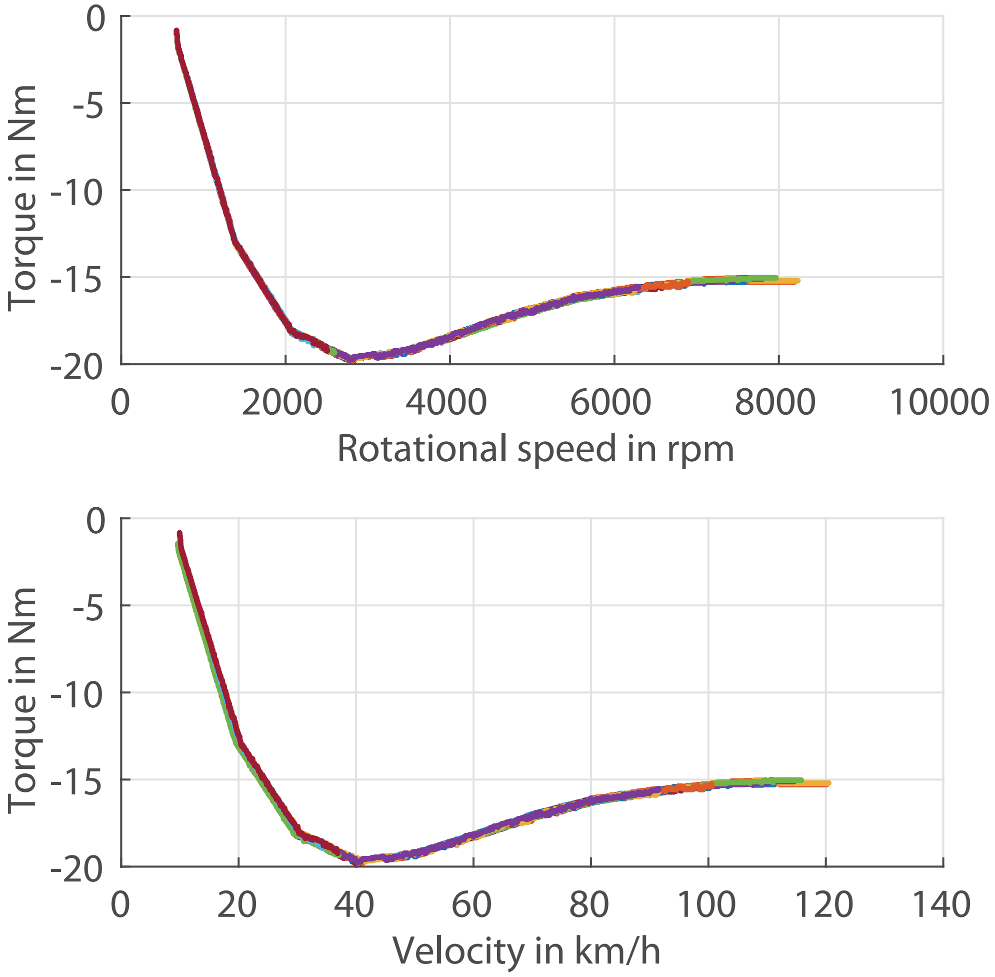

Figure 4.31.: Drag torque with gear D engaged. The torque is correlated to the traction motor. The different colours represents different measurements.

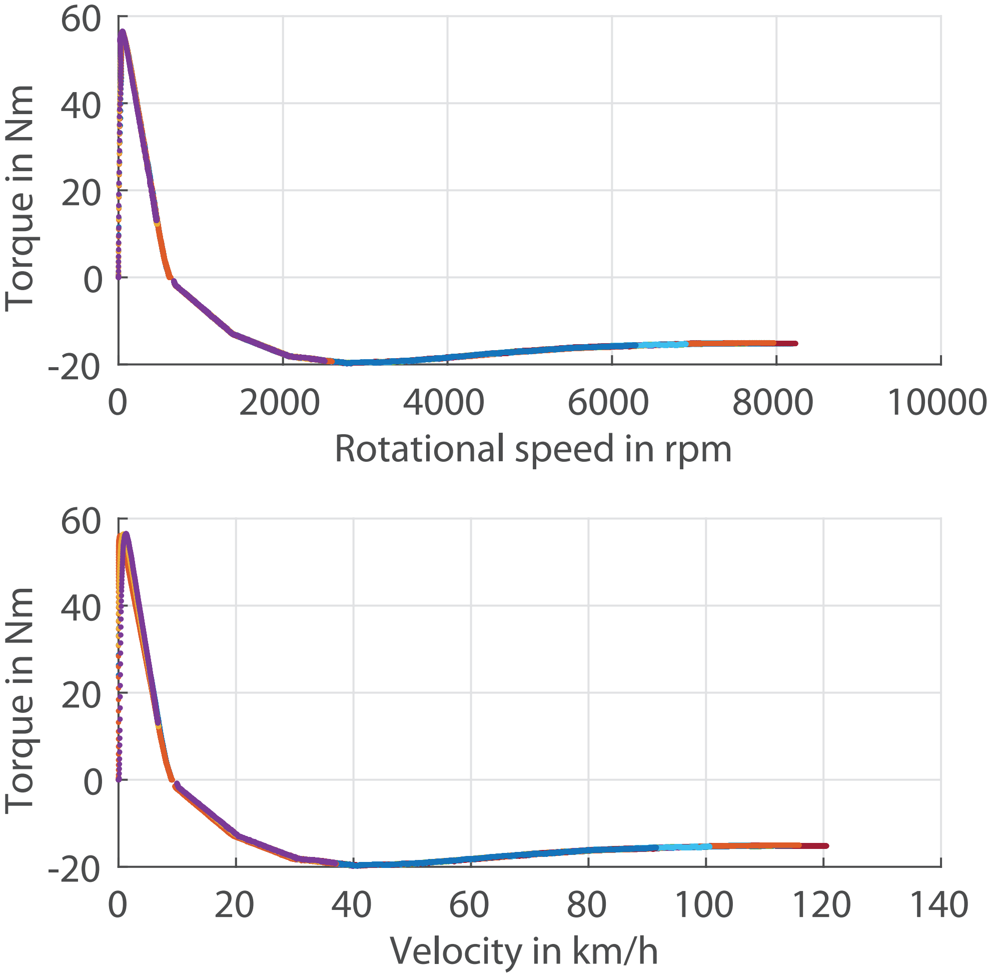

Figure 4.32.: Combined figure of the brake release measurements and the drag torque measurements. The different colours represents different measurements.

that both rotational speeds of the traction motor and the ICE are coherent between the first 14 s. These rotational speeds are correlated to the drive axle. Therefore, it is assumed that the clutch between the ICE and the driving axle is engaged. Actually, this operation mode should be described as engine mode (OPM 4). However, non of such operation mode is displayed on the CAN-Bus during the entire manoeuvre. Therefore, the drag torque has to be separated into two sections. In one section the clutch is still closed (area 2) and in the other it is opened (area 3), compare Figure 4.34.

Figure 4.34 shows that in the first few moments (area 1), where both torques are positive and an acceleration is performed, the torque difference between traction motor and axle is achieved by the ICE. The rotational speeds of the axle / traction motor and the ICE are

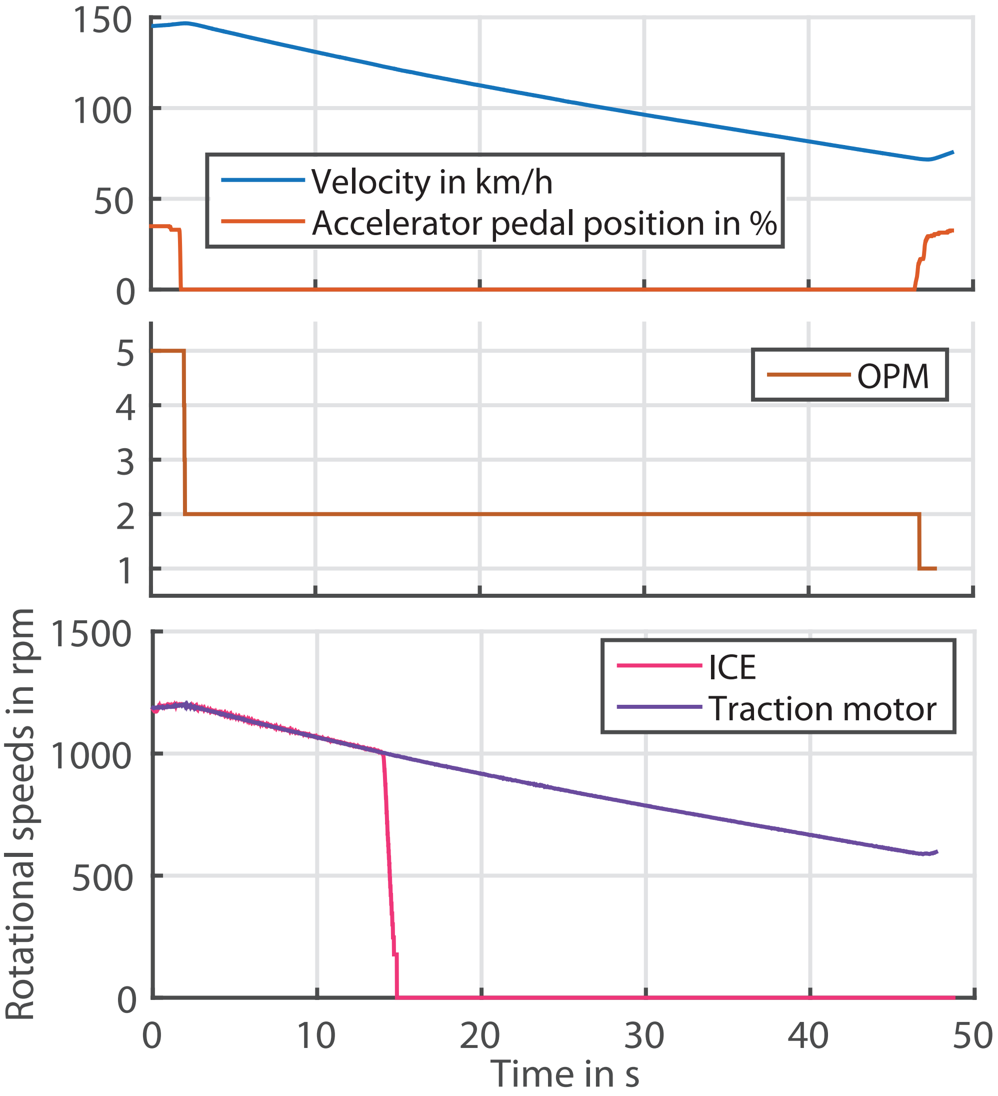

Figure 4.33.: Velocity, pedal position, operation mode and rotational speeds of the traction motor and ICE during the coast down manoeuvre. The rotational speeds are correlated to the drive axle.

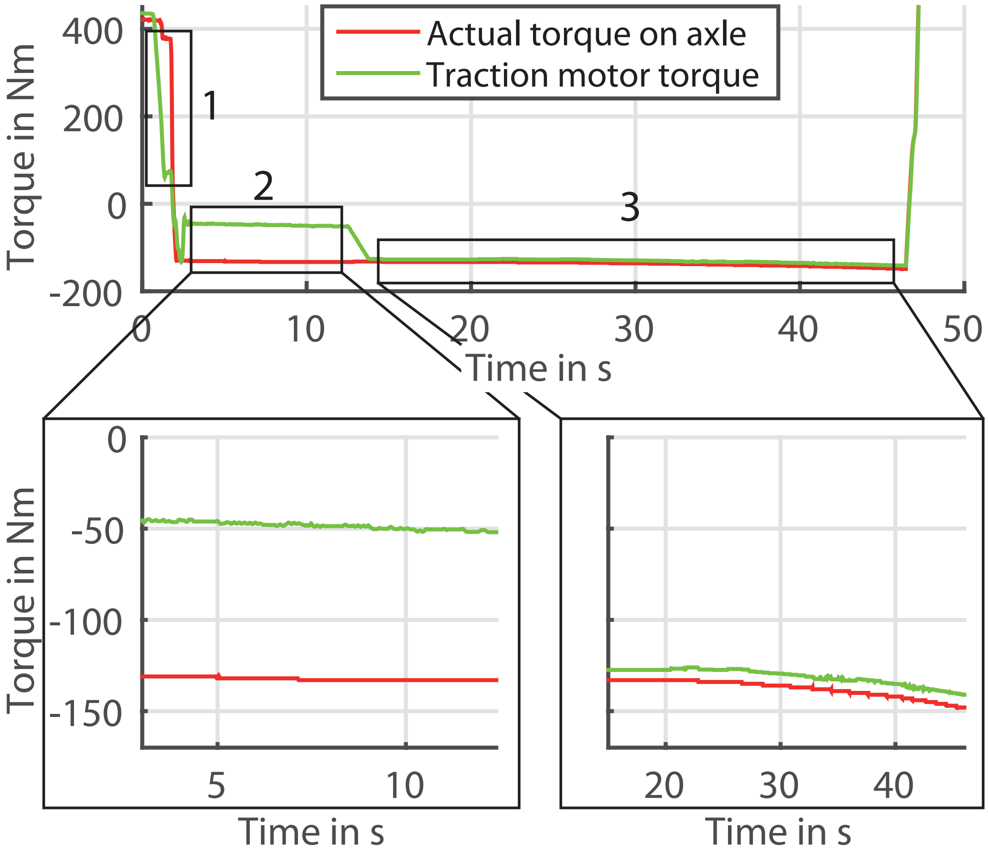

Figure 4.34.: The red line shows the actual torque on the driving axle. As the green line shows the traction motor torque correlated on the driving axle level. Area 2 shows the drag torque of the coupled state of the ICE and the drive axle. Area 3 displays the drag torque of the traction motor alone.

the same (considering all relevant gear ratios). At this rotational speed the ICE performs at its optimal load point. In area 1 the traction motor and the actual axle torque differ from each other. However, the rotational speeds are still the same, which allows the conclusion that the clutch is still closed. Therefore, the drag torque is now depending on the combustion engine and the traction motor. In this few seconds it would be more efficient if the traction motor recuperates the whole drag moment. The battery current (≈9 A), power (≈32 kW) or the SoC (<85 %) does not limit this process. Nevertheless the electric motor torque is too low to achieve the same drag torque behaviour like an ICE (i.e., high drag torque at high vehicle speed). Such an implementation gives the driver the feeling of a conventional ICE driven vehicle. Area 3 displays that the traction motor and actual torque are the same and therefore drag torque depends only on the traction motor.

To conclude, the vehicle and its operation strategy is very complex. The manufacturer has to consider more parameters than the SoC, the maximum power and the torque on the driving axle. Therefore, it may be possible that this coupled state is implemented to give the driver the impression of a conventional ICE behaviour. Consequently, the drag torque has to be separated under specific circumstances into the drag torque of the ICE and into the drag torque generated by the traction motor. From 14 coast down manoeuvres with engaged gear D only five measurements included some seconds with this coupled state. The same behaviour is found when the driving gear B is engaged. Similarly, only five out of 19 measurements contained this state for a few seconds. Therefore, it was hard to extract reasonable results for this coupled state.

Summary

The drag torque of traction motor is evaluated with the help of coast down manoeuvres with engaged gear. Figure 4.31 shows the results for the D gear and Figure A.4 for gear B engaged. The maximum torque for gear D is -20 Nm at a rotational speed of the electric motor of around 2800 rpm and -50 Nm at around 4000 rpm with gear B engaged. The drag torque of the ICE solely was not analysed since the engine state (OPM 4) was only used at higher speed and rarely activated.

5. Summary and Conclusion

This Master's thesis deals with the development of a holistic method to identify drivetrain parameters in real driving situations as well as on test benches without disassembling the vehicle. The motivation is to identify parameters which than can be implemented into a drivetrain simulation. With this simulation the development time and costs can be reduced significantly.

Chapter 1: Introduction. This chapter gives an overview of the present CO_2 limits and its further development of passenger vehicles. In addition, the different types of hybrid electric vehicles and their potential of reducing green house gases are discussed. Furthermore, the provided test vehicle is introduced with its different operation modes.
Chapter 2: Fundamentals and Methods. Within this chapter the different coordinate systems are addressed. For this thesis, a vehicle fixed levelled coordinate system with its origin in the centre of gravity (CoG) is used. The fundamental equations for longitudinal vehicle dynamics are stated as well as the driving resistance forces. In addition, the method of least squares is introduced. This method is used in various driving manoeuvres to identify parameters.
Chapter 3: Driving Manoeuvres. For this thesis, a manoeuvre roadmap was developed. In this chapter the performed manoeuvres with the provided HEV are represented and described. Table 3.3 gives an overview of all manoeuvres and the identified parameters.
Chapter 4: Parameter Identification. This chapters presents methods to identify parameters from a vehicle. At first, an average mean filter is introduced. It is used to filter the measured velocity and their derivatives. The dynamic tyre radius is identified through a rolling manoeuvre and is taken for almost all other identifications. To use a vehicle fixed coordinate system the CoG is needed. The x-y-position of the CoG can be determined with the contact forces of the tyres. A tilt measurement was not possible to obtain the z-position. Thus the height of the CoG is estimated with an approximation. At first, the suspension characteristic is estimated with loading weights above the suspension. With this method the linear component of the springs can be determined. Further, the damper coefficient is evaluated with the damping factor. Afterwards these parameters are validated with a simulation model within an optimisation process. The results from the optimisation process differ from the first evaluated estimations. The deviations can be explained because many assumptions and simplification for the simulation models have been made (e.g. no spring inclination, no spring damper conversion, only mass points).
The battery characteristics are evaluated through heavy braking and full load manoeu-

vres. Heavy braking manoeuvre may not be ideal to evaluate the maximum charging characteristic. Control units like ABS or ESC can interfere and the conventional friction brakes are used instead of the recuperation potential of the traction motor. The evaluation of the traction motor and generator is conducted with the help of full load manoeuvres. The evaluation yields that the electric motor has almost an instantaneous response time. The tow-start performance of the generator was also investigated during recuperation manoeuvres as well with a low battery SoC ($\approx 27\,\%$). In general the performance of the generator does not change. At low SoC the ICE is started more often.

The driving resistance was evaluated with coast down manoeuvres and calculated with the method of least squares. Successful coast down manoeuvres are difficult to perform. More successful attempts lead to more precise results. The operation strategy was identified with transition points evaluated from test bench and real driving manoeuvres. With these transition points an “increasing” and “decreasing” quasi-static pedal map can be determined. The combination of both results in a pedal map with a hysteresis. The advantage of the test bench is that all load points of the vehicle can be determined. The braking strategy of the vehicle was evaluated with the help of recuperation and other braking manoeuvres. With the calculation of the total braking torque, a clear result was delivered.

At first, it was considered that the drivetrain inertia can be achieved with coast down (without an engaged gear) measurements. Within the evaluation it was discovered that this was not possible, because the drivetrain inertia is comparable small to the chassis inertia and is easily influenced. However, the drivetrain inertia is obtained with the evaluation of full load manoeuvres and the method of least squares. The brake release manoeuvre is fully determined with the output parameters maximum torque, end velocity, needed time to reach the end velocity, maximum acceleration and the acceleration gradient. Finally, the drag torque from the traction motor was obtained. At high velocities the ICE is coupled to the drivetrain and has to be considered as well.

Final statement: With the proposed methods, drivetrain parameters can be obtained through real driving and test bench manoeuvres. These parameter can be implemented into drivetrain simulations. The objective of this Master’s thesis was to reduce time and expanses to identify specific drivetrain parameters.

List of Figures

1.1. Categorization of HEVs, adopted from [5]. 3

1.2. The four different operation modes of the testing vehicle. 5

2.1. Used coordinate system based on ISO 70000, adopted from [4]. 8

2.2. Vehicle body, axis, road and it all active forces, adopted from [4] 9

2.3. Vehicle with front powered drivetrain and gearbox. 12

3.1. Example of a full load manoeuvre. 16

3.2. Example of a drive away manoeuvre. 19

3.3. Example of a brake release manoeuvre. 19

3.4. Load variation manoeuvre example. 21

3.5. Relative x- and y- Position of the real driving cycle. 23

3.6. Velocity and height profile over the time of the real driving cycle. 23

4.1. Measurement equipment. 28

4.2. Current probes positions. 28

4.3. Example of an average mean filter, with a window size of 20 points. 31

4.4. Difference of the tyre radii. The parameter C is the centre of the tyre, M_P the instantaneous centre of rotation and Δz_S is the static spring compression, adapted from [4]. 31

4.5. Centre of gravity, adapted from [9]. 33

4.6. Tilt measurement, adapted from [9]. 35

4.7. Measurement to estimate the spring compression characteristic, adopted from [9]. . . . 38

4.8. Linear progressive spring characteristic. Distance s_{S0}, describes the end of the linear compression. At the distance s_{Sa} an additional spring is engaged. Adopted from [4]. . 40

4.9. Spring characteristics. 40

4.10. Spring damper simulation model, adapted from [4]. 42

4.11. Speed bump. Measured points in red, fitted and interpolated curve in blue. 43

4.12. Left: the pitch-rate and pitch with a good congruence of simulated and measured pitch and pitch-rate is shown. The optimisation process was performed with 20 km/h. Right: the pitch-rate and pitch have bad congruence and were performed with 10 km/h. The red lines are measured values and the green lines are the final optimisation results. . . 45

4.13. Cable potentiometer and wheel vector sensor to measure the relative velocity of the suspension, adopted from [9]. 46

4.14. Full load acceleration manoeuvre with battery current, voltage and power. 48

4.15. Velocity, battery voltage, battery current and battery power during a heavy braking manoeuvre. 50
4.16. Full load acceleration manoeuvre with the reaction time of the traction motor and the time difference between zero and 100 km/h. 51
4.17. Start up of the generator. Generator torque over time of a full load manoeuvre. 54
4.18. Generator evaluation from a full load manoeuvre 55
4.19. Generator behaviour with low SoC (≈27 %). 56
4.20. Generator behaviour of switching from engine mode to recuperation mode. 57
4.21. The velocities of eight coast down manoeuvres. Two of the eight are failed coast down attempts. 59
4.22. The overall driving resistance was calculated either with only successful or all attempts. Furthermore, it was calculated with the reference values given by the institution EPA. . 60
4.23. Static pedal map. The various colours represent different operation modes. The red points represent different load points. 62
4.24. Left: Quasi-static pedal map for real driving manoeuvres with driving manoeuvres just over the transition. Right: Quasi-static pedal map on a test bench with driving manoeuvres with constant APP or v. The different colours represent different operation modes. Red arrows represent quasi-static manoeuvres. 64
4.25. Transition points achieved from the test bench. 65
4.26. Quasi static “increasing” pedal map for real driving manoeuvres. 1: All transition points from real driving situations. 2: The points are averaged with a 5 km/h increment. 3: Additionally, the transitions points from the test bench are included. 4: With further optimisation the quasi-static pedal map is obtained. 66
4.27. Braking strategy. The cyan points represent the braking torque, the blue points the traction motor torque and the red line the max. recuperation characteristic of the traction motor. 68
4.28. Traction motor recuperation limit. 68
4.29. Torques from brake release manoeuvres correlated to the traction motor. 71
4.30. Acceleration and velocity of a brake release manoeuvre. 72
4.31. Drag torque with gear D engaged. The torque is correlated to the traction motor. The different colours represents different measurements. 74
4.32. Combined figure of the brake release measurements and the drag torque measurements. The different colours represents different measurements. 75
4.33. Velocity, pedal position, operation mode and rotational speeds of the traction motor and ICE during the coast down manoeuvre. The rotational speeds are correlated to the drive axle. 76
4.34. The red line shows the actual torque on the driving axle. As the green line shows the traction motor torque correlated on the driving axle level. Area 2 shows the drag torque of the coupled state of the ICE and the drive axle. Area 3 displays the drag torque of the traction motor alone. 77

A.1. Quasi-static pedal map, SoC above 27 %, Left: “Increasing” pedal map. Right: “Decreasing” pedal map. X

A.2. Pedal map, SoC below 27 %, Left: “Increasing” pedal map. Right: “Decreasing” pedal map. X
A.3. Pedal maps with hysteresis. Left: SoC above 27 %. Right: SoC below 27 %. XI
A.4. Drag torque with gear B engaged. The different colours represents different measurements. XII
A.5. Comparison of the drag torque between the test bench and the real driving situations. Both measurements results in the same outcomes. XIII

List of Tables

3.1. Full load variation examples. 16
3.2. Load variation examples. 21
3.3. Manoeuvre and Parameter Overview 25

4.1. Measured parameters. 29
4.2. Measured tyre parameters. 32
4.3. Centre of gravity – x-Position results. 34
4.4. Centre of gravity – y-position results. 35
4.5. Centre of gravity calculation results. 37
4.6. Results of the spring characteristic of the front spring. 39
4.7. Results of the spring characteristic of the rear spring. 39
4.8. Damper coefficients. 41
4.9. Simulation results in comparison to the estimated values. 44
4.10. Discharging battery characteristics. 47
4.11. Charging battery characteristics. 49
4.12. Results of the full load manoeuvres. 51
4.13. Jerks and comfort levels [25]. 52
4.14. Acceleration time $\tau_{0\rightarrow100}$. 52
4.15. Results of the generator characteristics of full load manoeuvres. 53
4.16. Results of the coast down manoeuvres. 58
4.17. List of all possible driving manoeuvres. Green: Velocity v of the vehicle; Blue: Accelerator pedal position APP; Red: Transition of the operation mode. 63
4.18. Results of the brake release manoeuvres. 72

A.1. Front spring measurement results IX
A.2. Front spring measurement results IX

Bibliography

[1] Manfred Burckhardt and Heinz Burg. *Berechnung und Rekonstruktion des Bremsverhaltens von PKW.* Verlag Information Ambs, 1988. ISBN - 978-3885500254.

[2] Daniel Görke. *Untersuchungen zur kraftstoffoptimalen Betriebsweise.* Springer, 2016. ISBN - 978-3-658-14163-9.

[3] Bernd Heißing, METIN Ersoy, and S Gies. *Fahrwerkhandbuch–Grundlagen, Fahrdynamik, Komponenten, Systeme, Mechatronik, Perspektiven. 2.* Springer Vieweg, 2013. ISBN - 978-3-658-01992-1.

[4] W. Hirschberg and H. Waser. Fahrzeugdynamik. Lecture notes. Institut of Automotive Engineering, Graz University of Technology. 2010.

[5] P Hoffmann. *Hybridfahrzeuge.* Springer-Verlag, 2010. ISBN - 978-3-7091-1780-4.

[6] BMW. *BMW i3.* http://www.bmw.com/com/de/newvehicles/i/i3/2015/showroom /technical_data.html. Accessed on: 02.06.2014.

[7] Uwe Kiencke and Lars Nielsen. *Automotive Control Systems: For Engine, Driveline, and Vehicle.* Springer, 2005. ISBN - 978-3-540-26484-2.

[8] Yong Seok Kim, Joonyoung Park, Tae Wook Park, Jae Sung Bang, and Hyun Sung Sim. Anti-jerk controller design with a cooperative control strategy in hybrid electric vehicle. In *Power Electronics and ECCE Asia (ICPE & ECCE), 2011 IEEE 8th International Conference on*, pages 1964–1968. IEEE, 2011.

[9] Daniel Kollreider. *Identifikation der Reifeneigenschaften als Grundlage zur Fahdynamikbewertung.* PhD thesis, Institute for Automotive Engineering, Graz University of Technology, 2009.

[10] Johannes Liebl, Matthias Lederer, Klaus Rohde-Brandenburger, Jan-Welm Biermann, Martin Roth, and Heinz Schäfer. *Energiemanagement im Kraftfahrzeug: Optimierung von CO2-Emissionen und Verbrauch konventioneller und elektrifizierter Automobile.* Springer-Verlag, 2014. ISBN - 978-3-658-04451-0.

[11] MATLAB. *Documentation, Matlab ver. R2014b.* The MathWorks Inc., 2014.

[12] Felix Matthies. *Beitrag zur Modellbildung von Antriebsträngen für Fahrbarkeitsuntersuchungen.* PhD thesis, Faculty IV, Electrical Engineering and Computer Science, Technische Universität Berlin, 2013.

[13] Manfred Mitschke and Henning Wallentowitz. *Dynamik der Kraftfahrzeuge.* Springer Fachmedien Wiesbaden, Wiesbaden, 2014. ISBN - 978-3-658-05068-9.

[14] Audi. *Audi A4 Avant 1.4 TFSI.* http://www.audi.at/a4/a4_avant/technik/technische_daten. Accessed on: 02.06.2014.

[15] Driveaccord.com. http://www.driveaccord.net/forums/86-9th-generation/80074-what-accords-cd-coefficient-drag.html. Accessed on: 02.06.2014.

[16] Lexus. *Lexus CT 200h.* http://www.lexus.eu/car-models/ct/ct-200h/#Introduction. Accessed on: 02.06.2014.

[17] Mercedes. *Mercedes CLA 250.* http://www.mercedes-benz.de/content/germany/mpc/mpc_germany_web-site/de/home_mpc/passengercars/home/new_cars/models/cla-class/c117/facts_/technicaldata/models.html. Accessed on: 02.06.2014.

[18] Nissan. *Nissan Altima 2013 2.5 SL.* http://www.caranddriver.com/reviews/2013-nissan-altima-25-sl-test-review. Accessed on: 02.06.2014.

[19] Teslaleiving.net. http://teslaliving.net/2014/06/14/clutches-and-creep/. Accessed on: 02.06.2014.

[20] Topspeed.com. http://www.topspeed.com/cars/honda/2014-honda-accord-hybrid-ar159503.html. Accessed on: 02.06.2014.

[21] Zustandsschätzung und Filterung. Lecture notes. Institute of Automation and Control, Graz University of Technology. 2007.

[22] Konrad Reif, Karl E Noreikat, and Kai Borgeest. *Kraftfahrzeug-Hybridantriebe: Grundlagen, Komponenten, Systeme, Anwendungen.* Springer-Verlag, 2012. ISBN - 978-3-8348-2050-1.

[23] Georg Rill. *Road Vehicle Dynamics: Fundamentals and Modeling.* CRC Press, 2011. ISBN - 978-1439838983.

[24] Dieter Schramm, Manfred Hiller, and Roberto Bardini. *Modellbildung und Simulation der Dynamik von Kraftfahrzeugen,* Volume 124. Springer, 2010. ISBN - 978-3-642-33888-5.

[25] Xi Wei and Giorgio Rizzoni. Objective Metrics of Fuel Economy, Performance and Driveability-a review. Technical report, SAE Technical Paper, 2004.

A. Appendix

Table A.1.: Front spring measurement results

Mass	Front right in kg	Front left in kg	Rear right in kg	Rear left in kg	Compression in mm
Idle state	484	479	360	406	403
+20 kg	501	499	362	404	401
+40 kg	521	520	362	403	396
+60 kg	544	538	360	405	390
+80 kg	565	557	360	405	383
+100 kg	581	577	363	404	381

Table A.2.: Front spring measurement results

Mass	Front right in kg	Front left in kg	Rear right in kg	Rear left in kg	Compression in mm
Idle state	484	480	358	402	397
+20 kg	487	474	383	427	392
+40 kg	473	469	404	450	387
+60 kg	468	463	429	477	382
+80 kg	462	457	455	502	378
+100 kg	456	452	480	526	373

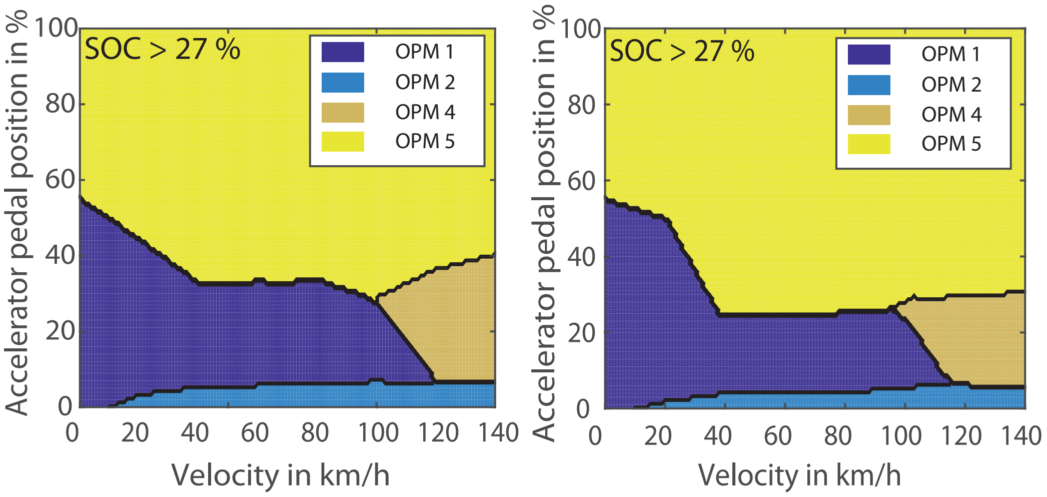

Figure A.1.: Quasi-static pedal map, SoC above 27 %, Left: “Increasing” pedal map. Right: “Decreasing” pedal map.

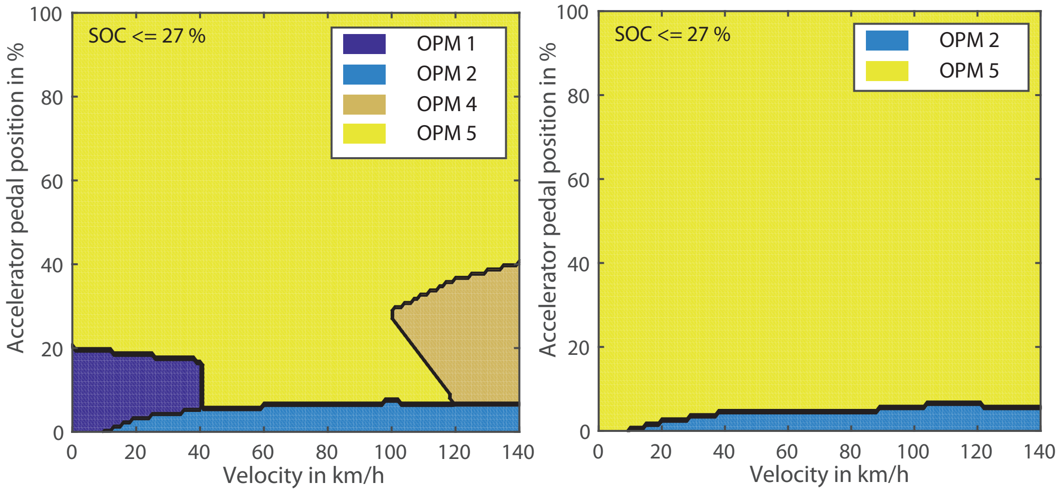

Figure A.2.: Pedal map, SoC below 27 %, Left: “Increasing” pedal map. Right: “Decreasing” pedal map.

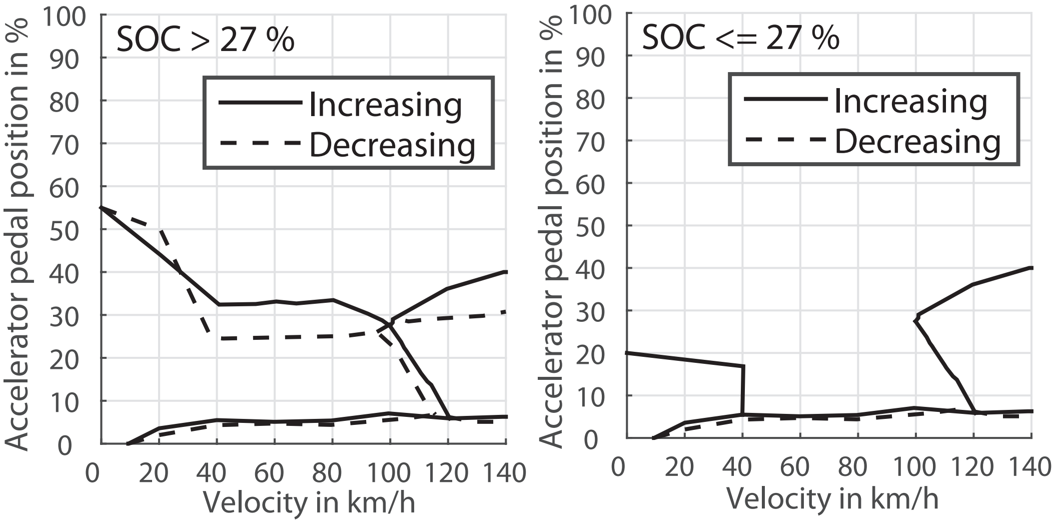

Figure A.3.: Pedal maps with hysteresis. Left: SoC above 27 %. Right: SoC below 27 %.

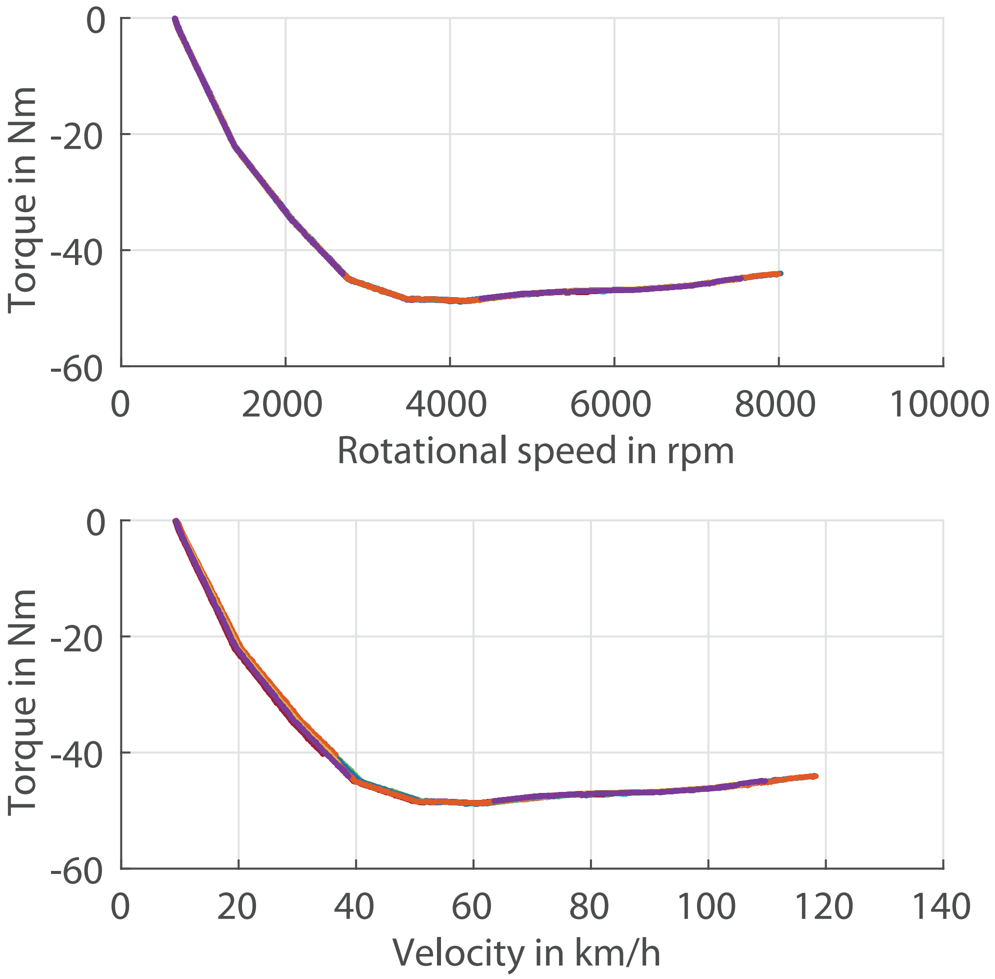

Figure A.4.: Drag torque with gear B engaged. The different colours represents different measurements.

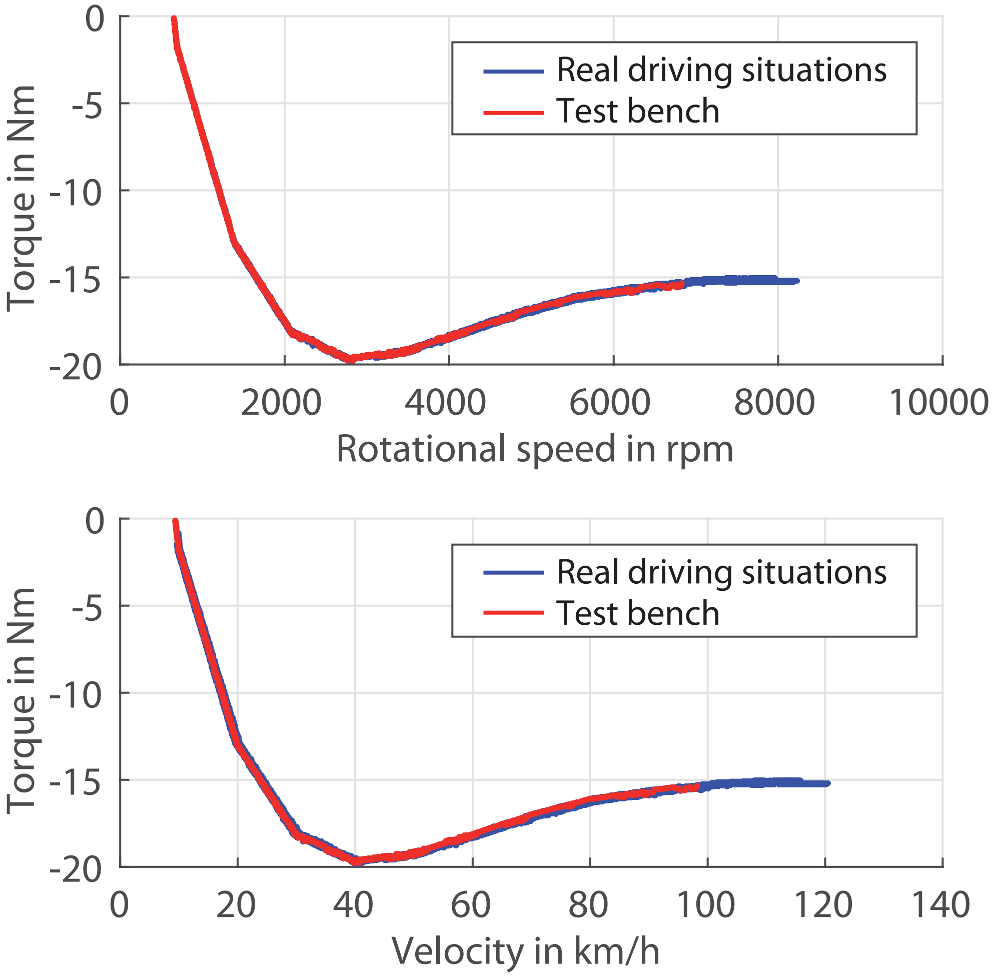

Figure A.5.: Comparison of the drag torque between the test bench and the real driving situations. Both measurements results in the same outcomes.